Hindered Transport in Composite Hydrogels

by
Kimberly Bryan Kosto

B.S., Chemical Engineering
Rensselaer Polytechnic Institute, 1999

Submitted to the Department of Chemical Engineering
in partial fulfillment of the requirements for the degree of

DOCTOR OF PHILOSOPHY IN CHEMICAL ENGINEERING

at the

MASSACHUSETTS INSTITUTE OF TECHNOLOGY

June, 2004

Signature of Author: _____
Department of Chemical Engineering
May 19, 2003

Certified by: _____
Professor William M. Deen
Carbon P. Dubbs Professor of Chemical Engineering
Thesis Supervisor

Accepted by: _____
Professor Daniel Blankschtein
Professor of Chemical Engineering
Chairman, Committee for Graduate Students

Hindered Transport in Composite Hydrogels

by
Kimberly Bryan Kosto

Submitted to the Department of Chemical Engineering on May 19, 2004 in partial fulfillment of the requirements for the degree of Doctor of Philosophy in Chemical Engineering

ABSTRACT

The ultimate goal of this research was to develop a greater understanding of the structural components needed to describe transport within the glomerular basement membrane (GBM). Specifically, dimensionless diffusive and convective hindrance factors were investigated by measuring macromolecular permeability through synthetic, two-fiber, agarose-dextran hydrogels at very small or very high Pe, respectively. By comparing diffusion and convection in the synthetic hydrogel with corresponding measurements in isolated rat GBM, further insight regarding the structure responsible for transport through the GBM was gained. In order to compare diffusive hindrances in the synthetic gels with those in isolated GBM, partitioning in agarose-dextran hydrogels was also examined. Additionally, hindered transport theories were tested.

In studying diffusion, partitioning, and convection, macromolecules with Stokes-Einstein radii (r_s) ranging from 2.7 to 5.9 nm were used. Gels with agarose volume fractions of 0.040 and 0.080 were studied with dextran volume fractions (assuming dextran acts as a fiber) ranging from 0 to 0.0076 and 0 to 0.011, respectively. For the diffusion studies, two globular proteins (ovalbumin and bovine serum albumin) and three narrow fractions of Ficoll, a spherical polysaccharide, were used. For the partitioning and convection studies, four narrow fractions of Ficoll were used.

Diffusivities of fluorescein-labeled macromolecules were measured in dilute aqueous solution (D_∞), agarose gels (D_a), and agarose-dextran composite gels (D) using fluorescence recovery after photobleaching. For both agarose concentrations, the Darcy permeability (κ) decreased by an order of magnitude as the dextran concentration in the gel was increased from zero to its maximum value. For a given gel composition, the relative diffusivity (D/D_∞) decreased as r_s increased, a hallmark of hindered diffusion. For a given test molecule, D/D_∞ was lowest in the most concentrated gels, as expected. As the dextran concentration was increased to its maximum value, 2-3 fold decreases in relative diffusivity resulted for both agarose gel concentrations. The reductions in macromolecular diffusivities caused by incorporating various amounts of dextran into agarose gels could be predicted fairly accurately from the measured decreases in κ, using an effective medium model. This suggests that one might be able to predict

diffusivity variations in complex, multicomponent hydrogels (e.g. those in body tissue) in the same manner, provided that values of κ can be obtained.

Equilibrium partition coefficients (Φ, the concentration in the gel divided by that in free solution) of fluorescein-labeled Ficolls in pure agarose and agarose-dextran composite gels were measured as a function of gel composition and Ficoll size. As expected, Φ generally decreased as the Ficoll size increased (for a given gel composition) or as the amount of dextran incorporated into the gel increased (for a given agarose concentration and Ficoll size). The decrease in Φ that accompanied dextran addition was predicted well by an excluded volume theory in which agarose and dextran were both treated as rigid, straight, randomly positioned and oriented fibers. Modeling dextran as a spherical coil within a fibrous agarose gel produced much less accurate predictions. The diffusional permeabilities of these gels were assessed by combining the current partitioning data with relative diffusivities, or diffusive hindrance factors ($K_d = D/D_\infty$), reported previously. The values of ΦK_d for a synthetic gel with 8.0% agarose and 1.1% dextran (by volume) were found to be very similar to those for the GBM in vitro, which also has a total solids content of ~10%.

The sieving coefficient (Θ), or the ratio of the macromolecular downstream concentration to that at the upstream membrane surface, was measured in high Peclet number flow where $\Theta = \Phi K_c$. The convective hindrance factor (K_c) is the macromolecular velocity in the gel due to bulk flow divided by that of the superficial fluid. The measured sieving coefficients of four narrow fractions of Ficoll in agarose and agarose-dextran composite gels decreased with each addition of dextran. For a given gel composition, Θ generally decreased as the size of the macromolecule increased. While theories describing hindered convection in random fiber matrices have yet to be developed, ΦK_c seems to correlate well with κ, for a given r_s, based on the predictions of parallel fiber theory for a number of different macromolecules and a variety of gel compositions. The inherent differences in averaging between the observable partition and sieving coefficients in gels with fiber spacing heterogeneity result in large apparent K_c, as substantiated by examination of hindered transport in parallel fiber media. Comparison of ΦK_c in agarose-dextran synthetic gels and isolated GBM continues to support the idea that the GBM transport properties can be explained by its mixture of thick and thin fibers, rather than its precise chemical composition.

Thesis Supervisor: William M. Deen
Carbon P. Dubbs Professor of Chemical Engineering

Acknowledgements

When I first joined the Deen group, one of the senior members, Jeff White, mentioned that "Getting a Ph.D. is a marathon." I did not appreciate those words of wisdom until I neared the completion of my thesis. Marathon or Ph.D., it was not the actual race, or thesis writing, that shaped who I have become or gave me the strength to finish. Rather, it was the training, preparation, and all those I met along the way that kept me going. I could not have crossed this finish line without the help of the many people who made this thesis possible.

I sincerely thank my advisor, Prof. William Deen, for his dedication, insight, and patience. His door was always open so both success and failure could be discussed at a moment's notice, if necessary. I also thank Profs. T. Alan Hatton and Alan Grodzinsky for their enthusiasm, encouragement, and many constructive comments during committee meetings and beyond. Building the FRAP was one of the most rewarding undertakings in my thesis work and I thank Prof. T. Alan Hatton for opening up his lab and supplying much of the equipment.

I thank Mr. Wright for irradiating every composite gel that I ever studied. Also, I greatly appreciate the time and effort of Tim Finegan, with whom I had many discussions regarding optics and lasers. His expertise certainly contributed to the development of the FRAP system and to my understanding of optics. I thank the two undergraduates with whom I worked, Christiana Obiaya and Swapna Panuganti, for their hard work and friendship. I thank all of my past and present lab members, Jeff White, Matt Lazzara, Bo Chen, Chen Wang, Ian Zacharia, Greg Zugates, Nitesh Nalwaya, Jason Fincher, Kristin Mattern, Helen Chuang, and Gaurav Bhalla, who taught me much and always made coming to lab more fun and worthwhile.

I had such a great first year class and made many friends who will always make me remember MIT with a smile. To all those on the "lunch knock" (in order of pick up), Kevin Dorfman, Jim Bielenberg, Ian Zacharia, April Ross, Ley Richardson, Paul Yelvington, and Patty (Sullivan) Bielenberg, it was always my favorite part of the day. Thanks guys!

I sincerely thank my parents for all their support and encouragement. They set a wonderful example that I can only hope to follow. Sis, thanks for being such a great sis and for not making me ride in the back seat anymore! I thank all my family for being so supportive of my dreams and especially my Aunt Sally who welcomed me into her hometown of Boston.

Great appreciation goes to my husband, Martin, for never being more than a phone call away, for always being able to make me smile, for teaching me that a trip to FAO Swartz can make you feel like a kid again, and for being a better person today than you were yesterday and challenging me to do the same.

Finally, I thank God.

Table of Contents

List of Figures

List of Tables

1 Background

1.1 Introduction

Hydrogels are materials in which a large volume of water is held within a crosslinked polymer network. They range in complexity from synthetic materials that contain a single polymer (e.g., polyacrylamide) to natural ones that are composites of several biopolymers. The current and potential uses of hydrogels in membrane and chromatographic separations, their increasing application in medical devices, and their occurrence in body tissues (e.g., basement membranes and cartilage) provide ample motivation for studying the transport of water and macromolecules in such materials. For macromolecular solutes in particular, a combination of steric and hydrodynamic effects causes diffusion and convection to be slower than in water. That is, the crosslinked polymers prevent macromolecules from occupying certain positions and limit their possible paths. Further, by acting as fixed obstacles, the crosslinked polymers alter the fluid stresses, thereby increasing the drag coefficient for a solute molecule and decreasing its mobility. Both effects lower the measurable permeability properties of the macromolecular solute.

While hydrogels are important to a wide variety of fields, as mentioned above, we are particularly interested in understanding transport within a biological hydrogel, the glomerular basement membrane (GBM). The GBM is part of the glomerular capillary wall across which blood from the heart is filtered in the initial stage of urine formation. The glomerular capillary walls act as barriers restricting most of the plasma proteins to the capillary lumen, while allowing water to permeate. Within the capillary wall, the GBM, which lies between the endothelial and the epithelial cell layers, plays a significant role in both hydraulic (Drumond and Deen, 1994) and macromolecular (Edwards et al., 1999) transcapillary transport.

There are a number of different properties that help describe the overall permeability of a synthetic or biological hydrogel including its hydraulic (Darcy) permeability as well as

macromolecular diffusion, partitioning, and convection within the gel. In section 1.2 that follows, past experimental findings and theoretical models for these four transport properties, as they relate to fibrous media, will be reviewed. These data and models have greatly advanced our ability to predict gel permeabilities based on structural information such as fiber radius, macromolecule size, and fiber volume fraction. Section 1.3 details recent progress towards understanding transport through in vitro and synthetic GBM. The chapter closes with an overview of the thesis work.

1.2 Transport in Fibrous Media

1.2.1 Darcy Permeability

The hydraulic permeability of a gel is an important parameter that can be used to elucidate information about gel structure. Hydraulic permeabilities through hydrogels are generally modeled by Darcy's law,

$$\mathbf{v} = \frac{-\kappa}{\mu}\nabla P \tag{1-1}$$

where κ is the Darcy permeability, $\mathbf{v}$ is fluid velocity vector, μ is viscosity, and P is pressure.

Jackson and James (1986) compiled measurements of hydraulic permeabilities in a number of fibrous materials ranging from wool and fiberglass to collagen and hyaluronic acid. They compared the data to existing theories describing flow through various arrangements of cylindrical rods. With their extensive comparison of theory to data, Jackson and James (1986) confirmed the functional dependence indicated by many of the applicable theories. The data essentially collapse onto a single curve when dimensionless Darcy permeability (κ/r_f^2, where r_f is the fiber radius) is plotted versus gel fiber volume fraction (ϕ), or

$$\frac{\kappa}{r_f^2} = f(\phi) \tag{1-2}$$

Darcy permeabilities of gels, which were not emphasized in the study by Jackson and James (1986), are often difficult to measure. Commonly, the flow is either so slow that it cannot be accurately determined, or the pressure so high that the gel might be destroyed. However, κ has been in measured in a few different gels including gelatin (Pallman and Devel, 1945; Signew and Egli, 1950), agar (Pallman and Devel, 1945), polyacrylamide (White, 1960; Weiss and Silberberg, 1977; Tokita and Tanaka, 1991; Kapur et al., 1996), poly(glyceryl methacrylate) (Leung and Robinson, 1990a; 1990b), and agarose (Johnson and Deen, 1996b; Johnston and Deen, 1999; 2002; White and Deen, 2002). The measurements in agarose were attained at reasonable pressures by mechanically supporting the gel with a polyester mesh. Darcy permeability measurements in synthetic composite gels are even more scarce, although White and Deen (2002) did measure κ in various concentrations of agarose gels that contained small amounts of crosslinked dextran.

Numerous models abound for predicting flow through parallel fiber arrays (Langmuir, 1942; Happel, 1959; Hasimoto, 1959; Kuwabara, 1959; Sparrow and Loeffler, 1959; Sangani and Acrivos, 1982; Drummond and Tahir, 1984). However, models involving flow through three-dimensional random arrays are more appropriate for the disordered structure found in many polymeric hydrogels. Jackson and James (1986) developed a model for predicting Darcy permeabilities in three-dimensional random fiber arrays based on fibers of uniform radius, which is given by

$$\frac{\kappa}{r_f^2} = \frac{3}{20\phi}(-\ln\phi - 0.931 + O(\ln\phi)^{-1}) \tag{1-3}$$

It is accurate to within an order of magnitude.

Several models based on a bimodal distribution of fiber radii have also been developed (Ethier, 1991; Huang et al., 1994, Clague and Phillips, 1997), but they are restrictive in the relative size distribution of radii for which they are applicable. Ethier's (1991) model predicts κ

for membranes comprised of two sizes of fibers with radii different enough that the thin fiber array appears homogeneous compared to the thick fiber array. The thick fibers were considered as barriers embedded in the thin fiber matrix, which was treated as an effective Brinkman medium characterized by its hydraulic permeability. Another heterogeneous fiber model was applied to the arterial intima by Huang et al. (1994) to predict the Darcy permeability through membranes with collagen and proteoglycan components. They assumed that the total resistance in the arterial intima equaled the sum of the resistances of the collagen and proteoglycan components, which were determined using the results of Sangani and Acrivos (1982) and the Carmen-Kozeny correlation, respectively. Clague and Phillips (1997) also analyzed water permeability in bimodal, random fiber systems. They calculated the hydraulic permeability by averaging the local permeabilities, determined using a numerical slender body theory, of many different regions in the fibrous gel. To optimize the results of their model, the ratio of the thick to thin fiber radius must be less than three.

1.2.2 Macromolecular Flux

While the Darcy permeability characterizes water flow, size dependent hindrance factors describe the transport of solutions containing macromolecules. To develop an understanding of macromolecular permeabilities in hydrogels, the convective and diffusive hindrance factors must be considered. The diffusive hindrance factor (K_d) is equal to the apparent diffusivity of the macromolecule within the gel (D) divided by the macromolecular free solution diffusivity (D_∞). The convective hindrance factor equals v_s/v, where v_s is the average velocity of the macromolecule due to bulk flow and v is the superficial fluid velocity. The relationship between the flux of a solute within a gel membrane and K_d and K_c is

$$\mathbf{N} = -K_d D_\infty \nabla C + K_c \mathbf{v} C \tag{1-4}$$

where C is the solute concentration averaged over the hydrogel on a scale that is large compared to the interfiber spacing, but small compared to the bulk gel sample. To express Eq. (1-4) in terms of the concentration of macromolecule in the external solutions, the macromolecular partition coefficient (Φ, macromolecular concentration inside the gel divided by that in the surrounding solution) must be used, as discussed below.

One way to describe the effects of molecular size on K_d, K_c, and Φ is to use hindered transport theories developed for membranes with long, regularly shaped (e.g., cylindrical) pores (Deen, 1987). Thus, a given gel might be viewed as having a certain effective pore size and pore number density. However, there is not a clear way to predict those pore parameters from actual compositional variables, such as the volume fraction of crosslinked polymer. Closer to reality are models that envision a gel as a network of polymeric fibers with fluid-filled interstices, similar to the concepts used in modeling Darcy permeability. In the three sections below, experimental measurements and fiber theories developed to predict macromolecular diffusion, partitioning, and convection are discussed.

1.2.2.1 Diffusion

Macromolecular diffusivities in hydrogels have been measured using a variety of methods, including fluorescence recovery after photobleaching (FRAP) (Hou et al., 1990; Jain et al., 1990; Moussaoui et al., 1992; Wattenbarger et al., 1992; Berk et al., 1993; Saltzman et al., 1994; Johnson et al., 1995; Johnson E. M. et al., 1996; Pluen et al., 1999), pulsed-field-gradient NMR (Gibbs et al., 1992), and holographic interferometry (Kosar and Phillips, 1995; Zhang et al., 1999; Gong et al., 2000). In general, K_d is found to decrease as molecular size and/or gel polymer concentration are increased.

In modeling diffusive hindrance in hydrogels, it is usually assumed that a single type of rigid, cylindrical fiber, of radius r_f, is arranged in either a random or spatially periodic array (Ogston, 1973; Phillips et al., 1989,1990; Clague and Phillips, 1996; Johnson E. M. et al., 1996; Amsden, 1998; Phillips, 2000). While structurally more realistic than a porous representation,

and sometimes quite accurate in predicting transport properties, the development of these models has been somewhat limited. One of the first models, proposed by Ogston (1973), is

$$K_d = \frac{D}{D_\infty} = \exp\left[-\left(\frac{r_s}{r_f} + 1\right)\sqrt{\phi}\right] \tag{1-5}$$

It is based on the probability that a spherical molecule of radius r_s could complete a step through a randomly oriented array of fibers.

Unfortunately, Eq. (1-5) neglects hydrodynamic effects on mobility. Phillips et al. (1989; 1990) were the first to account for solute-fiber hydrodynamic interactions. They compared rigorous results of generalized Taylor dispersion theory applied to lattices of bead-and-string type fibers with an "effective medium" approach. As opposed to the usual structurally detailed hydrodynamic models of fibrous membranes or gels, this effective medium model provided an alternative where the structure of the material is accounted for indirectly by employing a known value of the Darcy (or hydraulic) permeability, such as

$$F\left(\frac{r_s}{\sqrt{K}}\right) = \left[1 + \left(\frac{r_s}{\sqrt{K}}\right) + \frac{1}{9}\left(\frac{r_s}{\sqrt{K}}\right)^2\right]^{-1} \tag{1-6}$$

Phillips et al. (1989; 1990) asserted that $F \cong K_d$. In this type of model, the mobility of a diffusing macromolecule is related to the Darcy permeability by considering the drag on a sphere moving through a medium described by Brinkman's equation; larger Darcy permeabilities, which correspond to more open structures, yield greater mobilities.

Based on hydrodynamic arguments, Brady (1994) suggested that steric (S) and hydrodynamic (F) contributions to the diffusive hindrance factor were multiplicative. The steric factor, which is similar to an inverse tortuousity, is the relative diffusivity in the absence of hydrodynamic interactions between the fibers and the macromolecular solute. That is, it

describes the effect of excluding the center of a spherical solute molecule from a region of radius $r_f + r_s$ centered on any fiber.

Unfortunately, the most complete fiber matrix models, which include mobility as well as steric effects (Phillips et al., 1989,1990; Clague and Phillips, 1996; Johnson, E. M. et al., 1996; Phillips, 2000), apply only to the simplest structures. In particular, fiber arrays with two or more different radii (i.e., two-component gels) have been considered only in the context of water flow, as discussed above (Clague and Phillips, 1997). A major difficulty in modeling hindered diffusion is that hydrodynamic interactions in such systems are relatively long range. That is, the mobility of a diffusing macromolecule is affected by distant, as well as nearby, fibers. The need to consider many-body hydrodynamic interactions makes it challenging to model even one-component gels. However, the effective medium model, Eq. (1-6), which has been used (alone or coupled with a steric factor) previously to predict diffusive hindrances in media composed of a single fiber type (Phillips et al., 1989; Brady, 1994; Kosar and Phillips, 1995; Johnson, E. M. et al., 1996; Kapur et al., 1997), could be more generally applicable. In principle, this way of linking diffusivities to water flow data might be useful for predicting or correlating diffusivities in complex, multicomponent gels, provided that the Darcy permeability can be measured. Such data are available for certain synthetic or biological gels (e.g., Johnson, E. M. et al., 1996; Kapur et al, 1997; Bolton et al., 1998; White and Deen, 2002).

1.2.2.2 Partitioning

One of the quantities needed to characterize the permeation of solute i through a hydrogel is the equilibrium partition coefficient (Φ_i), which is the concentration of i within the gel ($\overline{C}_i$) divided by that in the surrounding bulk solution (C_i). That is, with the gel and solution at equilibrium,

$$\Phi_i = \frac{\overline{C}_i}{C_i} \tag{1-7}$$

where $\overline{C_i}$ is based on the total gel volume, including solids. Of particular interest for separations, drug delivery, and the analysis of physiological processes is how Φ_i for a macromolecular solute will be influenced by its size, charge, and bulk concentration, and by the composition and physical arrangement of the gel.

Beginning with the pioneering work of Ogston (1958), equilibrium partitioning of macromolecules in gels has typically been modeled by representing the crosslinked polymers as randomly positioned and oriented fibers, similar to the approaches for κ and K_d. For a dilute solution of spherical solutes i with radius r_i partitioning into a random array of long fibers of radius r_f, Ogston (1958) showed that

$$\Phi_i = \exp\left[-\phi\left(1+\frac{r_i}{r_f}\right)^2\right] \tag{1-8}$$

In these fiber matrix models, the fibers are generally treated as rigid rods. Usually, a single fiber radius has been employed, implying a single type of gel polymer. When long-range (e.g., electrostatic) forces are negligible and steric interactions are dominant, theoretical results for single-fiber arrays are available for various situations, including dilute solutions of spheres (Ogston, 1958), concentrated solutions of spheres (Fanti and Glandt, 1990a; 1990b), and dilute or concentrated solutions of spheroids (Lazzara et al., 2000) or random coils (White and Deen, 2000; 2001). For spheres, electrostatic interactions have also been considered (Johnson and Deen, 1996a; Buck et al., 2001).

Agarose gels, in bead or sheet form, have been an attractive system for testing these partitioning models (e.g., White and Deen, 2000; Laurent, 1967; Lazzara and Deen, 2004). In particular, it was found recently that Φ_i for BSA and several sizes of Ficoll in agarose gels closely followed the predictions of an excluded volume theory, for both dilute and concentrated solutions, when agarose was modeled as a fiber matrix with a uniform radius of 1.6 nm (Lazzara and Deen, 2004). Ficoll, a crosslinked copolymer of sucrose and epichlorohydrin, was chosen as

a test solute because it appears to behave much like a neutral, rigid sphere (Bohrer et al., 1984; Davidson and Deen, 1988).

Composite gels (i.e., ones that contain two or more types of crosslinked polymers) have received much less attention in partitioning studies than single-component gels, despite their biological importance and possible technological interest. Recently, a model was developed to describe partitioning of one or more solutes, with varying size and shape, in mono-, bi-, or polydisperse fibrous or porous media (Lazzara et al., 2000). Partition coefficients are determined by summing the excluded volumes of the confined phase (e.g., fibers) and the bulk phase (e.g., solute solution). Only steric factors are included and the model assumes that both the solutes and fibers are rigid. The excluded volume approach facilitates modeling non-spherical solutes, multiple solute mixtures, and fibrous mixtures in a single model.

1.2.2.3 Convection

Sieving coefficients, which can be measured via ultrafiltration, are a convenient measure of convective hindrance, especially when diffusion is negligible. The sieving coefficient (Θ) is the ratio of the downstream to upstream macromolecular solution concentrations (C_L and C_0, respectively),

$$\Theta = \frac{C_L}{C_0} \tag{1-9}$$

These external solution concentrations are related to the corresponding concentrations inside the gel by the partition coefficient. As long as the solutions are dilute, the partition coefficients at the upstream and downstream surfaces of the membrane will be equal.

The expression for macromolecular flux, Eq. (1-4), can be solved for the concentration profile within the gel during steady or pseudo-steady state sieving using ΦC_0 as a boundary condition at the upstream surface of the membrane. Flux matching at the downstream surface allows the flux to be quantified as

$$N = vC_L \tag{1-10}$$

Evaluating the concentration profile at the downstream surface of the membrane allows the sieving coefficient through a membrane with thickness L to be determined by

$$\Theta = \frac{\Phi K_c}{1-(1-\Phi K_c)\exp(-Pe)} \tag{1-11}$$

where

$$Pe = \frac{(\Phi K_c)vL}{(\Phi K_d)D_\infty} \tag{1-12}$$

At the two flow extremes, where Pe << 1 or Pe >> 1, diffusion or convection dominates so Eq. (1-11) can be simplified to

$$\Theta = 1 \qquad (\text{Pe} << 1) \tag{1-13}$$

or

$$\Theta = \Phi K_c \qquad (\text{Pe} >> 1) \tag{1-14}$$

respectively.

Most of the experimental findings and theoretical models that have been developed for random fiber matrices relate to Darcy permeability, diffusion, or partitioning, as discussed in detail above. Measurement and modeling of convective hindrance have received much less attention. Kapur et al. (1997) studied hindered convection in membranes with pores filled with polyacrylamide via sieving experiments performed in the regime where diffusion is negligible. Johnston and Deen (1999; 2002) determined K_c in agarose gels, supported by a polyester mesh, and accounted for both diffusion and convection during sieving. The only model for K_c that has been developed specifically for fibrous media is based on perpendicular flow through arrays of

identical parallel fibers (Phillips et al., 1989; 1990). However, an expression developed by Anderson and Malone (1974) for the osmotic reflection coefficient (σ_o) of neutral spherical solutes in cylindrical pores has been applied by Curry and Michel (1980) to predict the convective reflection coefficient for fibrous media. Anderson and Malone's (1974) expression, which is based on the partition coefficient (Φ), is given by

$$\sigma_o = (1-\Phi)^2 \tag{1-15}$$

Anderson (1981) showed Eq. (1-15) to be a good approximation of the osmotic reflection coefficient of spherical and non-spherical solutes in rectangular pores as well. He also found that the convective reflection coefficient was approximately equal to the osmotic reflection coefficient under the conditions studied. As a result of its applicability to a wide variety of solute and pore shapes, Curry and Michel (1980) speculated that Eq. (1-15) could also be applied to fibrous media.

1.3 Transport in a Biological Hydrogel, the Glomerular Basement Membrane (GBM)

1.3.1 Overview

Blood exiting the heart is fed to the kidneys via arteries and arterioles until it reaches tiny capillary tufts known as glomeruli. Each glomerulus is a biological ultrafilter that filters large amounts of plasma in the initial stage of urine formation, while retaining proteins within the bloodstream. The glomerular capillary wall has three main layers; namely, the endothelium, the glomerular basement membrane (GBM), and the epithelium. Flow from the capillary lumen first passes through the fenestrae in the endothelium, followed by the GBM fiber matrix, and finally exits into Bowman's space through the slit diaphragms between the foot processes of epithelial

cells. A recent article by Deen et al. (2001) reviews the key experimental and theoretical developments that have helped better define the structure of the glomerular capillaries.

Drumond and Deen (1994) developed a hydrodynamic model to determine the relative contribution of each capillary wall layer to the overall hydraulic permeability. The individual hydraulic permeabilities of the cellular layers and the GBM are additive, according to resistances in series. That is,

$$\frac{1}{k} = \frac{1}{k_{en}} + \frac{1}{k_{bm}} + \frac{1}{k_{ep}} \tag{1-16}$$

where the effective hydraulic permeability of layer i is given by k_i (*en* stands for endothelium, *bm* for basement membrane, and *ep* for epithelium). Flow resistances in both the endothelial fenestrae and through the epithelial filtration slits were determined via finite element solutions to Stokes' equation based on a unit cell that included one filtration slit and several endothelial fenestrae. The pertinent microstructural parameters of the glomerular capillary wall were estimated from morphometric studies in rats. Due to the microstructural complexity of the GBM, its hydraulic resistance was determined based on measurements of its Darcy permeability in isolated, compacted GBM (Robinson and Walton, 1989; Daniels et al., 1992; Walton et al., 1992; Edwards et al., 1997b, Bolton et al., 1998), as discussed below. Based on this analysis, Drumond and Deen (1994) concluded that the GBM and epithelial slit diaphragms each contribute about half of the overall glomerular capillary wall resistance to water flow.

As with hydraulic permeabilities, the concept of resistances in series can also be used to relate diffusive permeabilities,

$$\frac{1}{p} = \frac{1}{p_{en}} + \frac{1}{p_{bm}} + \frac{1}{p_{ep}} = \frac{1}{p_{bm}} + \frac{1}{p_{cell}} \tag{1-17}$$

where p_i is the diffusional permeability of the ith layer. Due to experimental limitations, the endothelial and epithelial diffusional resistances have been grouped together as $1/p_{cell}$. Using a confocal microscopy technique, the diffusive permeability can be measured in a single capillary loop of isolated basement membrane or intact glomerular capillary wall, p_{bm} and p, respectively (Daniels et al., 1993; Edwards et al., 1997a). Based on a comparison of these diffusional permeabilities, Edwards et al., (1997a) found that the cellular components are responsible for the majority of the diffusional resistance and they hypothesized that the slit diaphragm between the epithelial podocytes is the most resistant layer. However, the GBM was found to contribute about 13 - 26% of the diffusional resistance of the glomerular capillary wall, depending on the size of the diffusing macromolecule (Edwards et al., 1997a).

While hydraulic and diffusive permeability resistances are additive, the local sieving coefficient at any point along the glomerular capillary wall is based on the multiplicative effects of each layer. That is,

$$\Theta = \Theta_{en}\Theta_{bm}\Theta_{ep} \tag{1-18}$$

where Θ_i is the sieving coefficient for the ith layer. A completely selective layer will be characterized by $\Theta_i = 0$, while a completely nonselective layer will have $\Theta_i = 1$. Note that the sieving coefficient of each layer is dependent on the other, so they cannot be computed separately. As pointed out by Deen et al. (2001), due to the multiplicative relationship, regardless of the selectivity of an individual layer of the capillary wall, a change in Θ_i will effect Θ by the same percentage as it effects Θ_i. Note that Equation (1-18) is only valid locally since the plasma protein concentration increases as the blood travels through the glomerular capillary, which will change the values of the individual and overall sieving coefficients. The sieving coefficients will also be affected by the filtrate velocity. Eq. (1-18) is approximate since it does not include the effects of soluble proteins on macromolecular equilibrium partitioning (Lazzara and Deen, 2001). An estimate of the sieving coefficient in the GBM can be computed (in terms

of the epithelial sieving coefficient) by regarding it as a random fibrous media with one-dimensional flux given by Eq. (1-4) and following reasoning similar to that used in section 1.2.2.3 to derive the sieving coefficient of a fibrous gel (Edwards et al., 1999). As Θ_{ep} increases from 0 to 1, Θ_{bm} is predicted to vary from slightly greater than one (due to concentration polarization effects) to significantly less than one (Deen et al., 2001).

Since the GBM is made primarily of water and contains collagen, proteoglycans, and other fiber arrays, it is a biological hydrogel in which transport is characterized by the same parameters as detailed in section 1.2 for hydrogels in general. Due to its importance in both hydraulic and macromolecular permeability, as detailed above, the GBM is of particular interest in this study. Consequently, experiments with isolated GBM will be reviewed in section 1.3.2, followed by an attempt to account for these experimental measurements via fiber matrix theories in section 1.3.3. The chapter ends with an examination of synthetic agarose-dextran gels as possible analogs to the GBM in section 1.3.4.

1.3.2 Experimental Characterization of Isolated GBM

The 7 – 10% of the GBM that is not water (Robinson and Walton, 1987; Comper et al., 1993) consists of collagen IV, laminin, entactin, heparan sulfate proteoglycan, and fibronectin (Laurie et al., 1984). The negative charges abundant in heparan sulfate and other GBM proteoglycans contribute heavily to the overall negative charge of the GBM (Yurchenco and O'Rear, 1993). Numerous experimental investigations have sought to uncover the size and charge selectivity of the GBM relative to the two cellular layers surrounding it in the glomerular capillary wall (Robinson and Walton, 1989; Daniels et al., 1992; Walton et al., 1992; Daniels et al., 1993; Edwards et al., 1997a; Edwards et al., 1997b; Bolton et al., 1998). The use of dextran and various proteins, representative of those in the blood stream, as tracers to test macromolecular diffusion and permeability (Robinson and Walton, 1989; Daniels et al., 1992; Walton et al., 1992; Daniels et al., 1993) has recently been replaced by Ficoll (Edwards et al., 1997a; Edwards et al., 1997a; Bolton et al., 1998). Ficoll is a cross-linked copolymer of sucrose

and epichlorohydrin that is ideal for macromolecular permeability studies since it behaves like a neutral, rigid sphere (Davidson and Deen, 1988).

In order to study the permeability of the GBM, the cellular layers are commonly removed by detergent lysis (Ligler and Robinson, 1977; Daniels et al., 1992). After lysis, the isolated GBM retains much of its in vivo structure, which allows diffusion of fluorescently labeled macromolecules through the acellular capillary to be monitored by confocal microscopy (Edwards et al., 1997a). Alternatively, hydraulic and macromolecular permeabilities of isolated GBM can be measured by ultrafiltration though a homogeneous, compacted layer of the isolated GBM. Representative experimental measurements of the Darcy permeability of isolated GBM include 0.82 nm^2 (Edwards et al., 1997b), 1.15 nm^2 (Bolton et al., 1998), and 1.62 nm^2 (Robinson and Walton, 1989). Figure 1.1 shows ΦK_d and ΦK_c from these in vitro measurements of isolated GBM as a function of macromolecular Stokes radius.

Since many proteins and the GBM are negatively charged, Bolton et al. (1998) examined the charge selectivity of isolated, compacted GBM using Ficoll and Ficoll sulfate. At physiological conditions, it appears that the electrostatic interactions are screened well enough to dampen any noticeable charge selectivity within the GBM (Bolton et al., 1998).

1.3.3 Theoretical Reconciliation of GBM Transport Properties with GBM Structure

If the GBM is assumed to be composed solely of thick collagen fibers, the fiber matrix theories can only be used to predict Darcy and macromolecular permeabilities if an unrealistic volume fraction of fibers is used. Assuming the GBM is made entirely of fine fibers, the fiber matrix models work roughly well at predicting GBM Darcy permeabilities, but they fail miserably at predicting macromolecular permeabilities. Accounting for only fine fibers, the fiber matrix theories predict ratios of K_c to K_d that exceed 1000 (Bolton and Deen, 2001) which is unreasonable considering that K_c and K_d have been shown to be of about the same order of magnitude (Johnson, E. M. et al., 1996; Johnston and Deen, 1999; 2002). However, if the GBM

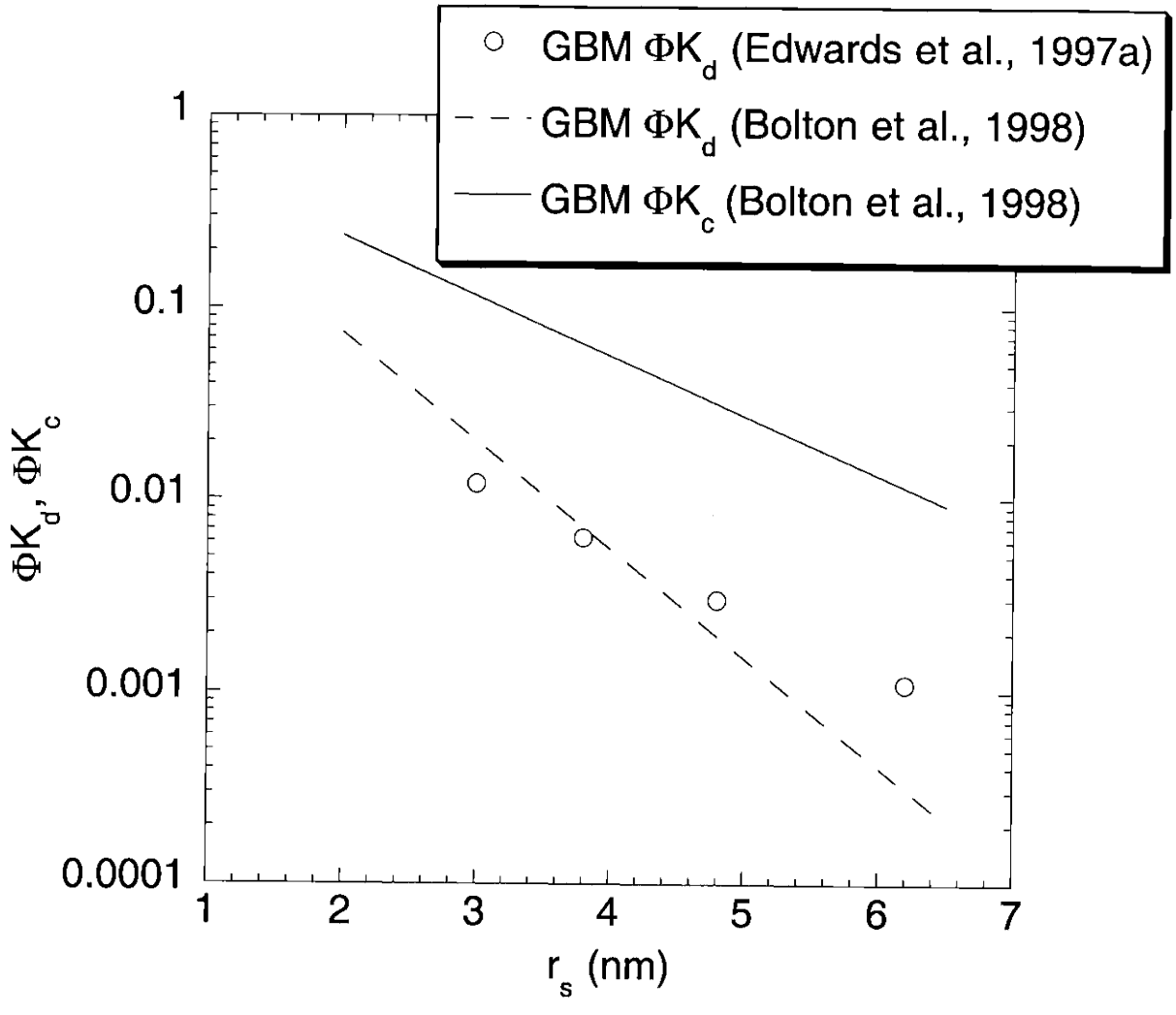

Figure 1.1 Diffusive (ΦK_d) and convective (ΦK_c) permeabilities for Ficoll in GBM as a function of Stokes radius (r_s). The GBM results are based either on confocal microscopy measurements of Ficoll diffusion across segments of cell-free capillary wall (Edwards et al., 1997a) or Ficoll sieving across filters prepared from isolated GBM (Bolton et al., 1998).

is modeled as a two-fiber gel comprised of coarse collagen fibers and fine glycosaminoglycan fibers, predicted Darcy permeabilities are similar to those measured in isolated GBM as long as ratio of the fine fiber volume fraction to the total fiber volume fraction is at least 0.4 (Bolton and Deen, 2001). Therefore, fibers of at least two different sizes are needed to represent the GBM. Since the GBM is composed of thick collagen IV fibers and thinner proteoglycan components (Laurie et al., 1984), which differ by an order of magnitude in radii (Yurchenco and O'Rear, 1993; Dea et al., 1973), it is not surprising that theories accounting for fibers of only one size do not well represent the GBM.

1.3.4 Synthetic Agarose-Dextran Composite Gels as Analogs to the GBM

In an experimental bimodal fiber membrane study, a synthetic membrane composed of crosslinked, thick agarose fibers and thin dextran fibers was used by White and Deen (2002) as an experimental model of the GBM. Agarose is ideal for fiber matrix studies because its Brownian motion is undetectable (Mackie et al., 1978) and it has little net charge. This neutral polysaccharide forms double helices in solution which aggregate into similarly sized fibers upon gelling (Arnott et al., 1974). Since agarose fibers range from 2 to 30 nm in diameter (Dormay and Candau, 1991; Belton et al., 1988), which about equals the 3 to 10 nm diameter of collagen fibers in the GBM (Farquar, 1981), experimental studies using agarose hydrogels are of particular interest. Similarly, the long, flexible dextran polymer chains with radii of 0.3 to 0.7 nm (Laurent and Killander, 1964), will approximate the proteoglycan components of the GBM, which have radii of about 0.5 nm (Dea et al., 1973). Since neither agarose nor dextran is charged, the synthetic GBM will be neutral, which is in contrast to the GBM in vivo that contains fixed negative charges (Bolton et al., 1998). However, a neutral model of the GBM is valid because at physiological ionic strength, electronic interactions are screened well enough to dampen any noticeable charge selectivity within the GBM (Bolton et al., 1998). White and Deen (2002) have measured Darcy permeabilities similar to those measured in the GBM in vitro using

their crosslinked agarose-dextran synthetic GBM, with similar total volume fraction to that in the GBM.

1.4 Thesis Overview

The ultimate goal of this research was to develop a greater understanding of the structural components needed to describe transport within GBM. As discussed above, two-fiber theories for hindered transport are inadequate and investigation of the actual GBM is limited. Consequently, experimentation with synthetic gels similar to the agarose-dextran composites that had such success in replicating in vitro Darcy permeabilities was undertaken. Dimensionless diffusive and convective hindrance factors were investigated by measuring macromolecular permeability through these synthetic, two-fiber, agarose-dextran hydrogels at very small or very high Peclet number, as is discussed in chapters 2 and 4, respectively. By comparing diffusion and convection in the synthetic hydrogel with corresponding measurements in isolated rat GBM, further insight regarding the structure responsible for transport through the GBM is gained. In order to compare diffusive hindrances in the synthetic gels with those in isolated GBM, partitioning in agarose-dextran hydrogels was also examined, as detailed in chapter 3. Additionally, available hindered transport theories were tested.

The work presented in chapter 2 has been accepted for publication in the *AIChE Journal*. The *Journal of Colloid and Interface Science* has accepted a manuscript based on the findings detailed in chapter 3. A manuscript based on chapter 4 is currently under development and will be submitted to the *Journal of Membrane Science*.

2 Diffusivities of Macromolecules in Composite Hydrogels

2.1 Introduction

In the work reported here, macromolecular diffusivities and Darcy permeabilities were measured in agarose-dextran composite gels of varying composition, and the utility of various fiber matrix models was examined. This data was meant to complement previous Darcy permeability measurements in similar gels that were consistent with in vitro GBM Darcy permeability and morphology (White and Deen, 2002). This study also provides information on hindered diffusion in more complex systems than those that are more commonly studied.

2.2 Materials and Methods

2.2.1 Gel Preparation

The gel synthesis procedure was similar to that used previously (White and Deen, 2002). Agarose (Type IV; Sigma, St. Louis, MO) was suspended in KCl-phosphate buffer (0.1 M KCl and 0.01 M sodium phosphate at pH 7.0) and heated in a 90°C oven for 4-6 h until it was completely dissolved. The hot agarose solution was poured carefully onto a 2.5 cm diameter woven polyester support (catalog #148 248; Spectrum Laboratories Inc., Rancho Dominguez, CA) that was placed on a heated glass plate. The mesh fibers in the support formed square openings of 43 μm and had a thickness of 70 μm, with 29% open area. After placing a second hot glass plate on top, the sample was cooled to room temperature and immersed in buffer overnight at 7°C. The gels to which dextran was to be added were immersed in 500 kDa dextran (Sigma, St. Louis, MO) solutions of either 50 or 150 mg/mL for at least 24 h, which greatly exceeds the diffusional equilibration time calculated from reported diffusivities for dextran in agarose (Key and Sellen, 1982). A 2 Mrad exposure to an electron beam (High Voltage Research Laboratory at Massachusetts Institute of Technology) was used to covalently link the dextran to the agarose. Following irradiation, each gel was equilibrated with a large volume of

buffer (2 mL, as compared to a typical gel volume of 0.025 mL) to remove free dextran. The agarose concentrations of 4.1 and 8.2% (w/v) were converted to volume fractions (ϕ_a) by dividing by 1.025 (Johnson et al., 1995); that is, $\phi_a = 0.040$ or 0.080. The volume fractions of immobilized dextran (ϕ_d), determined as described below, ranged from 0.0008 to 0.011. Samples used for water filtration and diffusion measurements underwent identical treatment, except that the diffusion samples did not require a polyester support. For every filtration sample, a diffusion sample was made from the same batch of gel.

2.2.2 Gel Dextran Concentration

The concentration of dextran incorporated into a given agarose gel was obtained by determining both the equilibrium partition coefficient and the fraction immobilized by the electron beam. The partition coefficient (Φ) is the concentration of free dextran in an untreated gel (based on total gel volume) divided by that in the external solution, at equilibrium. The fraction of the free dextran in the gel that was subsequently immobilized is denoted as η. To measure those quantities, 1.5 cm diameter disks were cut from agarose sheets prepared as described above. The thickness of each sample was measured using a micrometer, with the gel placed between two microslides of known thickness, allowing its volume ($V_g \cong 0.03$ mL) to be determined. The gel samples were equilibrated first with a large volume (2.5 mL) of 50 or 150 mg/mL dextran solution. Some were then irradiated and some left untreated. After thorough rinsing, each was equilibrated with a large volume (2.5 mL) of buffer and the final dextran concentration in the solution determined using a phenol sulfuric acid assay (Dubois et al., 1956). The large volume of solution used in each equilibration (V_0) made the mass of dextran in the gel negligible in each case. Accordingly, mass balances for each step yield

$$\Phi = \frac{C_u V_0}{C_0 V_g} \tag{2-1}$$

$$\eta = 1 - \frac{C_t}{C_u} \tag{2-2}$$

where C_0 is the dextran concentration in the initial solution, C_u the final concentration for untreated gels, and C_t the final concentration for treated (irradiated) gels, each in mass units. It follows that the volume fraction of immobilized dextran is

$$\phi_d = \eta \Phi C_0 \hat{V}_d \tag{2-3}$$

where the specific volume of dextran is $\hat{V}_d = 0.61$ mL/g (Bohrer et al., 1979).

2.2.3 Darcy Permeability

The Darcy permeability (κ) of each mesh-reinforced gel was measured as described previously (Johnson and Deen, 1996b; Johnston and Deen, 1999; White and Deen, 2002). The gel membrane was placed in a 3 mL ultrafiltration cell (Millipore, Bedford, MA) that was filled with the KCl-phosphate buffer and pressurized to 20 kPa using nitrogen. Samples of filtrate collected over timed intervals were weighed to determine the volume flow rate (Q). The gel thickness (δ), measured by confining the membrane between two microscope slides of known thickness and using a micrometer, ranged from 70 to 140 μm. From these measurements, κ was calculated as

$$\kappa = \frac{\mu Q \delta}{\beta A \Delta P} \tag{2-4}$$

where μ is the viscosity of water, A is the exposed membrane area, ΔP is the pressure drop, and β is a correction factor that accounts for the increased flow resistance due to the polyester mesh support. That factor, which increases with δ (Johnson and Deen, 1996b), ranged from 0.41 to 0.60 in these experiments.

2.2.4 Test Macromolecules

Fluorescein-labeled ovalbumin and BSA from Molecular Probes (Eugene, OR) were used without further purification. Narrow fractions of Ficoll were special-ordered from Pharmacia LKB (Piscataway, NJ). The three Ficoll fractions had weight-average molecular weights (M_W) of 21, 61, and 105 kDa. Based on information from the manufacturer, the polydispersity index (M_W/M_N, where M_N is number-average molecular weight) was 1.22, 1.15, and 1.13, respectively. The Ficolls were labeled using dichlorotryazinyl amino fluorescein (DTAF) (Sigma, St. Louis, MO) according to the method of De Belder and Granath (1973). The unreacted DTAF was removed using desalting chromatography columns (Bio-Rad, Hercules, CA) before the desired product was freeze-dried.

The properties of the five test macromolecules are given in Table 2.1. All diffusivities shown (D_∞) are those measured by us in bulk solution using FRAP, as discussed below. The Stokes-Einstein radius (r_s) for each major component was calculated from D_∞ using

$$r_s = \frac{k_B T}{6\pi\mu D_\infty} \tag{2-5}$$

where k_B is Boltzmann's constant and T is absolute temperature. Size-exclusion chromatography using Superdex 200 (Pharmacia Biotech, Piscataway, NJ) and 0.1 M PBS at pH 7.4 as eluent was used to estimate the fractional fluorescence attributable to either high or low molecular weight contaminants, which were interpreted as protein dimers or free fluorescein, respectively. The column was calibrated using macromolecules of known r_s, including 4 narrow fractions of Ficoll and a fluorescently labeled 2,000 kDa dextran. The limit of detection for either dimers or free fluorescein was about 1%. Hence, entries of "<0.01" in Table 2.1 correspond to nondetectable contaminants. Dimers were present in both protein samples, most prominently with BSA (16% of total fluorescence). The values of r_s shown for the dimers in Table 2.1 were estimated from

Table 2.1 Properties of Test Molecules. Diffusion coefficients, corrected to 20°C, are given as a mean ± standard error as detailed in the text. For the proteins and Ficolls, 4-6 samples were measured, while 2 samples were measured for DTAF.

Macromolecule	M_w	$D_{20,w}$ (10^{-7} cm^2/s) (monomer)	r_s (nm) (monomer)	r_s (nm) (dimer)	Dimer Fraction	Fluorescein Fraction
Ovalbumin	45,000	7.68 ± 0.17	2.8	4.1	0.05	<0.01
BSA	68,000	6.20 ± 0.12	3.5	5.0	0.16	0.05
Ficoll 21K	21,300	7.96 ± 0.35	2.7	--	<0.01	<0.01
Ficoll 61K	60,700	4.81 ± 0.09	4.5	--	<0.01	<0.01
Ficoll 105K	105,000	3.64 ± 0.05	5.9	--	<0.01	<0.01
DTAF	532	38.3 ± 1.4	0.6	--	--	--

their column elution times. Free fluorescein was detectable only in the BSA sample. The effects of these impurities on the diffusion measurements were generally small, as will be discussed.[1]

2.2.5 FRAP Diffusion Experiments

Image-based FRAP (Tsay and Jacobson, 1991; Berk et al., 1993) was used to determine the diffusion coefficients of the test macromolecules in the gels and in bulk solution. The FRAP system assembled for this purpose is shown schematically in Fig. 2.1. An argon-ion laser (LS 300; American Laser, Salt Lake City, UT), emitting visible light at 488 nm in TEM00 mode was used to irreversibly bleach the fluorescently labeled macromolecules. The laser light was split into two beams, one of which was attenuated by a plano-concave lens and the other concentrated by a plano-convex lens. By moving the latter, the diameter of the concentrated (bleaching) beam at the sample could be varied; that diameter was roughly 300 μm. Electronic shutters (Uniblitz, Rochester, NY) located in each beam path controlled the type of illumination that reached the sample and the exposure time. A dichroic mirror (505 nm; Omega Optical, Brattleboro, VT) reflected the laser light onto the sample, but transmitted the fluorescent emission, which was imaged by a CCD camera (Cohu, San Diego, CA) fitted with a 4x microscope objective (N.A. 0.11) and a 15x eyepiece. Images, digitized using a frame grabber (IMAQ-PCI 1409; National Instruments, Austin, TX), could be taken at a maximum rate of 30 s^{-1}. A series of images taken at time steps ranging from 1 to 60 s, depending on the diffusivity of the macromolecule (i.e., the time scale for fluorescence recovery), was analyzed to determine each diffusivity. At each time step, 5 images were taken in succession and averaged. From the original 640 by 780 pixels, a region 175 by 175 pixels centered on the bleached spot was saved for analysis. The spatial sampling rate, or distance between pixels, in either the horizontal or vertical direction was 3.8 μm, as measured by imaging a micrometer scale. The experiments were controlled and analysis done using Labview (National Instruments, Austin, TX) software. Diffusivities were measured at room temperature (22-28°C) and adjusted to 20°C by assuming that they vary as T/μ (Eq. 2-5).

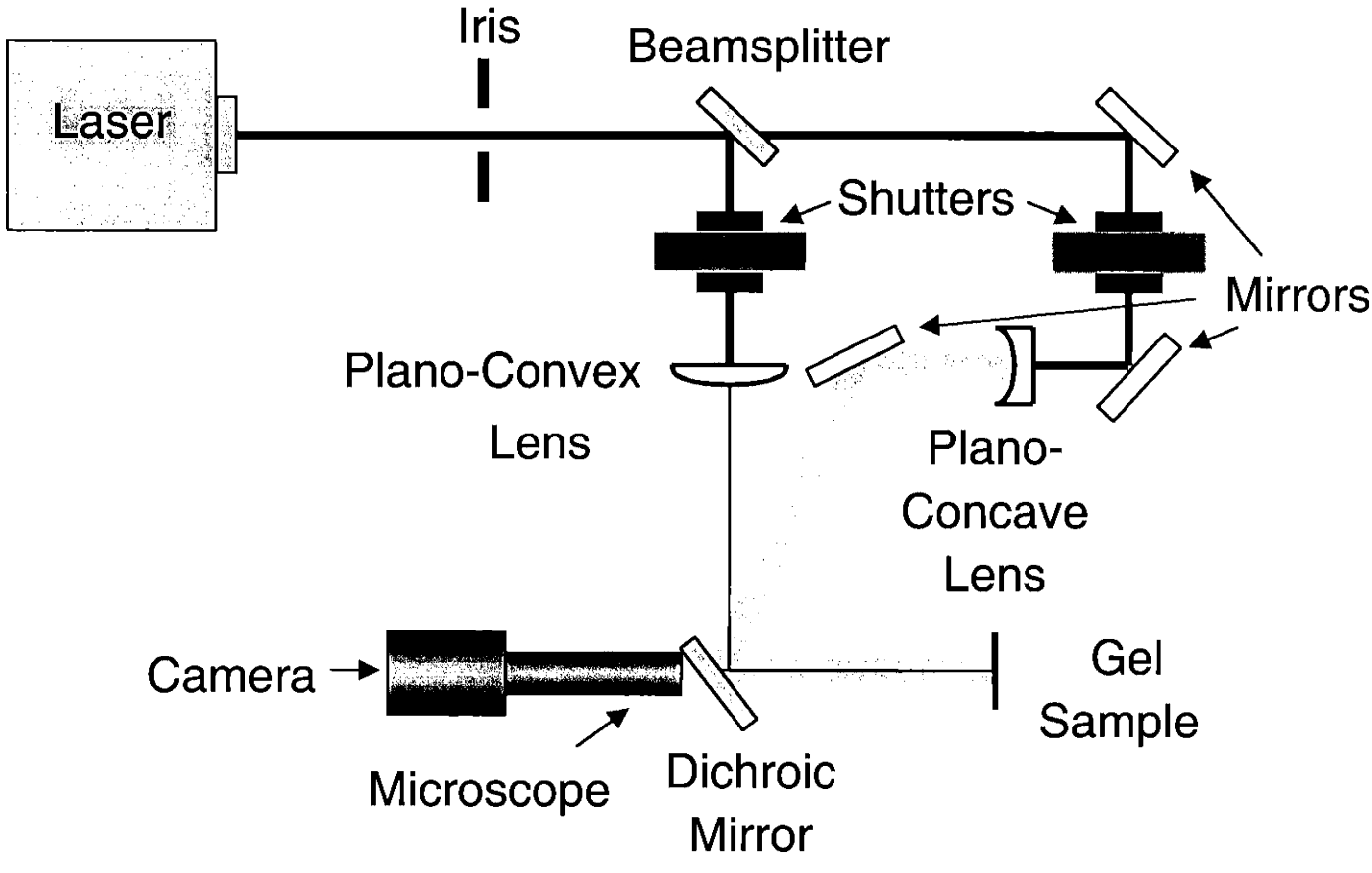

Figure 2.1 Schematic of FRAP system used to measure diffusivities. A 488 nm beam from an argon-ion laser was split into two beams, one of which was attenuated by a plano-concave lens and the other concentrated by a plano-convex lens. The 505 nm dichroic mirror reflected the 488 nm bleaching or attenuated laser beam onto the sample, while allowing the ~515 nm fluorescence emission to reach the camera.

Protein and Ficoll solutions were prepared by dissolving the test macromolecule in the KCl-phosphate buffer. The macromolecule concentrations ranged from 4 to 6 mg/mL, depending on the amount of fluorescence needed. The volume fraction of test macromolecules varied from 0.005 to 0.029, indicating that all solutions were dilute. To prepare for the FRAP measurements, the gel samples were first equilibrated with the fluorescent macromolecule solutions. The gels were then rinsed with buffer and placed between two glass slides with anti-reflection coatings (Edmund Industrial Optics, Barrington, NJ). Hematoseal (Fisher Scientific, Pittsburgh, PA) tube sealing compound was applied to the edges to prevent evaporation. For a given solution or gel sample, measurements were repeated 3 times at different locations. Diffusion coefficients were measured for each macromolecule in 4 to 8 gel samples with the same nominal agarose and dextran volume fractions. Gel and free-solution diffusivities were also determined for DTAF, which was assumed to be representative of any low-molecular-weight impurities.

2.2.6 FRAP Data Analysis

The diffusion coefficients were computed using spatial Fourier analysis of the digitized images (Tsay and Jacobson, 1991; Berk et al., 1993; Johnson, M. E. et. al., 1996). To allow for fluorescent impurities in the protein samples, as many as three components with differing diffusivities were considered. For three components, the transformed fluorescence intensity, relative to that before bleaching, is given by

$$f(t) \equiv \frac{\tilde{I}(u,v,t)}{\tilde{I}(u,v,0)} = (1-x_2-x_3)\exp(-4\pi^2(u^2+v^2)tD_1) + x_2\exp(-4\pi^2(u^2+v^2)tD_2) + x_3\exp(-4\pi^2(u^2+v^2)tD_3) \quad (2\text{-}6)$$

where x_i is the fraction of the fluorescence due to component i, D_i is the diffusivity of i, t is time, and u and v are spatial frequencies. The fluorescence fraction (x_i) is proportional to the number

concentration of i times the fluorescence per molecule. Setting one or two of the fluorescence fractions to zero reduces Eq. (2-6) to the form used for two components or one component, respectively. For a specified number of components, the diffusivity data were fitted to Eq. (2-6) (or its analogs) using the Levenburg-Marquardt routine (Labview; National Instruments, Austin, TX). A restriction that $f(t) \geq 0.38$ was applied to ensure that the edges of the Gaussian fluorescence profile were not cut off at any time during the fluorescence recovery (Berk et al., 1993). The eight lowest frequency pairs (u, v) following (0, 0), which produced similar recovery profiles with minimal noise, were the ones used to determine the diffusion coefficients. If the data from any one frequency pair had an absolute mean square error that was at least twice the average for all pairs, it was discarded.

For measurements in free solution, each protein diffusivity (D_∞) was first calculated using the contaminant fractions obtained from size-exclusion chromatography (Table 2.1). So that the diffusivity of the predominant component (protein monomer) would be the only fitted parameter, D_∞ of the dimer was estimated from its chromatographic radius. The D_∞ of free fluorescein was assumed to equal that measured for DTAF (Table 2.1). Usually, a fit based on a single diffusing species was practically indistinguishable from ones that included two or three components. If the difference in D_∞ was < 2.5%, the single species fit was used. The exception was BSA, where D_∞ was calculated by including all three components detected by chromatography.

Steric exclusion of molecules by the gels during the initial equilibration with the test solution would have reduced the relative amounts of dimer in the gel and increased the relative amounts of free fluorescein. These effects would be greatest for the most concentrated gels. It follows that if dimer fractions were small enough to be neglected in free solution diffusivity measurements, then they could be safely neglected in analyzing any gel data. However, free fluorescein effects (if any) would be amplified. Thus, the quality of single-component fits to the FRAP data was expected to deteriorate as molecular size and/or gel concentration was increased. An example of this phenomenon is shown in Fig. 2.2, in which fluorescence intensities for the largest Ficoll in 8.0% agarose are plotted as suggested by Eq. (2-6). In Fig.

2.2a, which shows results both for pure agarose and for free solution, the single-component fits were excellent. However, in Fig. 2.2b, which compares results for free solution with those for a more restrictive gel (dextran added to 8.0% agarose), the error in the single-component fit to the latter is unacceptable. As shown by the additional curve, the fit in Fig. 2.2b was improved greatly by including free fluorescein as a second component, with the diffusivity of free fluorescein estimated from that measured for DTAF at that gel composition. The one additional degree of freedom in the two-component fit was the fractional fluorescence due to free fluorescein, which was found to be 0.12 in this case. In general, when free fluorescein had to be invoked in fitting the FRAP data, the fluorescence fractions obtained were < 0.15. A free-fluorescein fraction of < 0.01 in bulk solution (the limit of detection by chromatography) would become 0.15 in the gel if the partition coefficient of the test macromolecule were < 0.067 times that of free fluorescein, which is quite reasonable for a concentrated gel. In other words, there was no inconsistency in fitting gel data with two components and free solution data with one component.

An analysis of the free solution data indicated that, in general, unbound fluorescein could be accurately distinguished (giving fluorescein fractions in accord with the chromatographic estimates) only if the macromolecule diffusivity was no more than 5% that of free fluorescein (as estimated using DTAF). When that criterion was met in a gel, a two-component fit (as in Fig. 2.2b) was considered to be an acceptable way to reduce the error. Otherwise, one-component fits were generally employed (as in Fig. 2.2a), and usually exhibited no more error than two-component fits. In the exceptional case of BSA, where three components were needed to accurately fit the free solution data, the gel fits were also based on three components.

In general, the variability between samples was larger than that among the 3 replicate measurements for each sample, so the standard error was computed based on the number of samples. When only 2 samples were examined, the error measure used was one-half of the difference between the two samples, plus the average standard error of the replicates.

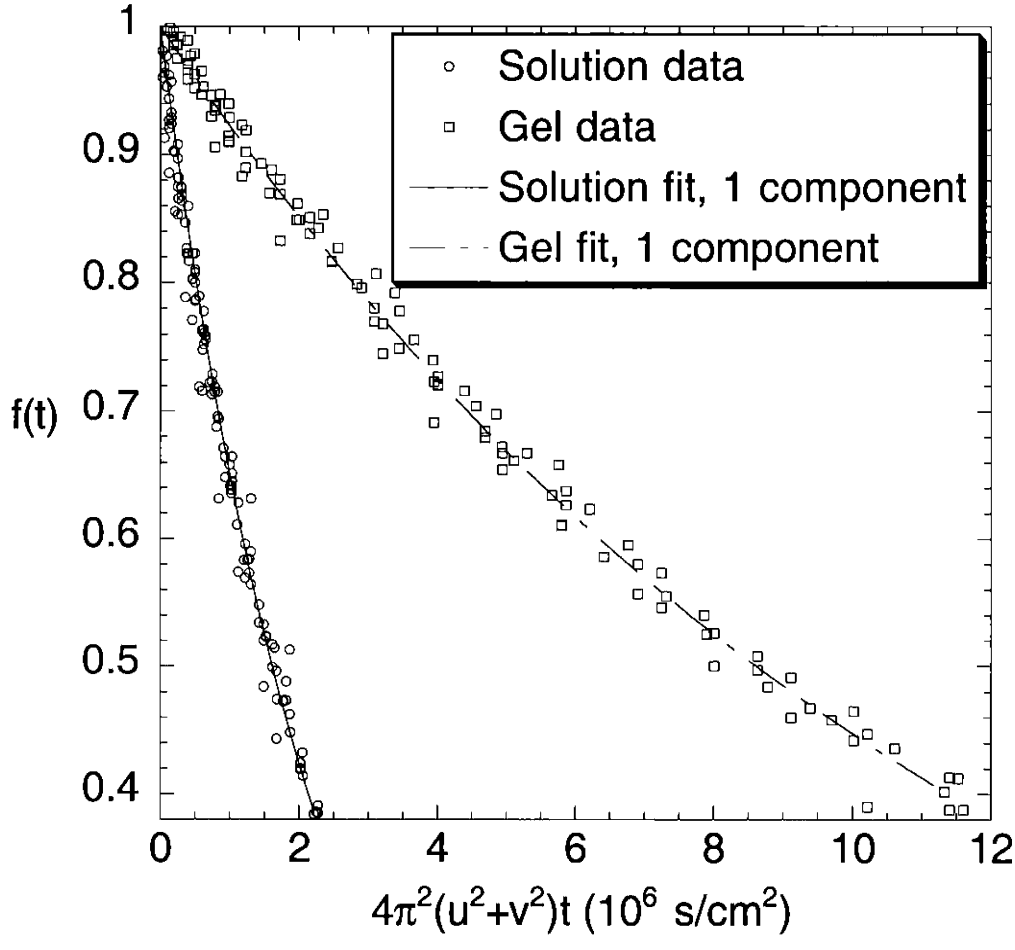

Figure 2.2a FRAP data for diffusion of 105 kDa Ficoll in buffer and in 8.0% agarose gels with or without dextran. (a) Pure agarose ($\phi_a = 0.080$) and free solution. Both curves represent one-component fits. (b) Composite gel ($\phi_a = 0.080$ and $\phi_d = 0.011$) and free solution. One- and two-component fits to the gel data are shown, the latter being much more accurate.

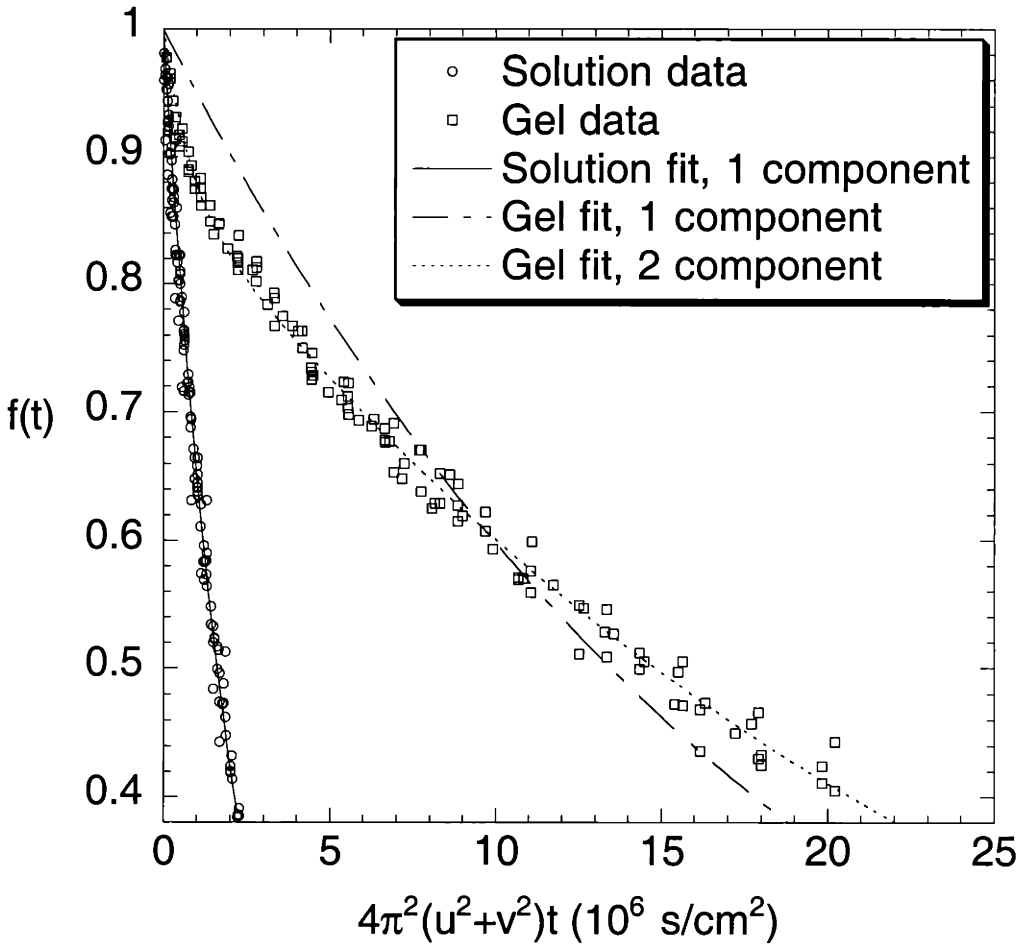

Figure 2.2b FRAP data for diffusion of 105 kDa Ficoll in buffer and in 8.0% agarose gels with or without dextran. (a) Pure agarose ($\phi_a = 0.080$) and free solution. Both curves represent one-component fits. (b) Composite gel ($\phi_a = 0.080$ and $\phi_d = 0.011$) and free solution. One- and two-component fits to the gel data are shown, the latter being much more accurate.

2.3 RESULTS

2.3.1 Gel Composition

The six gel compositions used, designated A-F, are given in Table 2.2. The first two data columns (ϕ_a and ϕ_d) are the volume fractions of agarose and immobilized dextran. Two agarose volume fractions, ϕ_a = 0.040 and 0.080, were each studied alone and with two levels of dextran. When present, dextran was the minority component, the highest value of ϕ_d being 0.011 (gel type F). The fraction of dextran immobilized (η, not shown) was found to increase with the dextran concentration in the initial equilibrating solution (C_0), reaching maximum values of 0.20 and 0.32 in 4.0% and 8.0% agarose, respectively. For gel type B, the results for η at the lower dextran concentration showed excessive variability, so that, to calculate ϕ_d for this case, η was estimated by linear interpolation in C_0. (It was found that η was a linear function of C_0 in 8.0% agarose.) Also shown in Table 2.2 are the values of C_0 and the partition coefficient measured for free dextran (Φ). As expected theoretically (White and Deen, 2001), Φ tended to decrease with increasing ϕ_a (for fixed C_0), and tended to increase with increasing C_0 (for fixed ϕ_a), although the differences were not always statistically significant.

It should be mentioned that the values of ϕ_d in Table 2.2 are roughly half those reported by White and Deen (2002) for similar gels. In that study, fluoresceinated dextran was used to determine η and ϕ_d. However, we noticed subsequently that such dextran solutions became gelatinous after electron beam irradiation, whereas unlabeled dextran was visibly unchanged. Accordingly, we employed only unlabeled dextran here. Because the solutions used to determine ϕ_d were identical to those used to prepare the gel samples for permeability and diffusivity measurements, the present estimates of gel dextran content should be more reliable.

Table 2.2 Properties of Composite Gels. ϕ_d and Φ are given as mean ± standard error for 8 samples.

Gel Type	ϕ_a	ϕ_d	C_0 (mg/mL)	Φ
A	0.040	0	0	----
B	0.040	0.0008[b]	50	0.39 ±0.02[a]
C	0.040	0.0076 ± 0.0009	150	0.43 ± 0.02[a]
D	0.080	0	0	----
E	0.080	0.0008 ± 0.0004	50	0.24 ± 0.01
F	0.080	0.0110 ± 0.0005	150	0.38 ± 0.01[a]

[a] These values were not statistically different, as determined by Tukey's method of multiple comparisons (Larson and Marx, 1986).
[b] Interpolated, assuming that η was proportional to C_0 (see text).

2.3.2 *Diffusion in Free Solution*

The diffusivities obtained for the proteins and Ficolls in free solution (D_∞) are given in Table 2.1. The present values for ovalbumin and BSA are each near the middle of the respective ranges in the literature. Those ranges, as summarized by Johnson et al. (1995), are 7.2×10^{-7} cm^2/s to 7.9×10^{-7} cm^2/s for ovalbumin and 5.8×10^{-7} cm^2/s to 6.4×10^{-7} cm^2/s for BSA. Accordingly, the values of molecular radius (r_s) for ovalbumin and BSA, which were calculated from D_∞ using Eq. (2-5), are also consistent with previous reports. Likewise, r_s for the Ficoll fractions was within 0.2% to 9.5% of measurements with corresponding unlabeled samples using quasielastic light scattering (Oliver et al., 1992).

2.3.3 *Diffusion in Agarose*

Relative diffusivities in pure agarose gels are plotted as a function of molecular radius in Fig. 2.3. The relative diffusivity is the diffusivity in the gel (D) divided by that in free solution (D_∞). Results are shown for 4.0% agarose (Fig. 2.3a) and 8.0% agarose (Fig. 2.3b). In each case, the present results for irradiated agarose (open symbols) are compared with previous data for untreated gels of approximately the same concentration (filled symbols, Johnson, E. M. et al., 1996). The protein and Ficoll diffusivities generally followed the same decreasing trend as molecular size was increased. The relative diffusivities in the irradiated gels decreased from about 0.7 to 0.5 in 4.0% agarose and from about 0.4 to 0.2 in 8.0% agarose, as molecular radius increased from 2.7 to 5.9 nm. Although the results overlapped, the values for irradiated gels tended to be slightly higher than those in untreated gels. Because the agarose concentrations in the previous untreated gels were somewhat lower than those in the present study (0.038 vs. 0.040, and 0.073 vs. 0.080), the actual effect of irradiation was somewhat greater than implied by the plots. Nonetheless, the increase in macromolecular diffusivities due to irradiation was much smaller than the 3-6 fold increase in Darcy permeabilities found previously (White and Deen,

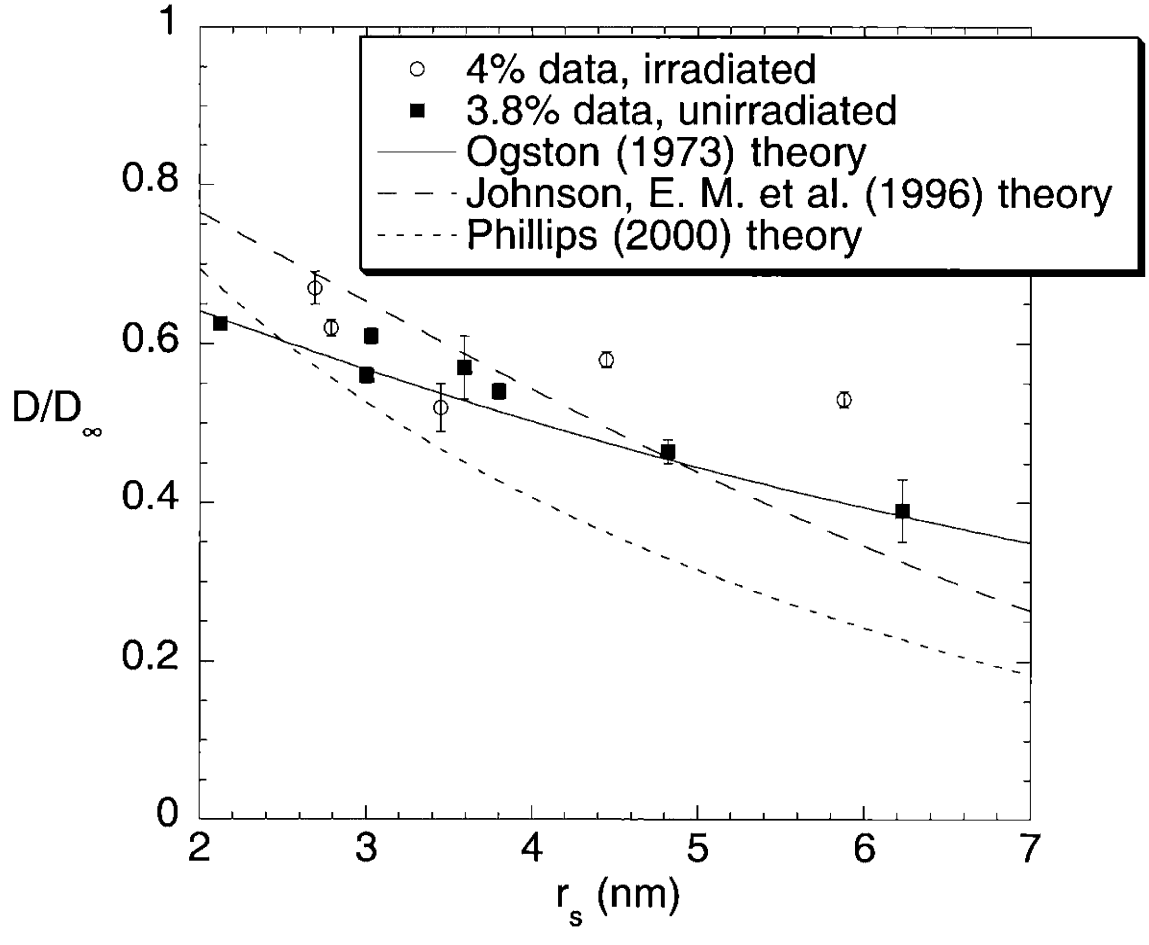

Figure 2.3a Relative diffusivities (D/D_∞) of proteins and Ficolls in pure agarose gels. (a) 4.0% irradiated (present study) and 3.8% unirradiated (Johnson, E. M. et al., 1996). (b) 8.0% irradiated (present study) and 7.3% unirradiated (Johnson, E. M. et al., 1996). The curves are theoretical predictions based on the models of Ogston (1973), Eq. (2-7); Johnson, E. M. et al. (1996), Eqs. (2-8) - (2-10); and Phillips et al. (2000), Eqs. (2-8), (2-9), and (2-11). See text for parameter values used in models.

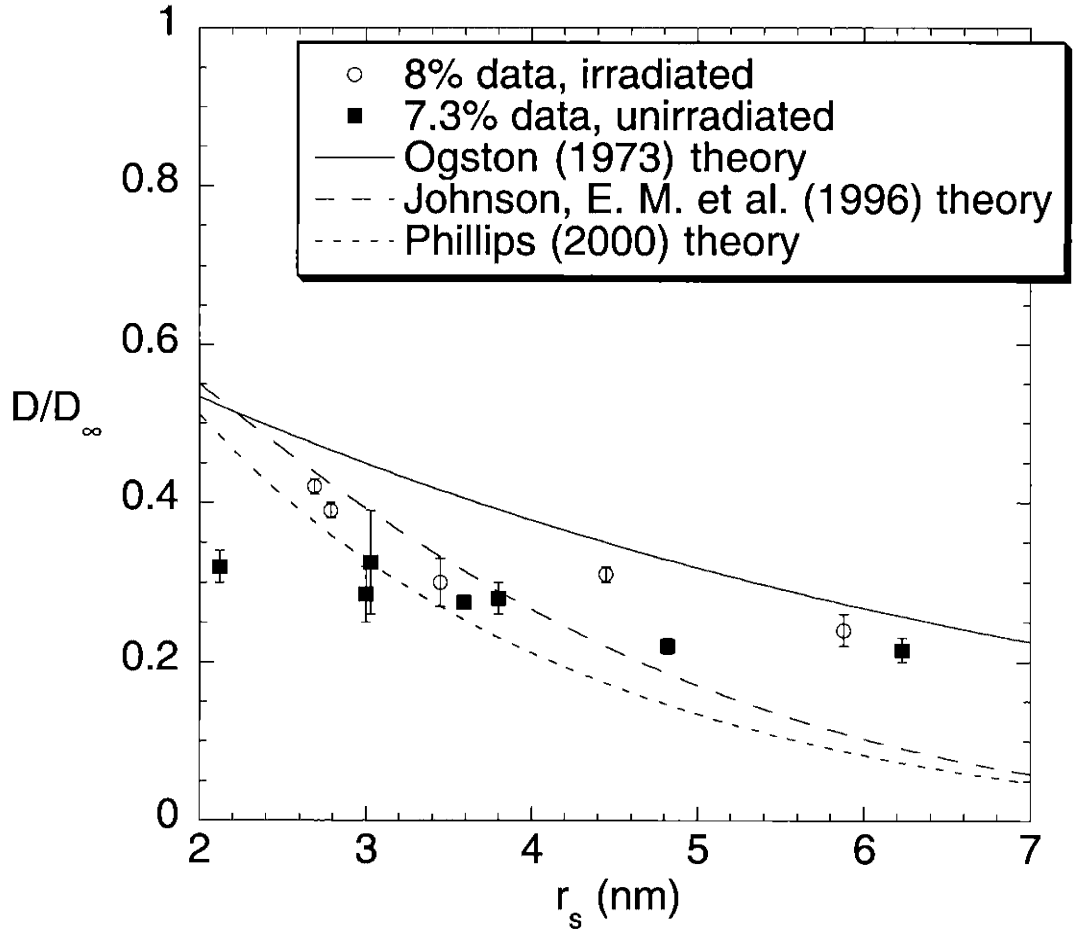

Figure 2.3b Relative diffusivities (D/D_∞) of proteins and Ficolls in pure agarose gels. (a) 4.0% irradiated (present study) and 3.8% unirradiated (Johnson, E. M. et al., 1996). (b) 8.0% irradiated (present study) and 7.3% unirradiated (Johnson, E. M. et al., 1996). The curves are theoretical predictions based on the models of Ogston (1973), Eq. (2-7); Johnson, E. M. et al. (1996), Eqs. (2-8) - (2-10); and Phillips et al. (2000), Eqs. (2-8), (2-9), and (2-11). See text for parameter values used in models.

2002). The curves in Fig. 2.3, which are predictions from various models, will be discussed later.

2.3.4 Diffusion in Agarose-Dextran Composites

The relative diffusivities of the proteins and Ficolls in agarose-dextran composite gels are given in Table 2.3, along with the results for pure agarose. Results for DTAF are also shown. The columns in Table 2.3 (A-F) correspond to the gel compositions in Table 2.2. As already shown in Fig. 2.3 for pure agarose, D/D_∞ generally decreased as the size of the diffusing macromolecule increased, for any given gel composition. Also, for a given macromolecule and a fixed agarose concentration (ϕ_a), D/D_∞ decreased as the amount of dextran (ϕ_d) was increased. Comparing the gels with the maximum dextran concentrations with pure agarose, there was generally a 2-3 fold reduction in relative diffusivity.

The precision of the relative diffusivities for BSA was reduced somewhat by the fact that the fractional fluorescence in the gels due to the dimer could not be determined reliably. As with the FRAP data in free solution, a three-component fit was used to interpret the data for BSA in each gel. However, the diffusivities of BSA and its dimer were too similar to use the dimer fraction in the gel samples as a fitting parameter. Accordingly, the fractional fluorescence due to the dimer was varied from 0 (corresponding to complete exclusion of dimer from the gel) to 0.16 (corresponding to equal partition coefficients of all three components). The lower amounts of dimer led to lower bounds for the relative diffusivity of BSA, whereas the higher amounts led to upper bounds; the mean values are shown in Table 2.3. There was less than a 10% difference between the lower and upper bounds.

2.3.5 Darcy Permeability

Figure 2.4 shows the Darcy permeability as a function of the dextran volume fraction in the gel, for both 4.0% and 8.0% agarose. The present results (open symbols) are compared with those obtained previously in gels prepared in the same way (filled symbols) (White and Deen,

Table 2.3 Relative Diffusivities (D/D_∞) in Gels. The compositions of gel types A-F are shown in Table 2.2. Except for BSA, D/D_∞ is given as mean ± standard error for 3-8 samples. For BSA, mean D/D_∞ and the corresponding error bars were calculated from the extremes of possible dimer fractions, 0.00 and 0.16, in a manner analogous to the case of a samples size of two (see text).

Molecule	A	B	C	D	E	F
Ovalbumin	0.62 ± 0.01	0.53 ± 0.01	0.37 ± 0.01	0.39 ± 0.01	0.33 ± 0.02	0.19 ± 0.00
BSA	0.52 ± 0.03	0.43 ± 0.02	0.27 ± 0.03	0.30 ± 0.03	0.26 ± 0.03	0.11 ± 0.02
Ficoll 21K	0.67 ± 0.02	0.56 ± 0.02	0.46 ± 0.01	0.42 ± 0.01	0.34 ± 0.01	0.24 ± 0.01
Ficoll 61K	0.58 ± 0.01	0.47 ± 0.03	0.31 ± 0.01	0.31 ± 0.01	0.22 ± 0.01	0.12 ± 0.00
Ficoll 105K	0.53 ± 0.01	0.41 ± 0.03	0.27 ± 0.01	0.24 ± 0.02	0.15 ± 0.00	0.08 ± 0.00
DTAF	0.74 ± 0.02	0.66 ± 0.02	0.54 ± 0.01	0.59 ± 0.01	0.53 ± 0.00	0.34 ± 0.00

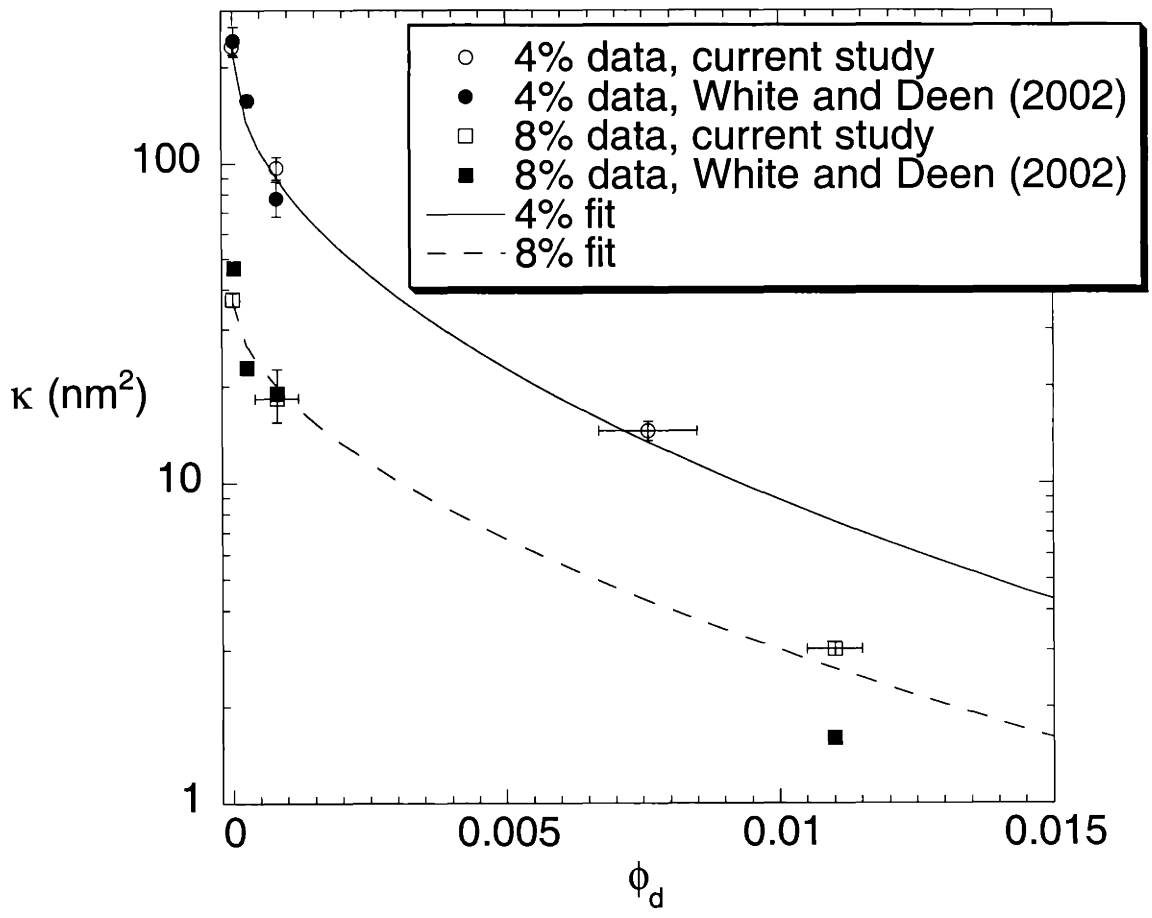

Figure 2.4 Darcy permeability (κ) of agarose and agarose-dextran composite gels. The present data are compared with those of White and Deen (2002). The curves are stretched exponential fits to the data in the form of Eq. (2-11a), where $F = \kappa/\kappa_a$ and κ_a is the value for pure agarose. For 4% agarose, a = 31.2 and b = 0.49; for 8% agarose, a = 31.7 and b = 0.55.

2002). In both cases, the data in Table 2.2 were used to relate C_0 to ϕ_d. (As already mentioned, the higher dextran volume fractions estimated previously are likely to be less reliable than those in Table 2.2.) For both agarose concentrations, κ decreased by an order of magnitude as the dextran concentration was increased from zero to its maximum value. The present results were very similar to those found previously, as shown. The curves are stretched exponential fits to all the data at each agarose concentration. For either agarose concentration, relatively little dextran was required to produce a significant reduction in κ. That is, Fig. 2.4 shows that incorporating $\leq$ 1% dextran (by volume) in either agarose gel had a greater effect on κ than did changing the agarose concentration from 4.0% to 8.0%.

2.4 DISCUSSION

Our principal finding was that the covalent binding of modest amounts of dextran to agarose resulted in up to 2-3 fold reductions in the diffusivities of proteins and Ficolls, relative to values in pure agarose gels. The reductions in diffusivity due to dextran incorporation were much less than those in the Darcy permeability, which decreased by up to 10-fold, as reported before (White and Deen, 2002). We focus now on the extent to which the results can be explained by available theories for hindered diffusion in fibrous media.

The diffusivities in pure agarose were compared with predictions from three models. One approach is that of Ogston (1973), who focused on the probability that a molecule of radius r_s can complete a step through a randomly oriented array of fibers of negligible thickness. When applied to a dimensionless fiber radius $\lambda = r_f/r_s$, and fiber volume fraction ϕ, the predicted relative diffusivity is

$$\frac{D}{D_\infty} = \exp\left[-\left(\frac{1}{\lambda}+1\right)\sqrt{\phi}\right] \tag{2-7}$$

In contrast to Eq. (2-7), where hydrodynamic effects on mobility are not considered, are two other results that combine both steric and hydrodynamic effects, due to Johnson, E. M. et al. (1996) and Phillips (2000), respectively. Both are based on the suggestion of Brady (1994) that the relative diffusivity be written as a product of a steric factor (S) and a hydrodynamic factor (F):

$$\frac{D}{D_\infty} = SF \tag{2-8}$$

The steric factor, which is similar to an inverse tortuousity, is the relative diffusivity in the absence of hydrodynamic interactions between the fibers and the macromolecular solute. That is, it describes the effect of excluding the center of a spherical solute molecule from a region of radius $r_f + r_s$ centered on any fiber. For randomly oriented arrays of fibers, the Brownian dynamics simulations of Johansson and Lofroth (1993) gave

$$S(f) = \exp(-0.84 f^{1.09}), \quad f = \left(1 + \frac{1}{\lambda}\right)\phi \tag{2-9}$$

This result was employed by both Johnson, E. M. et al. (1996) and Phillips (2000), whose models differ only in the evaluation of F. Johnson, E. M. et al. (1996) based the hydrodynamic term on the drag experienced by a sphere moving through a medium described by Brinkman's equation (Brinkman, 1947), as suggested in Phillips et al. (1989). Correcting an error in one of the coefficients that was pointed out in Solomentsev and Anderson (1996),

$$F\left(\frac{r_s}{\sqrt{K}}\right) = \left[1 + \left(\frac{r_s}{\sqrt{K}}\right) + \frac{1}{9}\left(\frac{r_s}{\sqrt{K}}\right)^2\right]^{-1} \tag{2-10}$$

This expression contains no explicit structural information; the effects of the gel structure are embodied in κ. In contrast, Phillips (2000) made use of the numerical results of Clague and Phillips (1996) for the drag on a sphere moving through a random array of fibers. Those results were correlated as a stretched exponential,

$$F(\phi,\lambda) = \exp(-a\phi^b) \tag{2-11a}$$

$$a = 3.727 - 2.460\lambda + 0.822\lambda^2 \tag{2-11b}$$

$$b = 0.358 + 0.366\lambda - 0.0939\lambda^2 \tag{2-11c}$$

The theoretical curves in Fig. 2.3 were based on the values of ϕ_a (Table 2.2) and κ for agarose (Fig. 2.4), together with a value of r_f (= 1.64 nm) inferred recently from equilibrium partitioning data for untreated agarose (Lazzara and Deen, 2004). The expression of Ogston (Eq. (2-7)) gave approximately the correct slope in the plots of relative diffusivity versus molecular radius at either agarose concentration, although it consistently overestimated the relative diffusivities in 8.0% agarose. A tendency of Eq. (2-7) to greatly overestimate relative diffusivities in unirradiated agarose gels was noted previously (Johnson, E. M. et al., 1996). The models of Johnson, E. M. et al. (Eqs. (2-8) - (2-10)) and Phillips (Eqs. (2-8), (2-9), and (2-11)) both yielded slopes that were too large. The results obtained with two other models for diffusion in gels (Amsden, 1998; Bosma et al., 2000) generally gave larger mean square errors when applied to our agarose data than did those shown in Fig. 2.3; those curves have been omitted for clarity. Thus, none of the available theories precisely captures the behavior of macromolecular diffusivities in pure agarose.

The only one of the models discussed above that can be applied readily to the diffusivity data in the agarose-dextran composite gels is the effective medium approach of Johnson, E. M. et al. (1996). That is, even if it is postulated that the composite gels can be modeled as a mixture of

randomly oriented fibers of differing radii, the other approaches cannot be extended readily to incorporate a second fiber type. In testing the predictive ability of the effective medium model for composite gels, we chose to focus on the diffusivity ratio D/D_a, where D_a is the value in pure agarose. Normalizing the gel diffusivity using the value in agarose tends to separate the ability of the model to predict D_a from its ability to predict the effects of the added dextran on D. An additional assumption we made is that S in the agarose-dextran gels is determined mainly by agarose. The idea that dextran does not contribute significantly to the steric factor for diffusion is supported by the fact that relative diffusivities of globular proteins in dextran solutions have been found to be described accurately by setting $S = 1$ in Eq. (2-8) and evaluating F using Eq. (2-10) (Kosar and Phillips, 1995). It appears also that S is near unity in hyaluronic acid solutions (Phillips et al., 1989) and polyacrylamide gels (Kapur et al., 1997), suggesting that steric hindrances to diffusion may be nearly absent, in general, if the polymeric obstacles are relatively flexible. In contrast to the polymers just mentioned, agarose forms rigid fibrils that do not exhibit detectable Brownian motion (Mackie et al., 1978). With the assumption that S was determined primarily by the agarose, applying Eqs. (2-8) and (2-10) to agarose gels with and without dextran gives

$$\frac{D}{D_a} = \frac{1 + \left(\frac{r_s}{\sqrt{\kappa_a}}\right) + \frac{1}{9}\left(\frac{r_s}{\sqrt{\kappa_a}}\right)^2}{1 + \left(\frac{r_s}{\sqrt{\kappa}}\right) + \frac{1}{9}\left(\frac{r_s}{\sqrt{\kappa}}\right)^2} \tag{2-12}$$

where κ_a is the Darcy permeability for pure agarose and the S terms have cancelled.

Figure 2.5 compares the experimental diffusivity ratios with the predictions from Eq. (2-12). For either 4.0% or 8.0% agarose, the model underestimated the effects of dextran at the lower dextran level (i.e., it overestimated D/D_a), but was quite accurate at the higher dextran level. Overall, given the simplicity of Eq. (2-12) and the absence of adjustable parameters, the

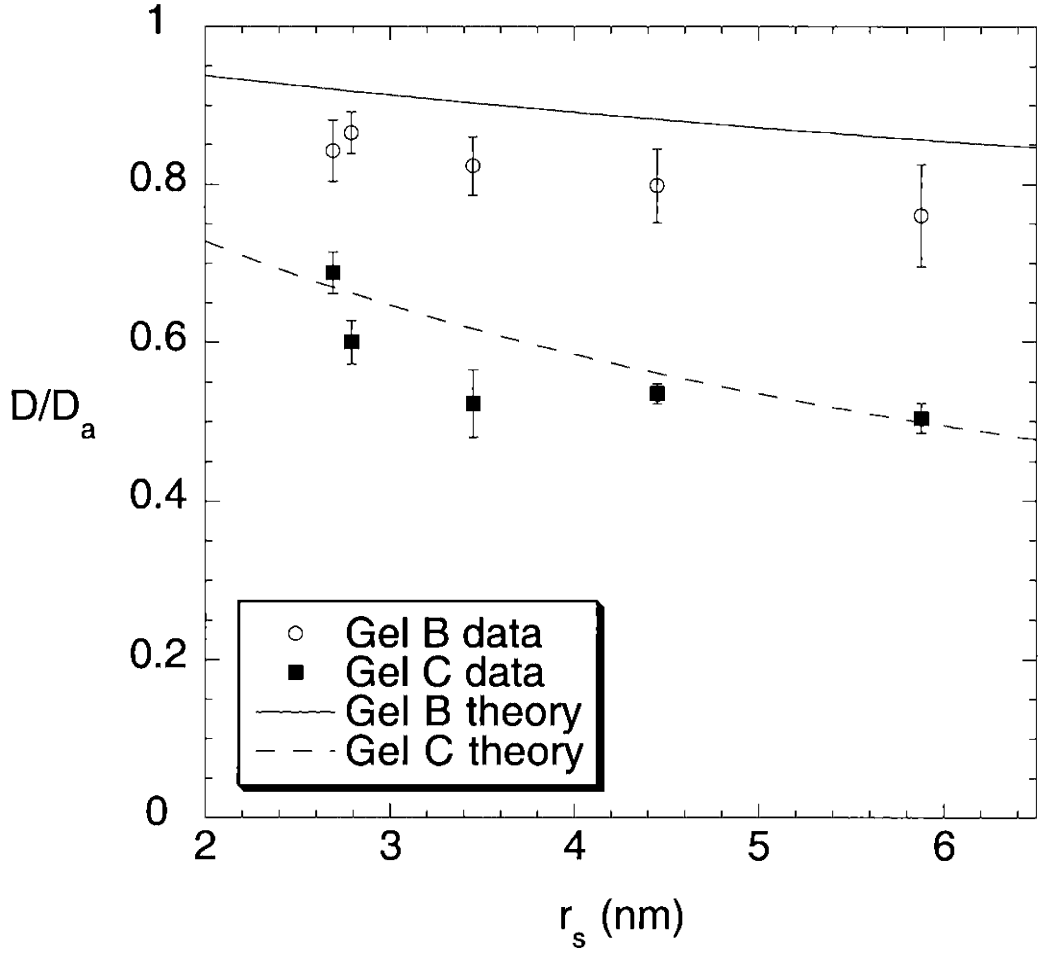

Figure 2.5a Diffusivities in composite gels relative to values in pure agarose. (a) 4.0% agarose with $\phi_d = 0.0008$ (Gel B) and $\phi_d = 0.0076$ (Gel C) (b) 8.0% agarose with $\phi_d = 0.0008$ (Gel E) and $\phi_d = 0.011$ (Gel F). The theoretical curves in each case are based on Eq. (2-12).

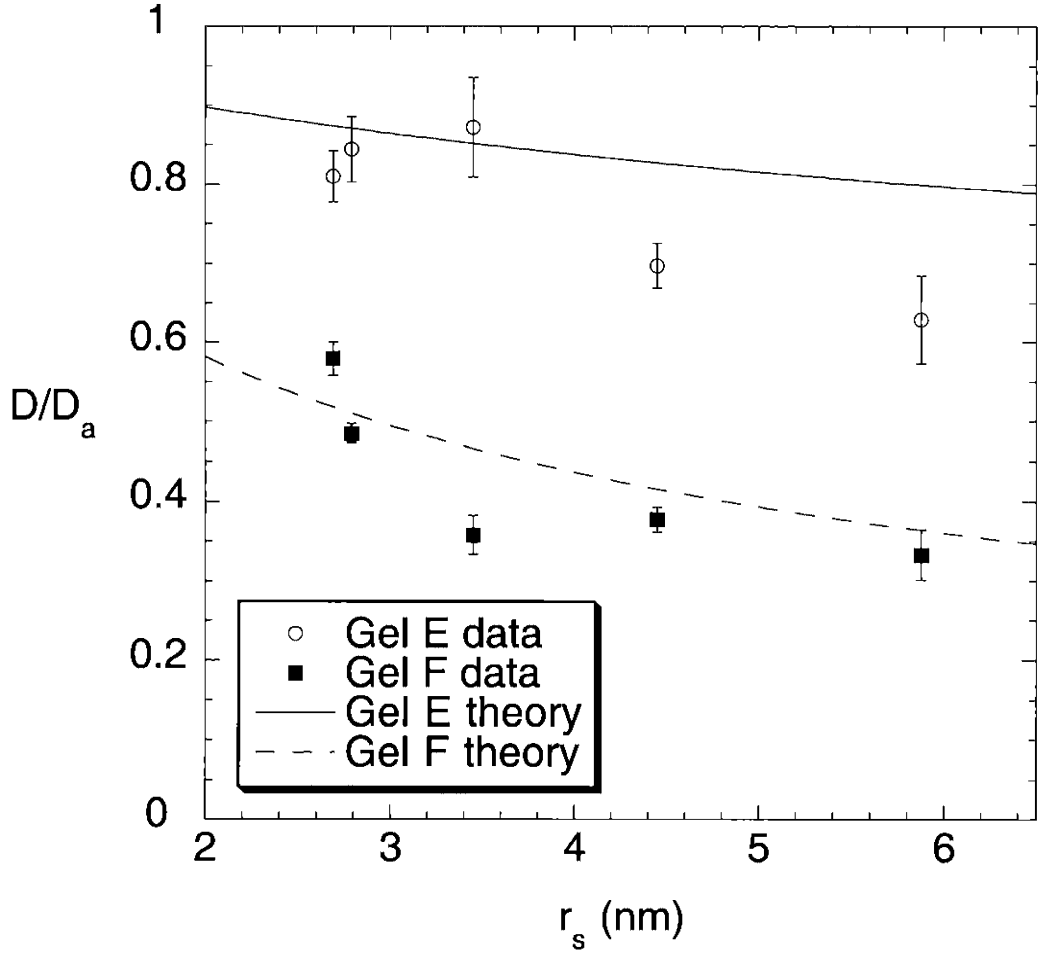

Figure 2.5b Diffusivities in composite gels relative to values in pure agarose. (a) 4.0% agarose with $\phi_d = 0.0008$ (Gel B) and $\phi_d = 0.0076$ (Gel C) (b) 8.0% agarose with $\phi_d = 0.0008$ (Gel E) and $\phi_d = 0.011$ (Gel F). The theoretical curves in each case are based on Eq. (2-12).

predictions are remarkably good. The agreement between the model and data in Fig. 2.5 supports the use of Eq. (2-10) for evaluating F in agarose and agarose-dextran gels. Moreover, it suggests that the limited success in predicting diffusivities in pure agarose (particularly the slopes in Fig. 2.3), may have been due mainly to problems with Eq. (2-9). Specifically, it suggests that Eq. (2-9), when applied to agarose, may have too strong a dependence of S on r_s.

The expression for S in Eq. (2-9) was obtained from simulations based on randomly positioned and oriented fibers of uniform radius (Johansson and Lofroth, 1993). Modeling untreated agarose in this manner led to very accurate predictions of equilibrium partition coefficients for BSA and several Ficolls (Lazzara and Deen, 2004), provided that the fiber radius was chosen as 1.6 nm. That value is close to the number-average fiber radius of 1.9 nm suggested by small-angle X-ray scattering data (Djabourov et al., 1989). However, attempts to predict Darcy permeabilities for agarose from fiber matrix models have generally yielded much poorer results (Johnson, E. M. et al., 1996; Clague and Phillips, 1997; Johnston and Deen, 1999; White and Deen, 2002). Complicating the situation is that electron beam treatments alter the structural properties of agarose, as evidenced by increases in diffusivity (present data) and Darcy permeability (White and Deen, 2002). Thus, it is not clear at present what geometric model(s) might be adopted to improve the results for S, either for treated or untreated agarose.

One feature of the present results is that the reductions in κ following dextran incorporation into agarose were proportionately much larger than those in D/D_∞. In general, changes in the Darcy permeability of gels will not necessarily be disproportionate to those in diffusivities. For example, Kapur et al. (1996, 1997), in studies of protein diffusion and water flow through polyacrylamide gels confined in porous membranes, found moderate and comparable percentage declines in κ and D/D_∞ as the polyacrylamide volume fraction was increased from 0.044 to 0.094. For a uniform, random fiber matrix, the dependence of κ on ϕ varies approximately as $-(\ln\phi)/\phi$ (Jackson and James, 1986). Thus, at relatively high volume fractions (as in the polyacrylamide study), κ is not nearly as sensitive to ϕ as it is at low volume fractions. In the

present study, where the more important volume fraction was ϕ_d, much larger changes in κ were seen because ϕ_d was much smaller.

In general, protein diffusivities may depend on pH, ionic strength, and protein concentration (Raj and Flygare, 1974). From pH 10.5 to about 5, BSA has a compact configuration, with a negative charge that diminishes as the isoelectric pH of 4.8 is approached. At still lower pH values (< 4.8), BSA acquires a net positive charge and undergoes a conformational change to a more expanded form. Raj and Flygare (1974) found that for BSA concentrations of 1-2% by weight and with pH between 6 and 7, the diffusivity was independent of pH, concentration, and ionic strength (within the range 0.01 - 0.50 M). Thus, the present results, which were obtained using dilute solutions at pH 7 and an ionic strength of 0.1 M, should have been insensitive to those factors. Moreover, because agarose and dextran are essentially neutral, no additional charge effects (beyond the intramolecular forces that influence the BSA conformation) are expected to have been present.

In conclusion, the reductions in macromolecular diffusivities caused by incorporating various amounts of dextran into agarose gels could be predicted fairly accurately from the measured decreases in Darcy permeability, using an effective medium model. This suggests that one might be able to predict diffusivity variations in complex, multicomponent hydrogels (e.g., those in body tissues) in the same manner, provided that values of κ can be obtained. Until more detailed structure-based models can be developed, ones that include multiple types of (possibly flexible) fibers, the effective medium approach seems to provide an attractive alternative for modeling diffusion in complex hydrogels.

Footnote

1. For ovalbumin and BSA, the r_s values for the monomers estimated from size-exclusion chromatography (3.1 and 3.7 nm, respectively) agreed well with those obtained using FRAP (Table 2.1). That was not true for a third protein, fluorescein-labeled IgG (from Jackson ImmunoResearch Laboratories, West Grove, PA). Chromatography of that IgG (MW = 160

kDa) yielded a monomer radius of 4.7 nm, a dimer radius of 6.1 nm, a dimer fraction of 0.05, and a fluorescein fraction of < 0.01. The FRAP data in free solution gave $D_\infty = (3.28 \pm 0.05) \times 10^{-7}$ cm^2/s, or a monomer r_s of 6.5 nm, larger even than that of the chromatographic dimer. Literature values of D_∞ for IgG (Putnam, 1975; Burczak et al., 1994) correspond to r_s = 5.4 to 5.6 nm. Because r_s could not be established unambiguously, experiments with IgG were discontinued.

3 Equilibrium Partitioning of Ficoll in Composite Hydrogels

3.1 Introduction

In the work reported here, equilibrium partition coefficients for several sizes of Ficoll were measured in agarose-dextran composite gels of varying composition, and the utility of excluded volume partitioning theory was examined. This data complements previous Darcy permeability measurements (White and Deen, 2002) as well as the hindered diffusivities discussed in chapter 2, and permits comparison of synthetic agarose-dextran gels with that of isolated GBM.

3.2 Materials and Methods

3.2.1 Test Macromolecules

Four narrow fractions of Ficoll, with weight-average molecular weights (M_W) of 21, 37, 61, and 105 kDa, were special-ordered from Pharmacia LKB (Piscataway, NJ). Based on information from the manufacturer, the polydispersity index (M_W/M_N, where M_N is number-average molecular weight) was 1.22, 1.18, 1.15, and 1.13, respectively. As detailed in section 2.2.4, the Ficoll fractions were labeled with dichlorotryazinyl amino fluorescein (DTAF) (Sigma, St. Louis, MO). These are the same fluoresceinated Ficolls as used in the diffusion study discussed in chapter 2. Size exclusion chromatography of the Ficoll samples using Superdex 200 (Pharmacia Biotech, Piscataway, NJ) showed no evidence of free fluorescein. The fluorescence recovery after photobleaching results from section 2.3.2 detail the free-solution diffusivity ($D_{i\infty}$) of each Ficoll, from which the Stokes-Einstein radii (r_s) was calculated as 2.7, 3.5, 4.5, and 5.9 nm for the 21, 37, 61, and 105 kDa narrow fractions of Ficoll, respectively. Those values differ by only 0.2-9.5% from measurements of corresponding unlabeled samples using quasielastic light scattering (Oliver et al., 1992). Dilute aqueous solutions were made by dissolving each Ficoll in a 0.01 M sodium phosphate, 0.1 M potassium chloride buffer at pH 7.0.

3.2.2 FRAP Diffusion Measurements

Image-based FRAP (Tsay and Jacobson, 1991; Berk et al., 1993) was used here to determine $D_{i\infty}$ of the 37 kDa Ficoll. Diffusivities for the other Ficolls were reported in chapter 2, together with details of the FRAP system, operating conditions, and data analysis. Briefly, a solution was prepared by dissolving the Ficoll fraction in the KCl-phosphate buffer to a final concentration of 2 mg/mL. The corresponding volume fraction of Ficoll was 0.006, indicating that the solution was dilute. The solution was drawn into microslides and FRAP measurements were performed at 3 different locations within each of two samples. The diffusion coefficients were computed from the FRAP data using spatial Fourier analysis of the digitized images.

3.2.3 Gel Preparation

Agarose (Type IV; Sigma, St. Louis, MO) was suspended in the KCl-phosphate buffer in a 90°C oven for 4-6 h, until the mixture appeared to be homogeneous. The agarose mixtures were rotated hourly to ensure adequate mixing. Then, the hot agarose solution was squeezed between two 90°C glass plates separated by microslide cover slips, to ensure a uniform thickness of 0.20-0.32 mm, depending on the number of cover slips used. The gels were allowed to cool to room temperature before being placed in buffer and stored overnight at 7°C. Agarose gel disks with a diameter of 1.5 cm were then cut using a metal punch. The disks were placed in either 50 or 150 mg/mL solutions of 500 kDa dextran (Sigma, St. Louis, MO) and allowed to equilibrate for at least 72 h. That period is several times the characteristic time for diffusion, based on the diffusivities for dextran in agarose given by Key and Sellen (Key and Sellen, 1982) and the thicknesses of the samples. A 2 Mrad exposure to an electron beam (High Voltage Research Laboratory, Massachusetts Institute of Technology) was used to covalently attach the dextran to the agarose. Following irradiation, the gels were placed in a large volume of buffer (2.5 mL), so that any dextran that was not immobilized would diffuse out. The agarose gel concentrations of 4.1 and 8.2% (w/v) were converted to volume fractions (ϕ_a) by dividing by 1.025 (Johnson et al., 1995). In other words, $\phi_a = 0.040$ and 0.080 for "4%" and "8%" agarose gels, respectively. The

concentrations of immobilized dextran were measured previously, as discussed in section 2.2.2, using the same preparation conditions. Based on the measured mass concentration and specific volume, the dextran volume fraction (ϕ_d) ranged from 0.0008 to 0.011. Thus, on this basis, dextran was always the minority component.

3.2.4 Partition Coefficient Measurements

To determine the partition coefficient of a given Ficoll in a gel sample (pure agarose or agarose-dextran composite), the gel was immersed in a large (2.5 mL) volume of solution containing approximately 0.6 mg/mL Ficoll, for at least 24 h. The immersion period always represented at least five characteristic times for diffusion, based on diffusivities measured in identical gels as detailed in sections 2.3.3 and 2.3.4, indicating that the Ficoll had ample time to equilibrate. The large solution volume (compared to the gel volume of 0.035-0.057 mL) ensured that the concentration of Ficoll in the solution remained nearly constant. The gel was then removed, rinsed thoroughly, and immersed in a large volume of Ficoll-free buffer (V_f = 2.5 mL) for another 24 h. That allowed virtually all the Ficoll that had entered the gel to diffuse back out into the buffer. After measuring the fluorescence of the initial and final Ficoll solutions, which was proportional to the corresponding concentrations (C_0 and C_f, respectively), the equilibrium partition coefficient was calculated as

$$\Phi = \frac{C_f V_f}{C_0 V_g} \tag{3-1}$$

where V_g is the volume of the gel. (The subscript denoting solute i has been omitted here, for simplicity.) The fluorescence of the Ficoll solutions was determined using a spectrofluorometric detector (Shimadzu, Columbia, MD) with excitation at 488 nm and emission at 515 nm. The gel volume was measured using a micrometer, with the gel placed between two microslides of

known thickness. Ficoll partition coefficients were measured four times for each set of conditions, and the results expressed as mean ± standard error.

3.2.5 Theory

The data were compared with predictions from a theory that is based entirely on steric interactions among the macromolecules in the solution and gel (Lazzara et al., 2000). Although fluorescein labeling gives Ficoll a small negative charge (Johnson, E. M. et al., 1996), agarose and dextran are essentially uncharged, and it was shown previously that the partitioning of labeled Ficolls in agarose was unaffected when ionic strength was increased beyond the levels used here (Lazzara and Deen, 2004). Thus, it is permissible to neglect electrostatic interactions in the present setting. Briefly, in this theory partition coefficients are computed by summing excluded volumes both in the confined phase (gel polymers and mobile macromolecules) and in the bulk solution (mobile macromolecules only). The approach is applicable (in principle) to any mixture of spherical or non-spherical solutes, either dilute or concentrated, and to an arbitrary number of gel components. In general, one nonlinear algebraic equation is generated for each type of mobile macromolecule.

Each of the present experiments involved a dilute solution of a single Ficoll, so that there was only one partition coefficient to consider and solute-solute interactions could be neglected. The confined phase had two components, agarose and dextran. Denoting the volume fractions of agarose and dextran in the gel as ϕ_a and ϕ_d, respectively, the excluded volume model reduces to

$$\Phi_i = \exp\left[-\phi_a \alpha_{ia} - \phi_d \alpha_{id}\right] \tag{3-2}$$

where the geometric parameters α_{ij} characterize the steric interactions between solutes of type i and fixed objects of type j. In all of the calculations to be discussed, the agarose fibrils were regarded as a single population of long, rigid rods. In what proved to be the more accurate

model, the immobilized dextran was viewed as a second type of fiber; in an alternative model it was represented as a spherical coil. For a spherical solute of radius r_i and long fibers of radius R_j, the excluded volume parameter is given by

$$\alpha_{ij} = \left(1 + \frac{r_i}{R_j}\right)^2 \tag{3-3}$$

For a spherical solute and a coil of effective radius a_j, the corresponding expression is

$$\alpha_{ij} = \left(1 + \frac{r_i}{a_j}\right)^3 \tag{3-4}$$

The values used for R_a, R_d, a_d, and ϕ_d will be discussed shortly. Note that the interpretation of ϕ_d depends on whether dextran is modeled as a rod or as a coil. For the rod (fiber) representation, ϕ_d was equated with the volume fraction calculated from the mass concentration and specific volume of dextran. For the coil model, the molecular volume for steric exclusion also includes all water contained within the assumed sphere, thus, ϕ_d for this case was much larger. It is also worth noting that the expression derived by Ogston (1958) for the partition coefficient of a spherical solute in a monodisperse fiber matrix is recovered by setting $\phi_d = 0$ in Eq. (3-2) and calculating α_{ia} according to Eq. (3-3).

3.3 Results and Discussion

The Ficoll partition coefficients measured in 4% and 8% agarose gels are shown by the discrete symbols in Figures 3.1 and 3.2, respectively. In each case, Φ is plotted as a function of the Stokes-Einstein radius of the Ficoll, with results given for pure agarose (irradiated as done in preparing the composite gels) and for low and high levels of dextran. The curves, which are

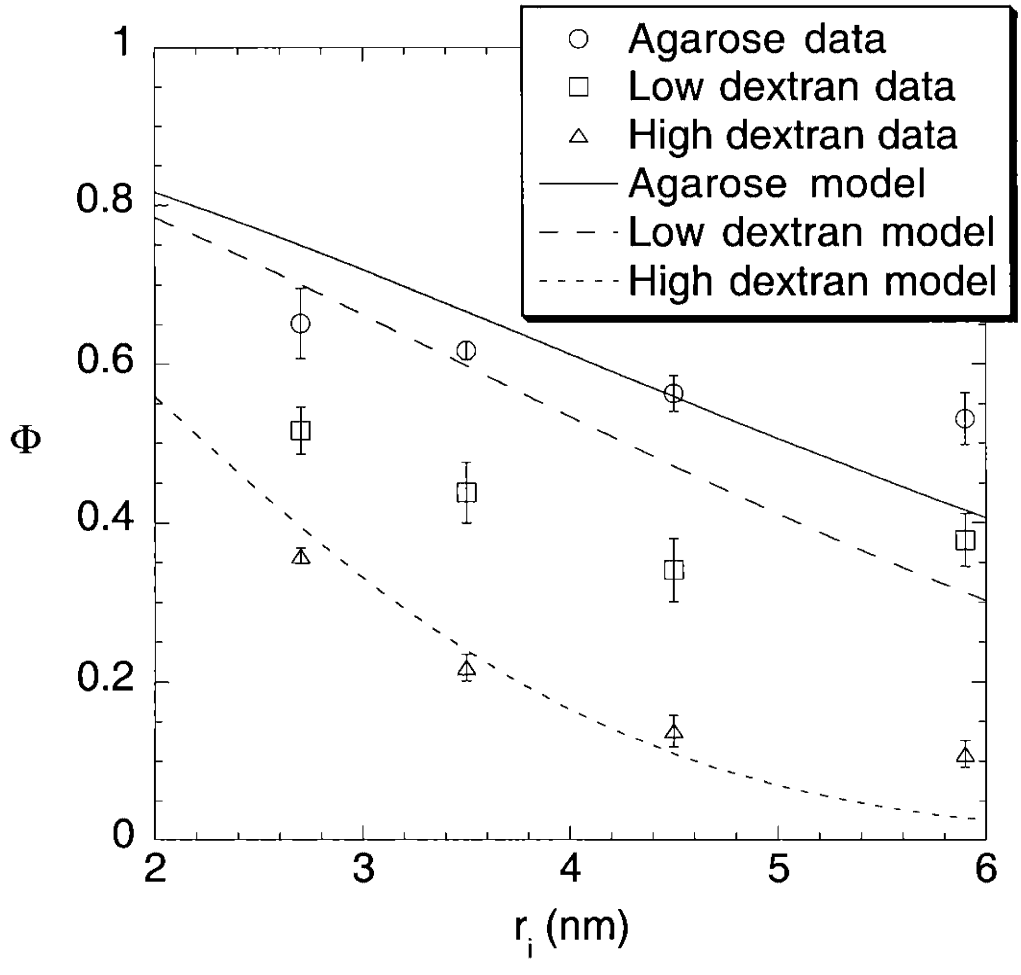

Figure 3.1 Equilibrium partition coefficients (Φ) of Ficoll in 4% agarose gels containing varying amounts of dextran. Data are shown for four Ficoll fractions with Stokes-Einstein radii (r_i) as indicated. The "low" and "high" dextran levels correspond to immobilized concentrations of 0.0013 and 0.012 g/mL, respectively. The model curves, which assume that dextran behaves as a fiber, are based on Eqs. (3-2) and (3-3) with $\phi_a = 0.040$, $\phi_d = 0.0008$ (low) or 0.0076 (high), $R_a = 1.6$ nm, and $R_d = 0.33$ nm.

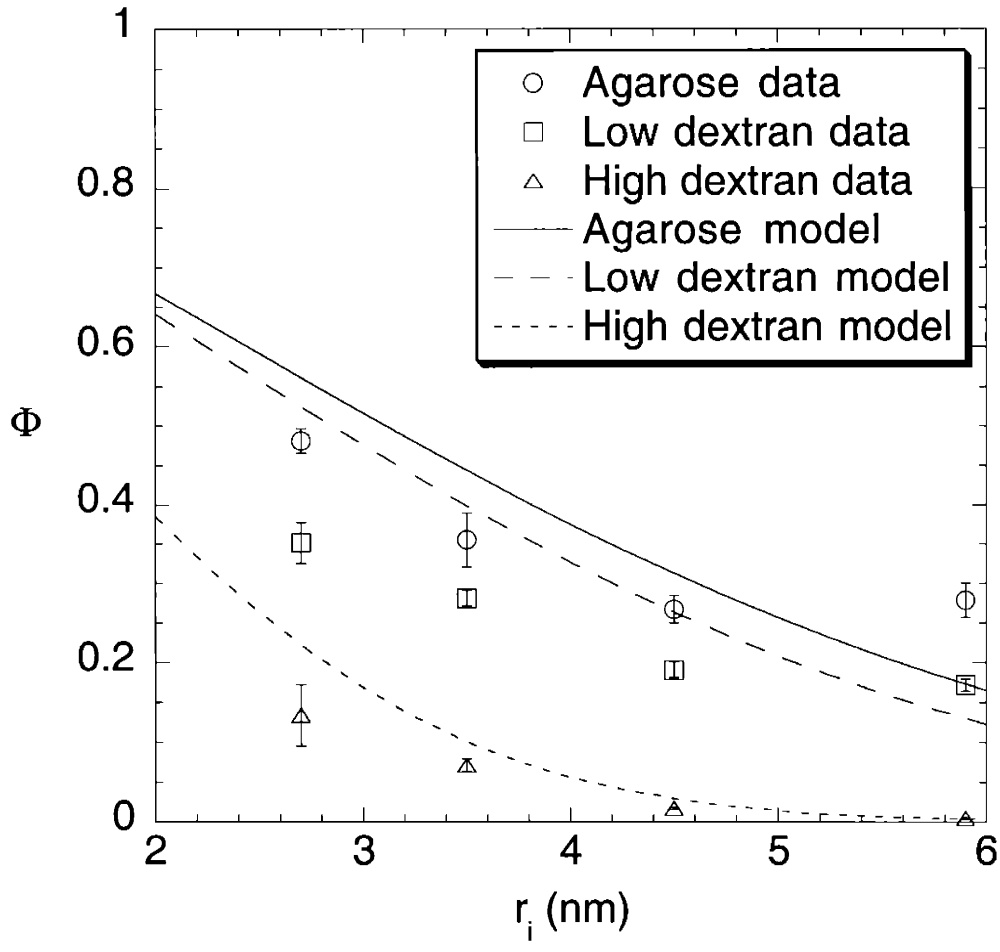

Figure 3.2 Equilibrium partition coefficients (Φ) of Ficoll in 8% agarose gels containing varying amounts of dextran. Data are shown for four Ficoll fractions with Stokes-Einstein radii (r_i) as indicated. The "low" and "high" dextran levels correspond to immobilized concentrations of 0.0013 and 0.018 g/mL, respectively. The theoretical curves, which assume that dextran behaves as a fiber, are based on Eqs. (3-2) and (3-3) with $\phi_a = 0.080$, $\phi_d = 0.0008$ (low) or 0.0110 (high), $R_a = 1.6$ nm, and $R_d = 0.33$ nm.

predictions from the excluded volume theory, are discussed below. As seen in either plot, Φ tended to decrease as the Ficoll size increased or as more dextran was linked to a given amount of agarose. A comparison of the data for pure (dextran-free) 4% and 8% agarose shows that Φ also decreased as the agarose concentration was increased. The "low" and "high" dextran data in the two plots are not directly comparable, because there were differences in the dextran concentrations incorporated into the 4% and 8% agarose gels.

Agarose fibrils have undetectable Brownian motion (Mackie et al., 1978), suggesting that it might be reasonable to model them as rigid rods. As already mentioned, that approach led to accurate predictions of BSA and Ficoll partition coefficients in unirradiated agarose gels, when the fiber radius was chosen as R_a = 1.6 nm (Lazzara and Deen, 2004). That value is made plausible by its similarity to the number-average radius of 1.9 nm inferred from SAXS data (Djabourov et al., 1989). Thus, we modeled the agarose fibrils in each case as a homogeneous population of long, randomly oriented rods of that radius. It was less clear *a priori* how the covalently bound dextran should be represented. The curves in Figs. 3.1 and 3.2 were generated by assuming that dextran too acts as a rigid rod. The radius of a dextran fiber (R_d = 0.33 nm) was estimated by using a monomer (α-D-glucopyranosyl residue) length of 0.47 nm, the specific volume of dextran of 0.61 mL/g (Bohrer, 1979), and a monomer molecular weight of 162 Da. The monomer length was estimated from an analysis performed by Arnott and Scott (Arnott and Scott, 1972) of atomic positions in α-D-glucose, based on a compilation of X-ray diffraction data. As seen in the plots, with these assumptions the excluded volume model predicted the observed trends fairly well. There were certain discrepancies at both agarose concentrations, but the overall agreement between the data and model suggests that dextran can be approximated as a second type of fiber.

A question that arises in modeling the bound dextran as a fiber is whether or not an extended dextran chain would be long enough to make end effects negligible in calculating the excluded volume, an assumption implicit in Eq. (3-3). Because the dextran chain is relatively thin (the cylindrical radius R_d is <12% of the Ficoll radius), each free end would exclude the

center of a Ficoll molecule from a volume that is nearly that of a hemisphere with radius r_i. With a monomer length of 0.47 nm, the contour lengths of a 500 kDa dextran (corresponding to M_W) and a 184 kDa dextran (corresponding to M_N) are calculated to be 1451 and 534 nm, respectively. For the largest Ficoll (where end effects would be proportionately greatest), the excluded volume due to two free ends of a dextran chain would be just 0.6% of the total for 500 kDa and 1.5% of the total for 184 kDa. For end effects to account for >5% of the excluded volume, the molecular weight would need to be <55 kDa. We conclude that, even though a certain amount of chain scission is likely to have occurred during the electron beam irradiation, end effects probably did not contribute significantly to the excluded volume.

An alternative model for the immobilized dextran is a water-filled coil, similar to what exists in free solution. The effective radius of such a coil for excluded volume purposes (a_d in Eq. (3-4)) was estimated from the partitioning data of Laurent (1963a, 1963b) for various proteins between water and dextran solutions. Results were given for cyanmethemoglobin, serum albumin, and γ-globulin, which range in Stokes radius from 3.1 to 5.5 nm, in 0-0.07 g/mL solutions of 450 kDa dextran (M_W), which is nearly identical to our dextran. We used only the data for dextran concentrations <0.025 g/mL, which we estimate as the critical concentration for chain overlap. (By comparison, the highest dextran concentrations in our 4% and 8% agarose gels were 0.012 and 0.018 g/mL, respectively.) Applying the excluded volume theory for dissimilar spherical molecules (Lazzara et al., 2000) to the eight relevant data points from Laurent (1963a, 1963b), we obtained a best-fit value of a_d = 11.1 nm. The fit to the Laurent results was excellent, with a root-mean-square error of just 2.4%. The "excluded volume radius" of 11.1 nm is somewhat smaller than either the radius of gyration (17.6 nm) or Stokes radius (14 nm) for this size of dextran (Nordmeier, 1993). Representing dextran as a sphere of 11.1 nm radius gave volume fractions that were an order of magnitude higher than those calculated for a rod of 0.33 nm radius. The values of ϕ_d used in the sphere and fiber models are summarized in Table 3.1.

Table 3.1 Agarose and Dextran Volume Fractions used in Partitioning Models.

Model	ϕ_a	ϕ_d (Low Dextran)	ϕ_d High Dextran
Fiber	0.040	0.0008	0.0076
	0.080	0.0008	0.0110
Sphere	0.040	0.0092	0.0870
	0.080	0.0092	0.1260

The ability of the two approaches to predict the effect of added dextran on Ficoll partitioning is compared in Figure 3.3. In this plot, the model predictions are the ordinate and the experimental results the abscissa. To focus on the effects of dextran, the predicted and measured partition coefficients are each normalized by the corresponding value in pure agarose. That is, each partition coefficient is expressed as a fraction of the agarose value (Φ_a). The 16 points for each model correspond to the 4 Ficoll sizes in each of 4 composite gels. As can be seen, the points for the fiber model cluster near the identity line. Although there was a tendency to underestimate the effects of dextran in the dilute gels (see also Figs. 3.1 and 3.2), the predictions were fairly accurate overall. In contrast, the points for the sphere model are all well above the identity line, indicating that the sphere model consistently underestimated the exclusion effect of dextran (i.e., overestimated the value of the Ficoll partition coefficient).

Although viewing the agarose-dextran gels as composites of randomly arranged coarse and fine fibers was quite effective in explaining the Ficoll partitioning results, especially in view of the simplicity of the model and the absence of fitted parameters, it does not account for certain aspects of agarose behavior. It has been found previously that electron beam irradiation of agarose gels increases their hydraulic (Darcy) permeability (White and Deen, 2002), and also increases the gel diffusivities of Ficolls and proteins, as discussed in section 2.3.3. Thus, irradiation apparently creates a more "open" structure. Comparisons of Ficoll partition coefficients measured in the present study, both in untreated agarose (data not shown) and irradiated agarose, suggest the same thing. That is, irradiation increased Φ_i by an average of 21±6%. An explanation of these effects of irradiation would require a more detailed model for the structure of agarose.

As noted at the outset, the agarose-dextran composite gels were developed as a possible experimental model for glomerular basement membrane (GBM). The present partitioning data, combined with diffusivities measured previously in identical gels (sections 2.3.3 and 2.3.4), permits certain comparisons to be made with GBM. A measure of the ability of a gel to hinder diffusion is the diffusivity of a test molecule in the gel divided by its value in free solution (K_d).

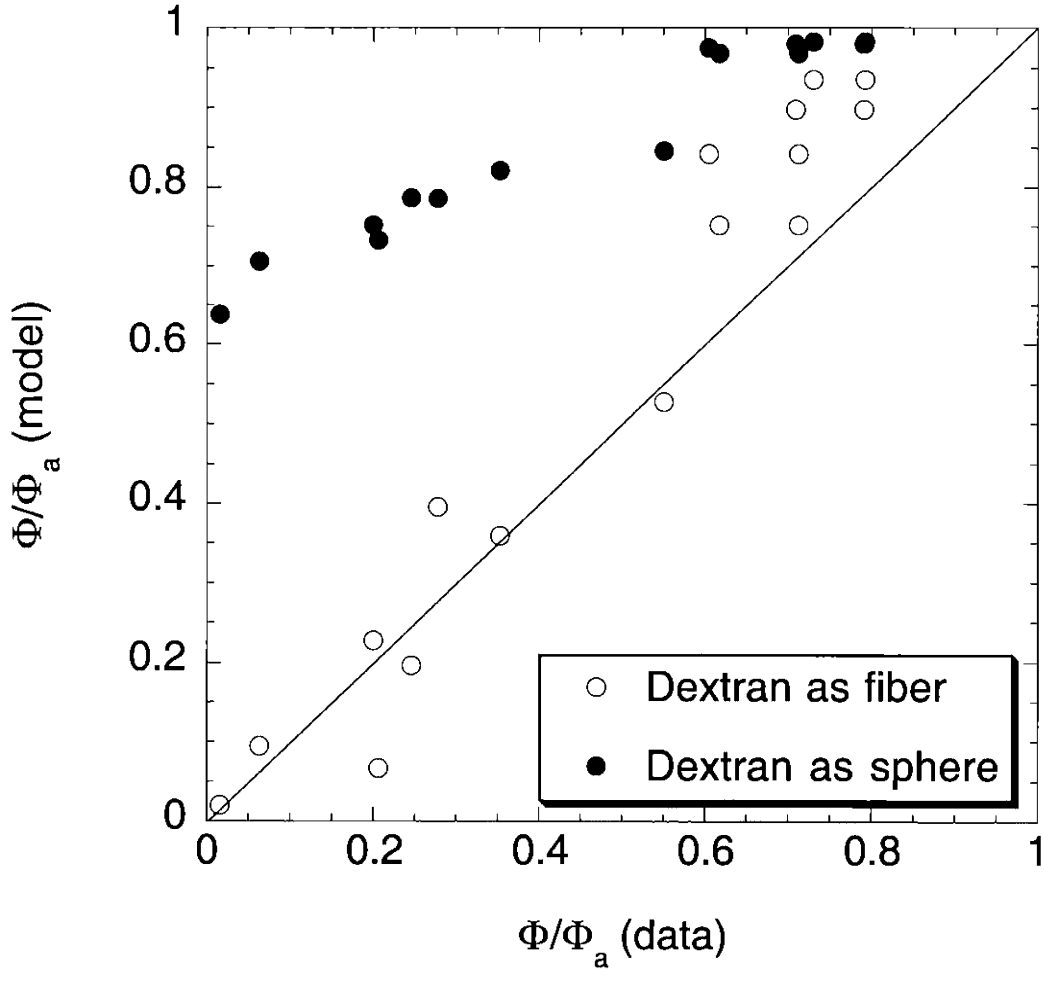

Figure 3.3 Ability of fiber and sphere models to predict the effects of immobilized dextran on Ficoll partitioning. Results are shown for four Ficoll fractions at each of two agarose concentrations (4% and 8%) and two dextran levels ("low" and "high"). Each measured or predicted partition coefficient (Φ) has been divided by the corresponding value in pure agarose (Φ_a). The fiber predictions were based on Eqs. (3-2) and (3-3) with parameter values as in Figs. 3.1 and 3.2; the sphere predictions were based on Eqs. (3-2) and (3-4) with a_d = 11.1 nm and the "sphere" volume fractions in Table 3.1.

The permeability of a gel membrane to a given solute is influenced by the partition coefficient as well as the diffusivity; in this case, the gel properties are embodied in the product, ΦK_d. As reviewed in Deen et al. (2001), measurements using isolated rat GBM have yielded estimates of ΦK_d for Ficolls of varying size. In choosing a suitable agarose-dextran gel for comparison, we note that a composite with $\phi_a = 0.08$ and $\phi_d = 0.01$ (i.e., 8% agarose with "high" dextran) has a total fiber volume fraction of 9%, similar to the 7-10% solid volume reported for GBM (Robinson and Walton, 1987; Comper et al., 1993). That agarose-dextran composite has been shown to have a Darcy permeability of 1.6-3.0 nm^2 (White and Deen, 2002) similar to the 1-2 nm^2 typically found for isolated GBM in vitro (Daniels et al., 1992; Edwards et al., 1997; Bolton et al., 1998). Accordingly, it is the one we selected for the comparison in Figure 3.4, in which values of ΦK_d are shown as a function of the Stokes radius of Ficoll. (Since K_d was not available for the 37 kDa Ficoll in agarose-dextran gels, that value of ΦK_d was calculated by interpolating the K_d results for the other Ficolls.) As may be seen, the values of ΦK_d in the agarose-dextran composite (circles) were quite similar to those found in GBM (i.e., cell-free glomeruli), either by confocal microscopy measurements of the diffusional permeability of narrow Ficoll fractions (squares, Edwards et al., 1997a), or by the analysis of sieving data obtained using polydisperse Ficoll (solid line, Bolton et al., 1998). That similarity supports the hypothesis that the permeability properties of GBM are determined primarily by its mixture of coarse and fine fibers. That is, its precise chemical composition seems to be secondary.

In conclusion, we showed that incorporating modest amounts of dextran into agarose gels significantly reduced the equilibrium partition coefficients of Ficolls. Those effects of dextran were predicted well by an excluded volume theory in which agarose fibrils were treated as coarse fibers and immobilized dextran chains as fine fibers. The ability of these agarose-dextran composite gels to mimic the hydraulic and diffusional permeability properties of GBM warrants further investigation of their transport properties. What has not been studied yet is the retardation experienced by macromolecules when there is bulk fluid flow (i.e., convective hindrances).

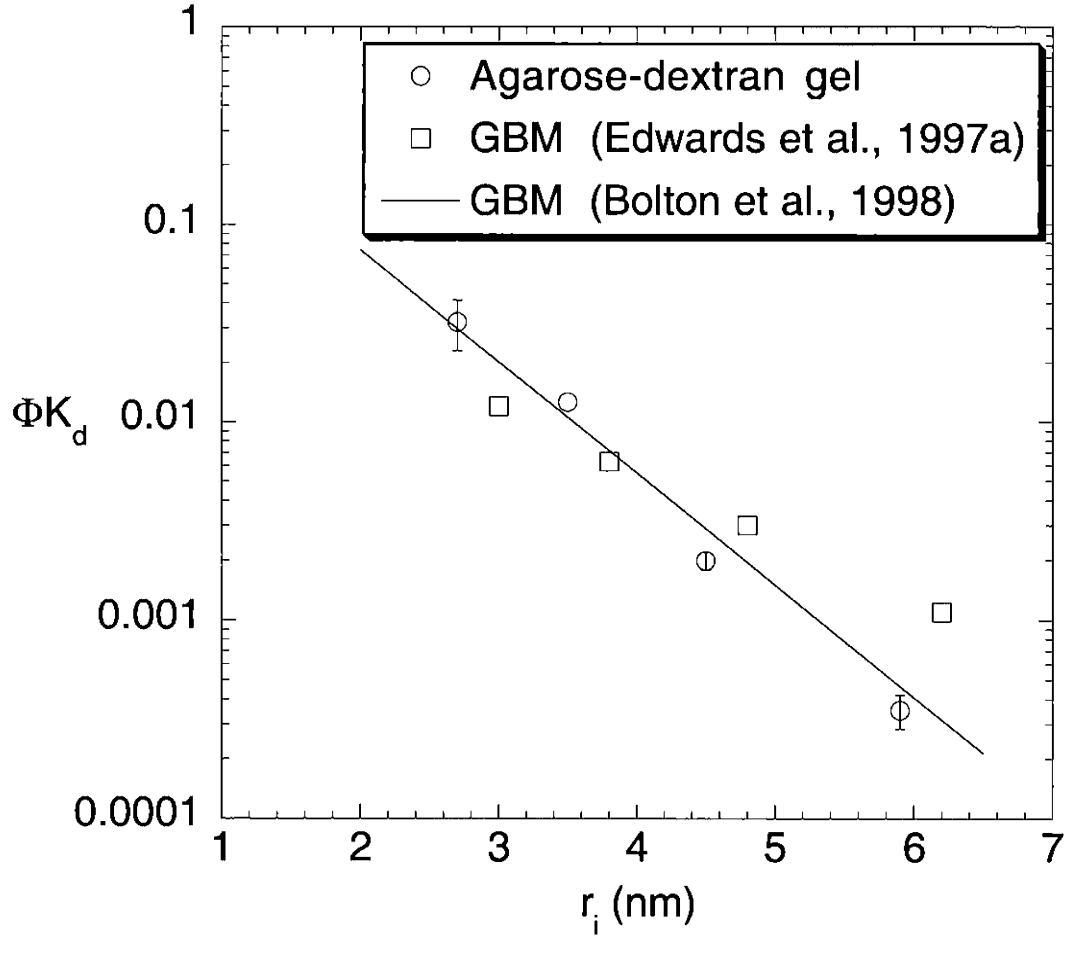

Figure 3.4 Comparison of Ficoll permeabilities of an agarose-dextran gel (8% agarose with "high" dextran) and isolated rat glomerular basement membrane (GBM). The permeability measure is the partition coefficient (Φ) times the gel-to-solution diffusivity ratio (K_d). The GBM results are based either on confocal microscopy measurements of Ficoll diffusion across segments of cell-free capillary wall (Edwards et al., 1997a) or Ficoll sieving across filters prepared from isolated GBM (Bolton et al., 1998).

4 Convection of Ficoll in Composite Hydrogels

4.1 Introduction

In the work presented here, sieving coefficients were measured at high Peclet number via ultrafiltration, for several sizes of Ficoll in agarose and agarose-dextran composite gels of varying composition. Experimental measurements of sieving in gels with monodisperse fiber radii are limited (Kapur et al., 1997; Johnston and Deen, 1999; 2002). To our knowledge, this is the first experimental study of convective hindrance in a synthetic composite gel. This hindered convection study complements previous investigations of Darcy permeability (White and Deen, 2002), hindered diffusion (chapter 2), and partitioning (chapter 3) in agarose-dextran composite gels that have similar hydraulic and diffusional permeabilities as those of the GBM.

4.2 Materials and Methods

4.2.1 Test Macromolecules

Four narrow fractions of Ficoll, with weight-average molecular weights (M_W) of 21, 37, 61, and 105 kDa, were special-ordered from Pharmacia LKB (Piscataway, NJ). Based on information from the manufacturer, the polydispersity index (M_W/M_N, where M_N is number-average molecular weight) was 1.22, 1.18, 1.15, and 1.13, respectively. As detailed in section 2.2.4, the Ficoll fractions were labeled with dichlorotryazinyl amino fluorescein (DTAF) (Sigma, St. Louis, MO). These are the same fluoresceinated Ficolls as used in the diffusion and partitioning studies discussed in chapters 2 and 3. Size exclusion chromatography of the Ficoll samples using Superdex 200 (Pharmacia Biotech, Piscataway, NJ) showed no evidence of free fluorescein. The fluorescence recovery after photobleaching results from section 2.3.2 detail the free-solution diffusivity ($D_{i\infty}$) of each Ficoll, from which the Stokes-Einstein radii (r_s) was

calculated as 2.7, 3.5, 4.5, and 5.9 nm for the 21, 37, 61, and 105 kDa narrow fractions of Ficoll, respectively. Those values differ by only 0.2-9.5% from measurements of corresponding unlabeled samples using quasielastic light scattering (Oliver et al., 1992). Dilute aqueous solutions were made by dissolving each Ficoll in a 0.01 M sodium phosphate, 0.1 M potassium chloride buffer at pH 7.0. In all cases, the concentration of the Ficoll solution was 0.02 mg/mL.

4.2.2 Gel Preparation

The gel synthesis procedure was very similar to that described in section 2.2.1. Agarose (Type IV; Sigma, St. Louis, MO) was dissolved in KCl-phosphate buffer (0.1 M KCl and 0.01 M sodium phosphate at pH 7.0) and heated in a 90°C oven for 4-6 h until it was completely dissolved. The hot agarose solution was poured carefully onto a 2.5 cm diameter woven polyester support (catalog #148 248; Spectrum Laboratories Inc., Rancho Dominguez, CA) that was placed on a heated glass plate. The mesh fibers in the support formed square openings of 43 μm and had a thickness of 70 μm, with 29% open area. After placing a second hot glass plate on top, the sample was cooled to room temperature and immersed in buffer overnight at 7°C. The gels to which dextran was to be added were immersed in 500 kDa dextran (Sigma, St. Louis, MO) solutions of either 50 or 150 mg/mL for at least 24 h, which greatly exceeds the diffusional equilibration time calculated from reported diffusivities for dextran in agarose (Key and Sellen, 1982). A 2 Mrad exposure to an electron beam (High Voltage Research Laboratory at Massachusetts Institute of Technology) was used to covalently link the dextran to the agarose. Following irradiation, each gel was equilibrated with a large volume of buffer (2 mL, as compared to a typical gel volume of 0.025 mL) to remove any unattached dextran. The agarose concentrations of 4.1 and 8.2% (w/v) were converted to volume fractions (ϕ_a) by dividing by 1.025 (Johnson et al., 1995); that is, $\phi_a = 0.04$ or 0.08. The volume fractions of immobilized dextran (ϕ_d), detailed in section 2.3.1, ranged from 0.0008 to 0.011.

4.2.3 Darcy Permeability

The Darcy permeability (κ) of each mesh-reinforced gel was measured as described in section 2.2.3. The gel membrane was placed in a 10 mL ultrafiltration cell (Millipore, Bedford, MA) that was filled with the KCl-phosphate buffer and pressurized to between 0.69 and 30.6 kPa, using nitrogen. These pressures were chosen, as discussed below, to ensure that the high Peclet number limit (Eq. (1-14)) would apply in determining the sieving coefficient. Samples of filtrate collected over timed intervals were weighed to determine the volume flow rate (Q). The gel thickness (δ), measured by confining the membrane between two microscope slides of known thickness and using a micrometer, ranged from 70 to 150 μm. From these measurements, κ was calculated as

$$\kappa = \frac{\mu Q \delta}{\beta A \Delta P} \tag{4-1}$$

where μ is the viscosity of water, A is the exposed membrane area, ΔP is the pressure drop, and β is a correction factor that accounts for the increased flow resistance due to the polyester mesh support. That factor, which increases with δ (Johnson and Deen, 1996b), ranged from 0.41 to 0.59 in these experiments.

4.2.4 Sieving

Following the Darcy permeability measurement, the apparent sieving coefficient (Θ') of each gel was determined. The ultrafiltration cell, filled with buffer from the Darcy permeability measurement, was emptied and refilled with a solution of 0.02 mg/mL of one of the fluoresceinated Ficolls. The stirring rod was set at approximately 220 rpm, as indicated by an optical tachometer, and the cell was repressurized. The cell was equilibrated and the collection line purged for 40 to 90 minutes, which was about 1.5 - 3 times the period required for purging, followed by a period of 40 to 90 minutes during which the filtrate was collected. The

concentrations of the filtrate (C_f) and the initial and final bulk retentate (C_{bi} and C_{bf}, respectively) solutions were linearly proportional to fluorescence intensity, which was measured using a spectrofluorometric detector (Shimadzu, Columbia, MD) with excitation at 488 nm and emission detection at 515 nm. The apparent sieving coefficient was calculated from the measured bulk retentate and filtrate concentrations as

$$\Theta' = \frac{C_f}{0.5(C_{bi} + C_{bf})} \tag{4-2}$$

The initial and final retentate concentrations differed by a maximum of 14%. The Ficoll mass balance is given by

$$V_{bi}C_{bi} = 0.5(C_{bi} + C_{bf})(V_{bi} - V_f) + C_f V_f \tag{4-3}$$

where V_{bi} is the initial volume of bulk retentate, and V_f is the total volume of filtrate collected during both the equilibration and measurement periods. It was typically closed to within 1% and was never off by more than 3%.

The apparent sieving coefficient was greater than the true sieving coefficient (Θ), which is given by

$$\Theta = \frac{C_f}{C_m} \tag{4-4}$$

due to concentration polarization at the surface of the membrane, which creates an increase in the concentration at the upstream membrane surface (C_m) compared to that of the bulk retentate (C_b). Concentration polarization in the ultrafiltration cell used in the present study has been described in detail by Johnston et al. (2001). They modeled flow in the ultrafiltration system using laminar boundary layer theory based on rigid body rotation above a stationary surface (Bödewadt flow)

and compared those rigorous results with that of simpler global and local stagnant film representations.

The local stagnant film model (hybrid model), developed by Johnston et al. (2001), is based on the assumption that stagnant film theory is locally applicable, but it allows the mass transfer coefficient (k_{sf}), and hence the film thickness, to vary with radial position so the average can be computed rigorously. An expression for the local mass transfer coefficient in the absence of filtration was determined from a least squares fit to the numerical results of the boundary layer theory. The boundary layer model predictions were validated previously for BSA in a 10 ml ultrafiltration cell identical to the one used here, given that the angular velocity (γ) of the fluid in the cell was 0.36 times the angular velocity of the stirrer (γ_s) (Johnston et al., 2001). It was expected that the stirring velocity exceed that of the liquid in order to balance the torque on the fluid from the sides and bottom of the ultrafiltration cell. For negligible osmotic pressure, the hybrid model predicted values of Θ that differed from the boundary layer theory predictions by a maximum of 15% for dimensionless filtration velocity (α) ranging from 0 to 1. The dimensionless filtration velocity is defined as

$$\alpha = \frac{v}{\sqrt{\nu_k \gamma}} Sc^{\frac{2}{3}} \tag{4-5}$$

where ν_k is the kinematic viscosity. For $\alpha = 0$ to 0.4, which was typical in this study, the hybrid model produces almost identical sieving coefficient predictions as those of the full boundary layer model, but with less computational complexity. Consequently, the hybrid model was used to correct for concentration polarization according to Eqs. (4-5) - (4-8). As detailed in Johnston et al. (2001), the hybrid model yields

$$\frac{\Theta'}{\Theta} = 2\int_0^1 \frac{B(Y)(1-Y)}{1-\Theta[1-B(Y)]} dY \tag{4-6}$$

where $$Y = 1 - \frac{r}{R} \tag{4-7}$$

and $$B(Y) \equiv \frac{C_m(Y) - C_f(Y)}{C_b - C_f(Y)} = \exp\left[\frac{\alpha}{0.6381Y^{-1/3} - 0.410Y}\right] \tag{4-8}$$

where r is the radial coordinate, R is the radius of the membrane, and Y is the reversed dimensionless radial coordinate. The expression in the denominator of the exponential in $B(Y)$ determines k_{sf} based on the least squares fit to the boundary layer theory, as discussed above. Using iteration, Eq. (4-6) was numerically integrated to determine the value of Θ that made the equality true for a given measurement of Θ'.

Using the concentration of Ficoll at the membrane surface in the van't Hoff equation, the osmotic pressure was found to be negligible compared with the applied transmembrane pressure. Based on C_m, the osmotic pressure was at most 0.45% of ΔP, which corresponded to the smallest Ficoll and the most permeable, least concentrated gel (4% agarose with no dextran), where the least pressure was applied to the system. With negligible osmotic pressure, concentration polarization has no effect on the filtrate velocity, making it independent of radial position, a requirement of Eqs. (4-5) - (4-8).

Since the osmotic pressure was negligible, the Darcy permeability could also be determined during the sieving experiment and compared with the measurement performed prior to sieving to ensure that the properties of the gel had not changed significantly. The two measurements of Darcy permeability generally differed by less than 10%. As discussed below, this variation was an effect of the time period over which the gel was subjected to flow. Additionally, the fluctuation was less than the gel-to-gel Darcy permeability fluctuations.

As discussed in section 1.2.2.3, as the flow velocity through the gel increases from zero, Θ decreases from 1 to the high Pe limit given by Eq. (1-14). To ensure that Eq. (1-14) was valid,

the pressure (flow velocity) was doubled in a series of sieving experiments performed on the same gel, until the true sieving coefficient leveled off to a constant value. This check was performed for the smallest and the largest Ficoll in both the 4% and 8% agarose gels with zero and high dextran concentration.

4.3 RESULTS

4.3.1 Darcy Permeability

The average Darcy permeabilities in each of the six gel compositions are detailed in Table 4.1. The present results are very similar with those obtained in section 2.3.5 and those previously measured in gels prepared by the same method (White and Deen, 2002). As shown in Fig. 4.1, which plots κ for the 4% and 8% agarose gels, each with zero, high, and low dextran levels, versus ΔP, the Darcy permeability was shown to be independent of the applied transmembrane pressure. The Darcy permeability in the gels containing dextran did often increase slightly over the time, but generally by less than 10%. This minor increase was possibly due to the loss of a small amount of dextran that was physically entangled within the agarose gel, but not chemically crosslinked. As discussed later, for all but the smallest κ, a 10% change in κ results in a much smaller change in the measured Θ. For both agarose concentrations, κ decreased by an order of magnitude as the dextran concentration was increased from zero to its maximum value.

Table 4.1 Darcy Permeabilities of Composite Gels. κ is given as the mean ± standard error for 15 samples in gels with $\phi_a = 0.08$, $\phi_d = 0.011$, 13 samples in gels with $\phi_a = 0.08$, $\phi_d = 0$, and 12 samples for the remaining gel compositions.

ϕ_a	ϕ_d	ΔP (kPa)	v (10^{-5} cm/s)	κ (nm^2)
0.04	0	0.69 ± 0.02	11.0 ± 0.5	264.1 ± 9.8
	0.0008	1.81 ± 0.02	12.7 ± 0.6	110.2 ± 4.2
	0.0076	7.20 ± 0.06	9.2 ± 0.7	19.5 ± 1.4
0.08	0	7.00 ± 0.08	12.1 ± 0.7	34.1 ± 1.9
	0.0008	9.97 ± 0.05	8.1 ± 0.3	16.1 ± 0.5
	0.011	30.60 ± 0.06	4.8 ± 0.2	2.9 ± 0.1

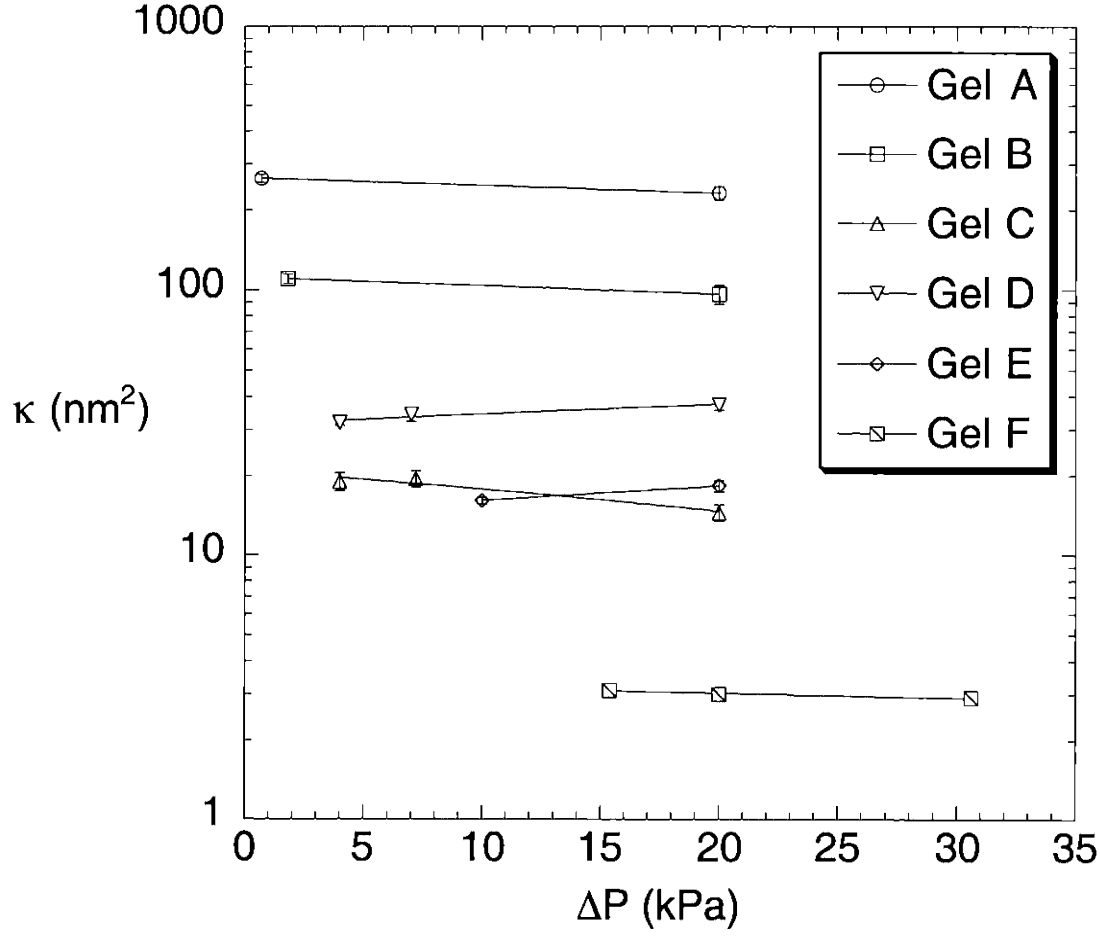

Figure 4.1 Darcy permeability (κ) of agarose and agarose-dextran gels, as a function of the applied transmembrane pressure (ΔP). Results are shown for six different gel compositions, namely; $\phi_a = 0.040$, $\phi_d = 0$ (Gel A), $\phi_a = 0.040$, $\phi_d = 0.0008$ (Gel B), $\phi_a = 0.040$, $\phi_d = 0.0076$ (Gel C), $\phi_a = 0.080$, $\phi_d = 0$ (Gel D), $\phi_a = 0.080$, $\phi_d = 0.0008$ (Gel E), and $\phi_a = 0.080$, $\phi_d = 0.011$ (Gel F).

4.3.2 Sieving

As mentioned above, in each gel, $\Theta = \Phi K_c$, since all sieving experiments were performed with a pressure high enough to ensure that the flow through the gel was purely convective. The results of sieving experiments performed at increasing pressures are shown in Fig. 4.2 for several representative gel compositions using either the smallest or largest Ficoll size. The apparent or actual sieving coefficients are plotted versus the filtrate velocity. As the filtrate velocity was doubled, Θ remained relatively constant, illustrating that the high Peclet number limit had been reached.

Figure 4.2 also shows that the concentration polarization correction, Eqs. (4-5) - (4-8), was accurate, as evidenced by significant increases in the value of Θ' with each increase in filtrate velocity as concentration polarization became increasingly important. The effects of the concentration polarization correction were moderate, resulting in values of Θ that were an average of 9% less than Θ'. The correction became greater as the macromolecule size or gel concentration increased (i.e. Θ' decreased) or as filtrate velocity increased. The maximum concentration polarization correction was needed for the largest Ficoll sieving through the 4% agarose gel with high dextran, where Θ' exceeded Θ by and average of 29%.

The true sieving coefficients of the four narrow Ficoll fractions, measured in 4% and 8% agarose gels, are shown in Figs. 4.3 and 4.4, respectively. They are also given in Table 4.2 along with their corresponding uncorrected values. In each case, Θ is plotted as a function of the Stokes-Einstein radius of the Ficoll, with results given for pure agarose (irradiated as done in preparing the composite gels) and for composite gels with low and high levels of dextran. As seen in either plot, Θ tended to decrease as Ficoll size increased or as more dextran was linked to a given amount of agarose. A comparison of the data for pure (dextran-free) 4% and 8% agarose shows that Θ also decreased as the agarose concentration increased. The "low" and "high" dextran data in the two plots are not directly comparable, because there are differences in the dextran concentrations incorporated into the 4% and 8% agarose gels, as noted in Table 4.1.

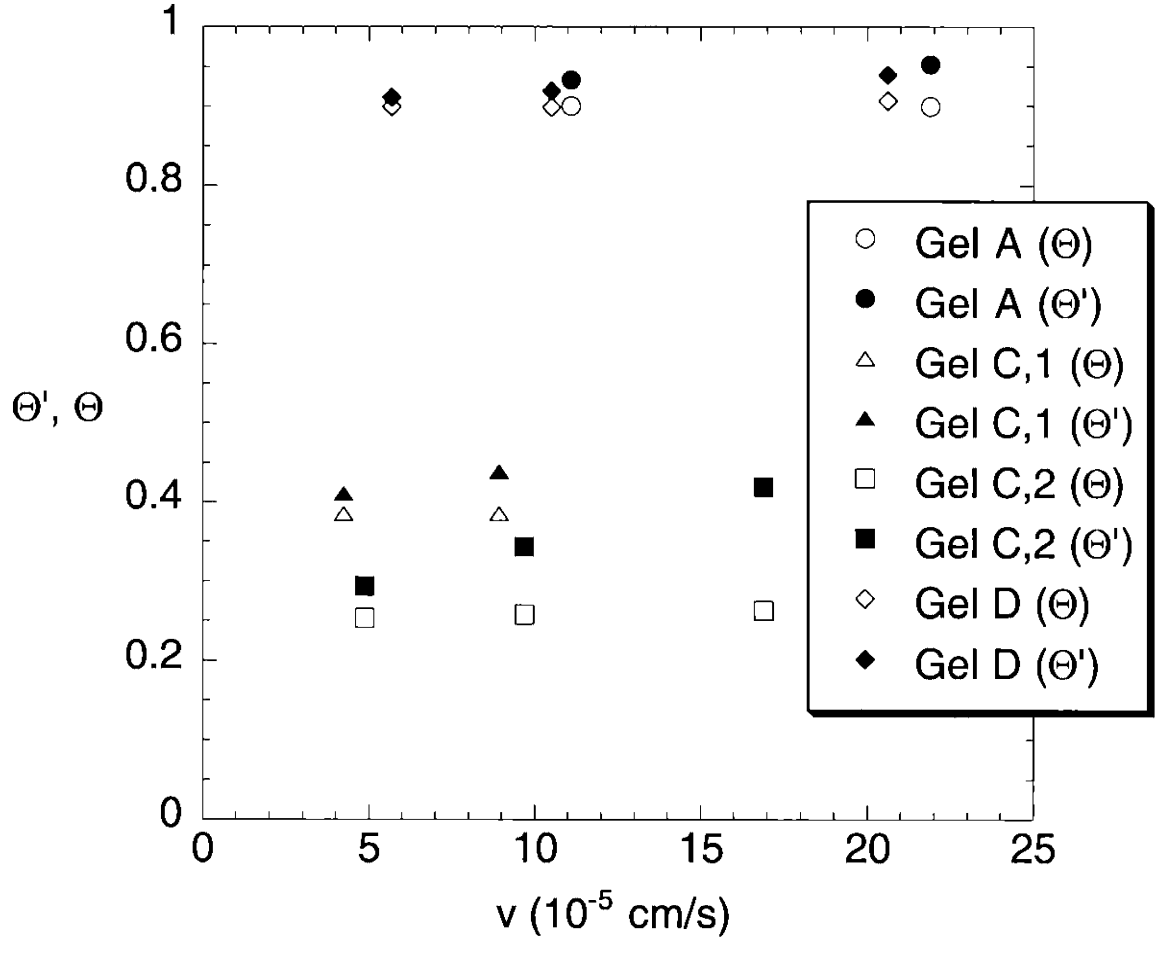

Figure 4.2 Apparent and actual sieving coefficients (Θ' and Θ, respectively) measured in gels with $\phi_a = 0.040$, $\phi_d = 0$ (Gel A), $\phi_a = 0.040$, $\phi_d = 0.0076$ (Gel C), and $\phi_a = 0.080$, $\phi_d = 0$ (Gel D) for several different filtrate velocities, performed in series on the same gel sample. For Gel C, results are shown for two different samples, as indicated.

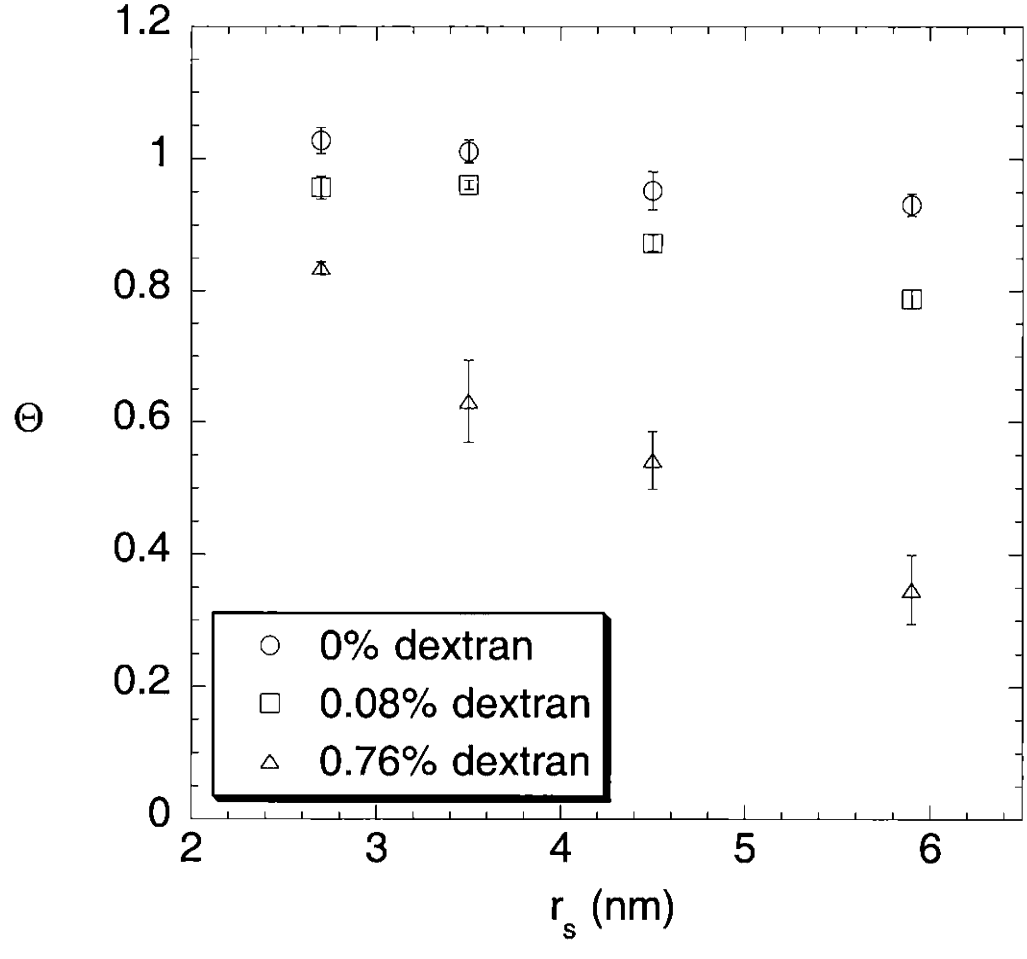

Figure 4.3 True sieving coefficients (Θ) of Ficolls, as a function of Stokes-Einstein radius (r_s), in 4% agarose gels containing varying amounts of dextran. Data are shown for four Ficoll fractions as the mean ± standard error for 3 samples.

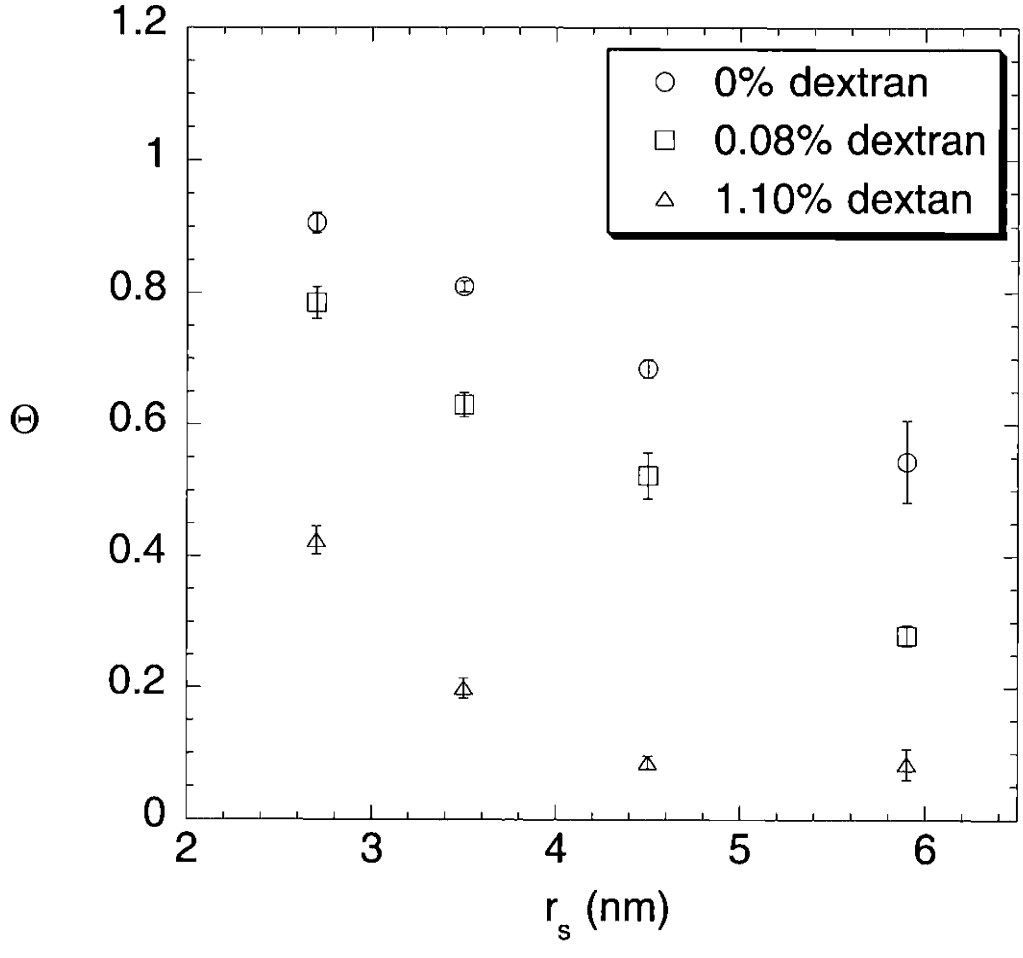

Figure 4.4 True sieving coefficients (Θ) of Ficolls, as a function of Stokes-Einstein radius (r_s), in 8% agarose gels containing varying amounts of dextran. Data are shown for four Ficoll fractions as the mean ± standard error for 3 - 6 samples.

Table 4.2a Sieving Coefficients and Darcy Permeabilities for 4% Agarose Composite Gels. κ, Θ', and Θ are given as the mean ± standard error for 3 samples.

ϕ_d	r_s (nm)	κ (nm^2)	Θ'	Θ
0	2.7	230.9 ± 10.3	1.03 ± 0.02	1.03 ± 0.02
	3.5	243.8 ± 14.9	1.01 ± 0.02	1.01 ± 0.02
	4.5	296.1 ± 12.5	0.97 ± 0.01	0.95 ± .03
	5.9	285.5 ± 11.3	0.95 ± 0.01	0.93 ± 0.02
0.0008	2.7	103.7 ±8.0	0.97 ± 0.01	0.96 ± 0.02
	3.5	113.8 ± 9.6	0.97 ± 0.01	0.96 ± 0.01
	4.5	115.6 ± 2.0	0.92 ± 0.01	0.87 ± 0.01
	5.9	107.7 ± 13.3	0.86 ± 0.02	0.79 ± 0.02
0.0076	2.7	19.2 ± 2.7	0.87 ± 0.01	0.84 ± 0.01
	3.5	20.2 ± 3.8	0.69 ± 0.06	0.63 ± 0.06
	4.5	17.6 ± 3.1	0.61 ± 0.05	0.54 ± 0.04
	5.9	21.0 ± 2.5	0.45 ± 0.06	0.35 ± 0.05

Table 4.2b Sieving Coefficients and Darcy Permeabilities for 8% Agarose Composite Gels. κ, Θ', and Θ are given as the mean ± standard error for 3-6 samples.

ϕ_d	r_s (nm)	κ (nm^2)	Θ'	Θ
0	2.7	31.9 ± 0.9	0.92 ± 0.01	0.91 ± 0.02
	3.5	38.4 ± 5.2	0.86 ± 0.00	0.81 ± 0.01
	4.5	29.2 ± 1.6	0.76 ± 0.01	0.69 ± 0.01
	5.9	36.8 ± 6.8	0.66 ± 0.06	0.54 ± 0.06
0.0008	2.7	16.9 ± 1.2	0.82 ± 0.02	0.79 ± 0.02
	3.5	15.7 ± 1.1	0.68 ± 0.01	0.63 ± 0.02
	4.5	18.7 ± 2.6	0.59 ± 0.03	0.52 ± 0.04
	5.9	15.4 ± 1.0	0.35 ± 0.02	0.28 ± 0.02
0.011	2.7	2.76 ± 0.1	0.45 ± 0.02	0.43 ± 0.02
	3.5	3.0 ± 0.1	0.22 ± 0.02	0.20 ± 0.02
	4.5	2.9 ± 0.2	0.10 ± 0.01	0.09 ± 0.01
	5.9	3.2 ± 0.2	0.10 ± 0.03	0.08 ± 0.02

4.4 DISCUSSION

4.4.1 Darcy Permeability as an Indicator of Hindered Convection in Agarose Based Gels

In agarose and agarose-dextran gels similar to those studied here, Darcy permeability has previously been shown to reflect the multi-body hydrodynamic interactions between a diffusing macromolecule and a fixed fiber matrix. As discussed in section 2.4, the effect of dextran on K_d (ratio of the macromolecular diffusivity in the gel to that in free solution) was largely explained using an effective medium model that was a function only of κ and r_s. The ability of κ to capture the effects of dextran on K_d, suggests that perhaps κ can also be used to predict ΦK_c. In Fig. 4.5, ΦK_c is plotted as a function of κ for various sizes of macromolecules in the irradiated agarose and agarose-dextran composite gels. It indicates that the rate of approach to $\Phi K_c \sim 1$ decreased as the size of the macromolecule increased. For a given size of macromolecule, sieving through gels with similar κ resulted in similar ΦK_c, despite the fact that the gels varied in agarose and dextran content. The dependence of ΦK_c on κ is particularly evident in the 4% agarose, 0.76% dextran gels and the 8% agarose, 1.1% dextran gels which had very similar Darcy permeabilities and were characterized by similar ΦK_c for a given r_s.

Also included in Fig. 4.5 are curves based on theoretical predictions of K_c, κ, and Φ calculated for flow normal to a square array of parallel fibers. This fiber arrangement was used because the only available convective hindrance theory developed specifically for fibrous media (Phillips et al., 1990) is based upon a parallel fiber array. The four theoretical curves correspond to r_s of 2.7, 3.5, 4.5, and 5.9 nm and an agarose fiber radius of 1.6 nm (Lazzara and Deen, 2004). Interestingly, the theory predicts ΦK_c relatively accurately despite the fact that it is based on convection normal to a square array of parallel fibers, rather than a random fiber matrix that more closely resembles the gel structure. Both the data and theory indicate that at very small

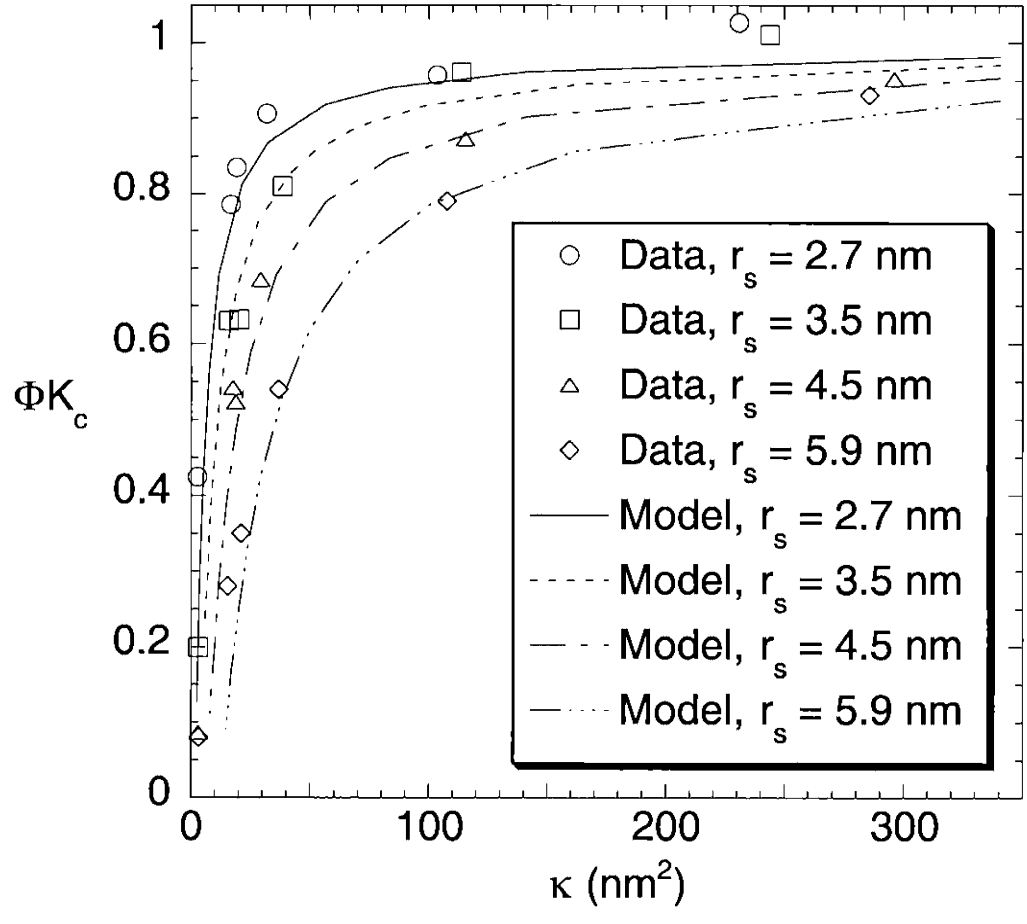

Figure 4.5 Convective hindrances of Ficoll in irradiated agarose and agarose-dextran composite gels. The ordinate is the product of the partition coefficient (Φ) and the ratio of solute velocity in the gel to the superficial fluid velocity (K_c). The abscissa is the Darcy permeability (κ). The theoretical curves are based on the model of Phillips et al. (1990) for flow normal to square arrays of parallel fibers.

Darcy permeabilities, ΦK_c will be quite sensitive to changes in κ. As κ increases, ΦK_c becomes increasingly insensitive to variations in κ.

For the theoretical curves K_c, κ, and Φ were calculated as detailed below, with the ratio λ given as the solute radius divided by the fiber radius. For arrays of bead-and-string fibers of radius r_f and volume fraction ϕ^*

$$K_c = 1 + B\phi^* + \Gamma\phi^{*2} \tag{4-9}$$

where

$$B = 5.1712 - 0.9724\left(\frac{1}{\lambda}\right) - 1.1355\left(\frac{1}{\lambda}\right)^2 + 0.2511\left(\frac{1}{\lambda}\right)^3 \tag{4-10a}$$

$$\Gamma = -9.97883 + 8.9787\lambda - 31.6717(\lambda)^2 - 2.9586(\lambda)^3 \tag{4-10b}$$

Eqs. (4-9) and (4-10) are correlations derived by Phillips et al. (1990) to fit their results for $0.5 \leq \lambda \leq 5$ over various ϕ^* ranges, so the fits are not necessarily accurate outside those ranges.

Phillips et al. (1989; 1990) base their calculations on bead-and-string fibers, but note that the Darcy permeability predicted in an array of their bead-and-string fibers is very similar to that predicted from models based on an array of cylindrical fibers. Replotting their data versus fiber spacing or fiber volume fraction, the agreement was noticeably better when equal fiber spacing was assumed rather than equal volume fraction. The volume fraction of beads in a fiber (ϕ^*) was 0.65 times the volume fraction of the corresponding cylindrical fiber (ϕ), for a dimensionless distance between beads within a fiber (d) of 0.05, as used by Phillips et al. (1990). That is,

$$\phi^* = 0.65\phi \tag{4-11}$$

where

$$\phi^* = \frac{\frac{4}{3}\pi}{(2+d)l^2} \tag{4-12}$$

$$\phi = \frac{\pi}{l^2} \tag{4-13}$$

The dimensionless distances d and l (the distance between the centers of adjacent fibers) were made dimensionless using r_f.

The Darcy permeability corresponding to the value of K_c predicted from the bead-and-string model was calculated for water flow normal to a square array of parallel cylindrical fibers, which was given by Sangani and Acrivos (1982) as

$$\kappa = \frac{r_f^2}{8\phi}(-\ln\phi - 1.476 + 2\phi - 1.774\phi^2 + 4.076\phi^3 + O(\phi^4)) \tag{4-14}$$

In order to compare the predictions for K_c and κ with the present data, Φ was calculated using an expression derived from excluded volume theory (Lazzara et al., 2000). Since the r_s of interest were all at least 1.7 times r_f, the bead-and-string fibers with spacing between beads of $0.05r_f$ will have approximately the same excluded volume per unit length as a cylinder with radius r_f, resulting in

$$\Phi = 1 - \phi(1+\lambda)^2 \tag{4-15}$$

4.4.2 Darcy Permeability as an Indicator of Hindered Diffusion in Agarose Based Gels

The correlation between ΦK_c and κ in gels of different compositions and for theoretical predictions based on a parallel fiber arrays motivates investigation of similar parameters in hindered diffusion. Johnson, E. M. et al. (1996) measured K_d in unirradiated agarose gels with volume fractions of 0.038, 0.055, and 0.072. For the unirradiated agarose (Johnson, E. M. et al., 1996) and irradiated agarose and agarose-dextran gels, K_d are compared with κ in Fig. 4.6. For a

given macromolecular size, K_d in the irradiated and unirradiated agarose and agarose-dextran gels varied similarly with κ. The curves in Fig. 4.6 are the predictions of two different fiber matrix theories, which are detailed below. The agreement between the different fiber theories is impressive considering that one is based on a square array of parallel fibers, while the other models diffusion through a three-dimensional random fiber matrix.

The diffusive hindrances used to derive the dashed curves in Fig. 4.6 are from Phillips et al. (1990), which are given by

$$K_d = \exp(-A\phi^{\frac{3}{4}}) \tag{4-16}$$

where

$$A = 5.1768 - 4.0075\lambda + 5.4388(\lambda)^2 - 0.6081(\lambda)^3 \tag{4-17}$$

Equations (4-16) and (4-17) describe macromolecular diffusion through a square array of parallel fibers. As in Fig. 4.5, for the Phillips et al. (1990) model curve, κ is calculated using the expression of Sangani and Acrivos (1982), Eq. (4-14).

The solid curves predict relative macromolecular diffusivities in a three-dimensional random cylindrical fiber matrix (Phillips, 2000) based on their corresponding κ. The values of K_d are given by

$$K_d = \exp(-0.84 f^{1.09})\exp(-a\phi^b) \tag{4-18}$$

where

$$f = (1+\lambda)^2\phi \tag{4-19a}$$

$$a = 3.727 - 2.460\frac{1}{\lambda} + 0.822\left(\frac{1}{\lambda}\right)^2 \tag{4-19b}$$

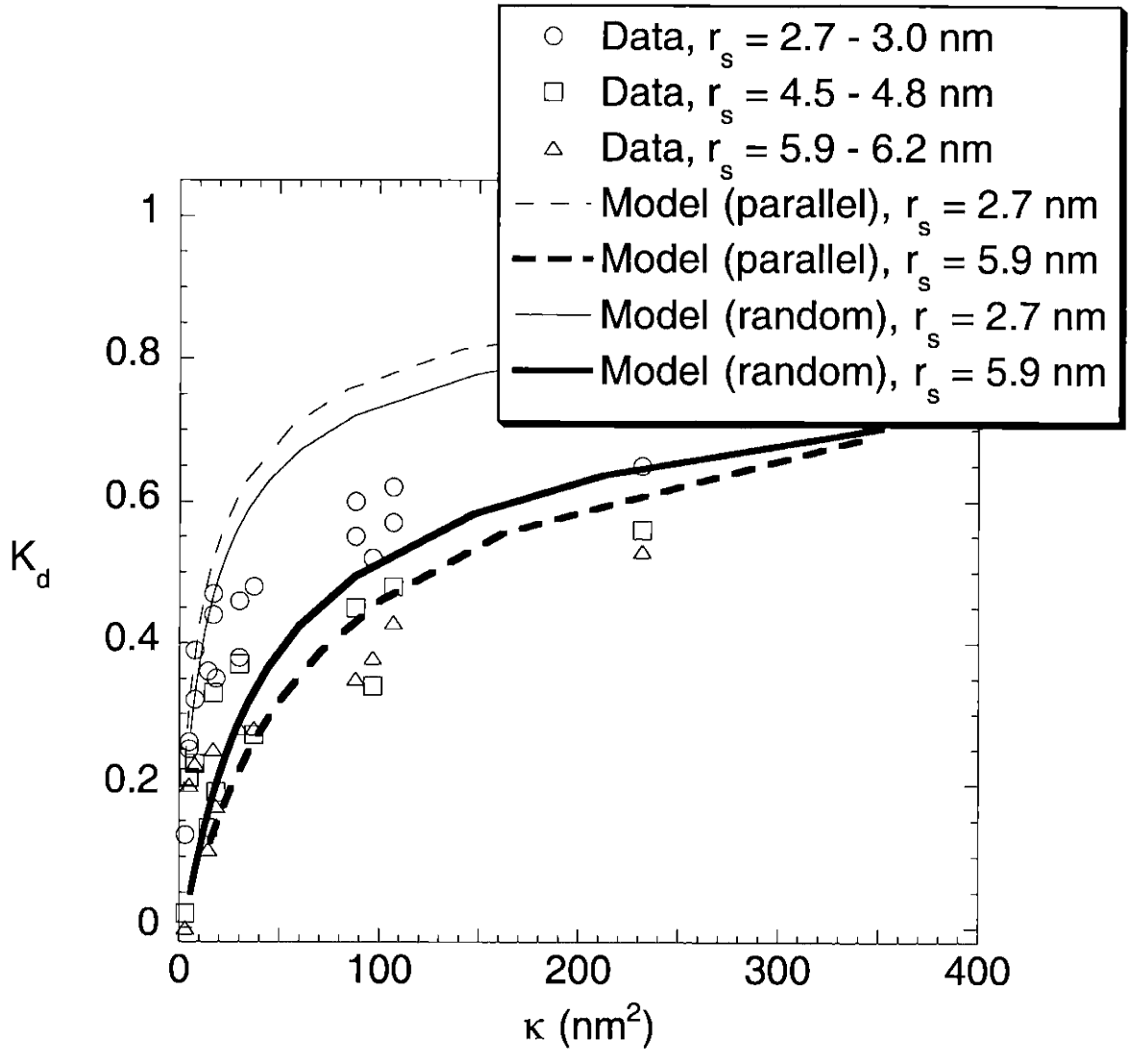

Figure 4.6 Comparison of the diffusive hindrance factor (K_d) for proteins and Ficoll in unirradiated agarose gels (Johnson, E. M. et al., 1996) and Ficoll in irradiated agarose and agarose-dextran gels, as a function of Darcy permeability (κ). The two sets of theoretical curves predict diffusive hindrances in square arrays of parallel fibers (Phillips et al., 1990) (dashed curves) and three-dimensional random fiber arrays (Phillips, 2000) (solid curves).

$$b = 0.358 + 0.366\frac{1}{\lambda} - 0.0939\left(\frac{1}{\lambda}\right)^2 \tag{4-19c}$$

The corresponding κ model for the random fiber matrix, developed by Clague and Phillips (1997), gives inverse κ as a weighted average of the inverse Darcy permeabilities for flow parallel to (κ_p) and normal to (κ_t) fibers in a square array at volume fractions of $\phi/3$ and $2\phi/3$, respectively. That is,

$$\frac{1}{\kappa} = \frac{1}{\kappa_p(\phi/3)} + \frac{1}{\kappa_t(2\phi/3)} \tag{4-20}$$

The models for flow parallel to and normal to fibers in a square array are given by Drummond and Tahir (1984) as

$$\kappa = \frac{r_f^2}{4\phi}\left(-\ln(\phi) - 1.476 + 2\phi - \frac{\phi^2}{2} + O(\phi^4)\right) \tag{4-21}$$

and by Eq. (4-14), respectively.

A comparison of ΦK_d versus κ is shown in Fig. 4.7 for experimentally determined Φ (section 3.3) and K_d (sections 2.3.3 and 2.3.4) in gels similar in composition and preparation as those used here. As in Fig. 4.6, the curves in Fig. 4.7 are from Phillips et al. (1990) (dashed curves) and Phillips (2000) (solid curves) but with theoretical predictions for Φ calculated according to Eq. (4-15) and Eq. (4-22), respectively. Equation (4-22), developed by Ogston (1958) for partitioning of macromolecules in a random fiber matrix, is

$$\Phi = \exp\left[-\phi(1+\lambda)^2\right] \tag{4-22}$$

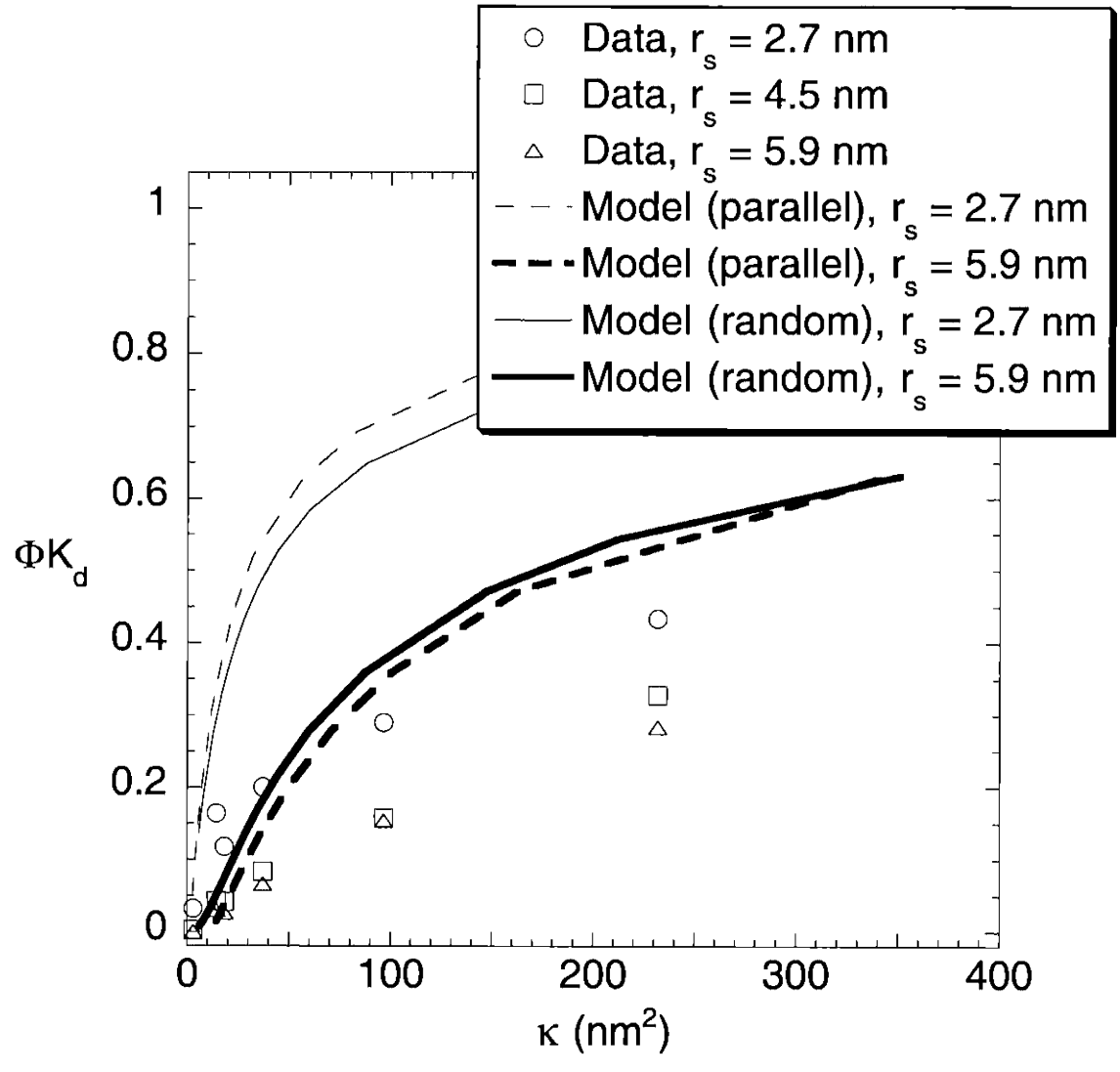

Figure 4.7 Comparison of the diffusive hindrance factor (K_d) times the partition coefficient (Φ) for Ficoll in irradiated agarose and agarose-dextran gels, as a function of Darcy permeability (κ). The two sets of theoretical curves predict diffusive hindrances in square arrays of parallel fibers (Phillips et al., 1990) (dashed curves) and three-dimensional random fiber arrays (Phillips, 2000) (solid curves) with Φ predicted by Eq. (4-15) and (4-22), respectively.

The agreement between the two theories remains good. However, both theories greatly overpredict ΦK_d in the agarose and agarose-dextran gels at all values of r_s. Additionally, a comparison of Figs. 4.5 and 4.7 indicates that ΦK_c is more sensitive to κ than is ΦK_d.

4.4.3 Hindered Convection in Polyacrylamide Gels

In one of the few other studies of hindered convection in fibrous gels, Kapur et al. (1997) measured sieving coefficients of RNAse and BSA at high Pe in cylindrical pores filled with polyacrylamide. Since they also measured Darcy permeabilities in gels of the same preparation, their data provides another opportunity to assess the ability of the parallel fiber model of Phillips et al. (1990) to predict ΦK_c, given κ, in three-dimensional disordered media. In order to plot the sieving data of Kapur et al. (1997), κ must be estimated at each ϕ in which they measured ΦK_c, since they did not measure κ in the sieving samples. For polyacrylamide volume fractions greater than 0.04, κ was estimated from the fit given by Kapur et al., (1996). Their power law expression was

$$\kappa = 4.35 \times 10^{-4} \phi^{-3.34} \quad (nm^2) \tag{4-23}$$

However, two of the gels in which Kapur et al. (1997) measured sieving coefficients had volume fractions that fall below the range in which Eq. (4-23) is valid. In their water permeability study, Kapur et al. (1996) also determined κ at two volume fractions that are very similar to those used in the sieving study that cannot be predicted by Eq. (4-23). They found that κ was approximately 27 nm^2 and 23.6 nm^2 at volume fractions of 0.026 and 0.032, respectively. From these data and Eq. (4-23), the sieving data of Kapur et al. (1997) is plotted against κ and compared with the predictions of Phillips et al. (1990) parallel fiber convective hindrance theory in Fig. 4.8. To determine the theoretical curves in Fig. 4.8, K_c, κ, and Φ were calculated according to Eqs. (4-9) - (4-10), (4-14), and (4-15), respectively. As given in Kapur at al.

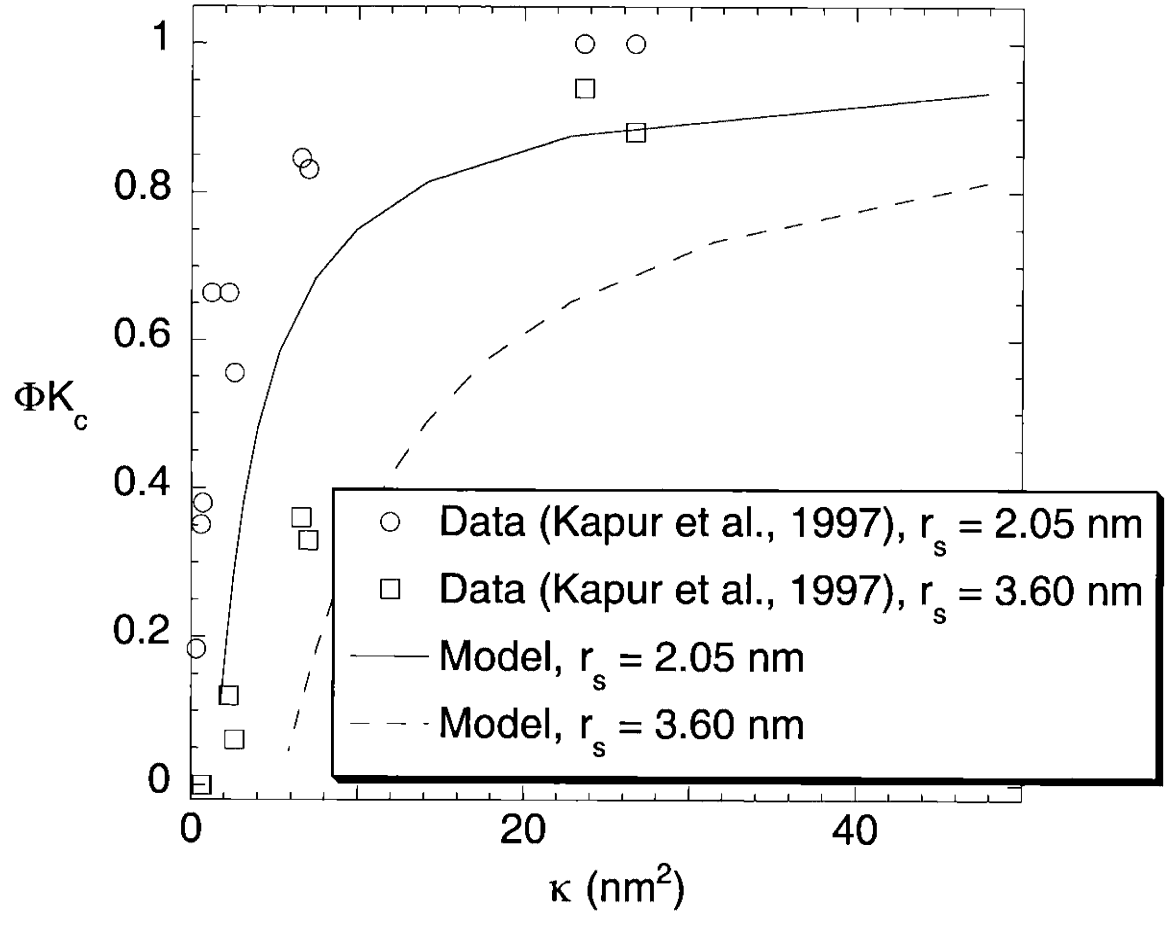

Figure 4.8 Sieving coefficients of RNAse (r_s = 2.05 nm) and BSA (r_s = 3.60 nm) measured at high Pe in polyacrylamide gels, as a function of Darcy permeability (κ). The sieving coefficient under these conditions is equivalent to ΦK_c. The data are from Kapur et al. (1997). The theoretical curves, which predict convective hindrance in parallel arrays of fibers are based on the model of Phillips et al. (1990) with Φ given by Eq. (4-15).

(1997), 2.05 nm, 3.60 nm, and 0.06 nm were used for the Stokes radii of RNAse and BSA and the fiber radius of polyacrylamide, respectively. It should be noted that for BSA in polyacrylamide, $\lambda = 6$, which is slightly outside the range of values for which Eqs. (4-9) and (4-10) are strictly valid. The agreement between the parallel fiber theory and the data is not nearly as good as for the agarose and agarose-dextran gels. That is, the theoretical curves tend to significantly underpredict ΦK_c. Because the model is based on an array of rigid fibers, the flexibility of polyacrylamide may have contributed to the discrepancies in Fig. 4.8, in addition to the deviations from parallel fiber arrangement.

Additionally, Kapur et al. (1997) found that the empirical correlation for the reflection coefficient (σ), given as

$$1-\sigma = \Phi K_c = \left[1+127(\lambda\phi)^4\right]^{-1} \tag{4-24}$$

fit their data very well for both RNAse and BSA. Previously, a comparison of unirradiated agarose with Eq. (4-24) also supported the dependence of ΦK_c on $\lambda\phi$, but a significant increase in the constant from 127 to 2400 was needed to fit the data of Johnston and Deen (1999; 2002). Fig. 4.9 compares irradiated pure 4% and 8% agarose gels with Eq. (4-24), again based on an agarose fiber radii of 1.6 nm (Lazzara and Deen, 2004). The remarkably good quantitative agreement is somewhat surprising, and may be coincidental.

4.4.4 Apparent K_c Calculations Based on Sieving and Partitioning Measurements

Equilibrium partition coefficients of narrow fractions of Ficoll in gels of the same preparation and composition as those used here were measured as described in section 3.3. Therefore, it appears that K_c can be calculated as the ratio of the sieving coefficient measured at high Peclet number, now indicated by $(\Phi K_c)_S$, over the equilibrium partition coefficient. Figures 4.10 and 4.11 compare the apparent K_c, or $(\Phi K_c)_S/\Phi$, against Stokes radius in the 4% and 8%

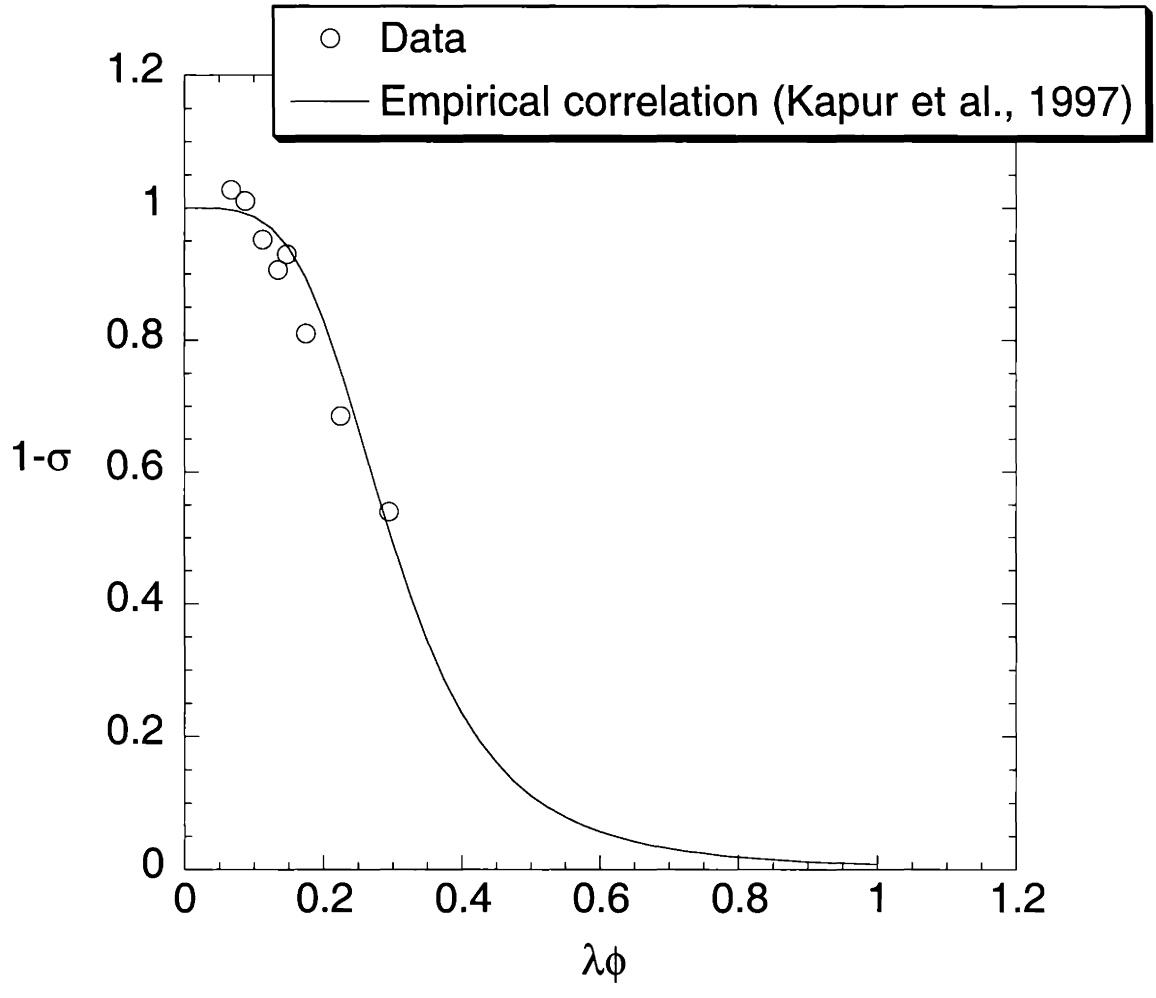

Figure 4.9 Reflection coefficient for Ficoll in 4% and 8% irradiated agarose gels with no dextran. The curve is calculated from Eq. (4-24), an empirical expression suggested by Kapur et al. (1997).

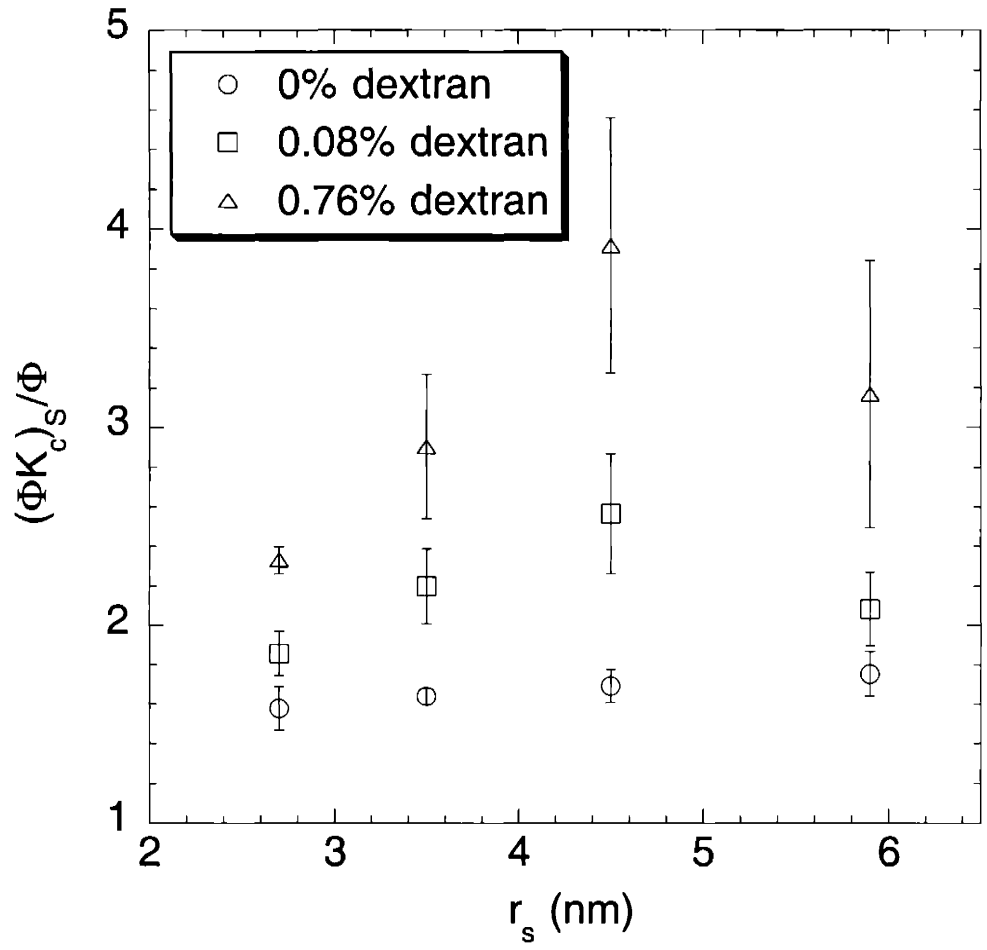

Figure 4.10 The ratio of the volume flow averaged convective hindrance, measured via sieving, to the area averaged partition coefficient, $(\Phi K_c)_s/\Phi$, is plotted against macromolecular Stokes radius (r_s) for 4% agarose and agarose-dextran composite gels.

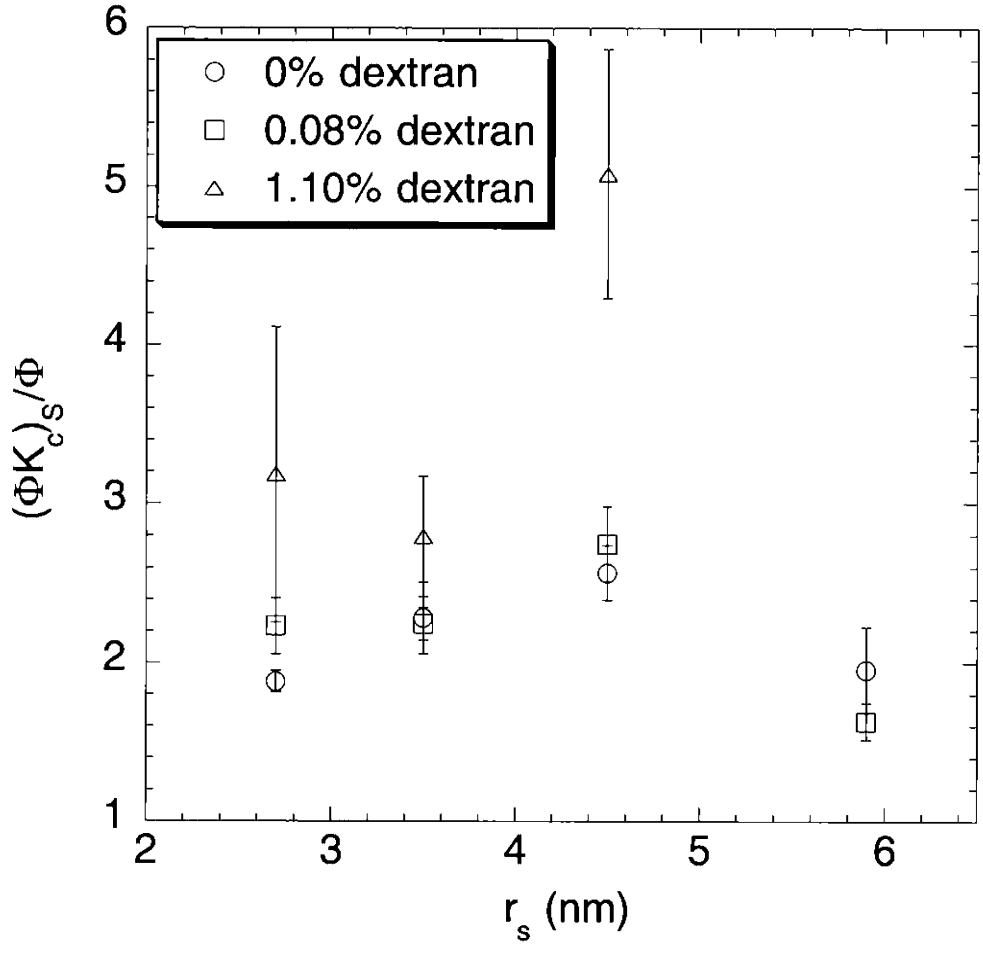

Figure 4.11 The ratio of the volume flow averaged convective hindrance, measured via sieving, to the area averaged partition coefficient, $(\Phi K_c)_s/\Phi$, is plotted against macromolecular Stokes radius (r_s) for 8% agarose and agarose-dextran composite gels. Note that the high dextran result for r_s = 5.9 nm has been omitted since it was significantly larger than the others ($(\Phi K_c)_s/\Phi \sim 18$) due to its extremely small partition coefficient.

agarose gels, respectively. For each agarose volume fraction, gels with zero, low, and high dextran are shown. $(\Phi K_c)_s/\Phi$ appears to peak at an intermediate solute size. Also, the apparent K_c was always greater than one and generally increased as dextran was added to a given agarose gel. These apparent K_c values were much higher than predicted by existing theory. For flow normal to a square array of parallel fibers, K_c is plotted against λ (or r_s) as shown in Fig. 4.12, with $r_f = 1.6$ nm. Predictions are shown for several different bead-and-string fiber volume fractions ranging from 0.005 to 0.080. While K_c is greater than one over a given range of λ for all of the volume fractions shown (macromolecules cannot occupy spaces close to the fibers where the velocity is lowest, due to their finite volume), it is generally less than 1.1. Experimentally, values of K_c up to 1.54 have been measured in agarose gels (Johnston and Deen, 2002), which are also significantly larger than the theoretical maximums. Johnston and Deen (1999; 2002) measured sieving coefficients in unirradiated agarose gels under conditions in which both diffusion and convection were significant. To determine K_c from their data, they calculated Φ using Eq. (4-22) from Ogston (1958) and estimated K_d for a given ϕ from the measurements of Johnson, E. M. et al. (1996).

To account for the unusually large apparent K_c in the agarose based gels, the gel structure was considered more closely. Based on their small-angle x-ray scattering data for pure agarose, Djabourov et al. (1989) found a bimodal distribution of agarose fiber radii, where 87% of the fibers had a 1.5 nm radius, and 13% had a 4.5 nm radius, giving a number-average fiber radius of 1.9 nm. Models predicting Darcy permeability in random fiber matrices based on a single size of fibers (Jackson and James, 1986) or two differently sized fibers (Clague and Phillips, 1997) using either the number-average or bimodal fiber distribution of Djabourov et al. (1989), respectively, have consistently underestimated those measured in unirradiated (Johnson and Deen, 1996b) and irradiated (White and Deen, 2002) agarose gels. The discrepancies generally increased with decreasing gel concentration. For a given volume fraction of fibers of a single radius, the Darcy permeability is well known to be proportional to the squared fiber radius. As a

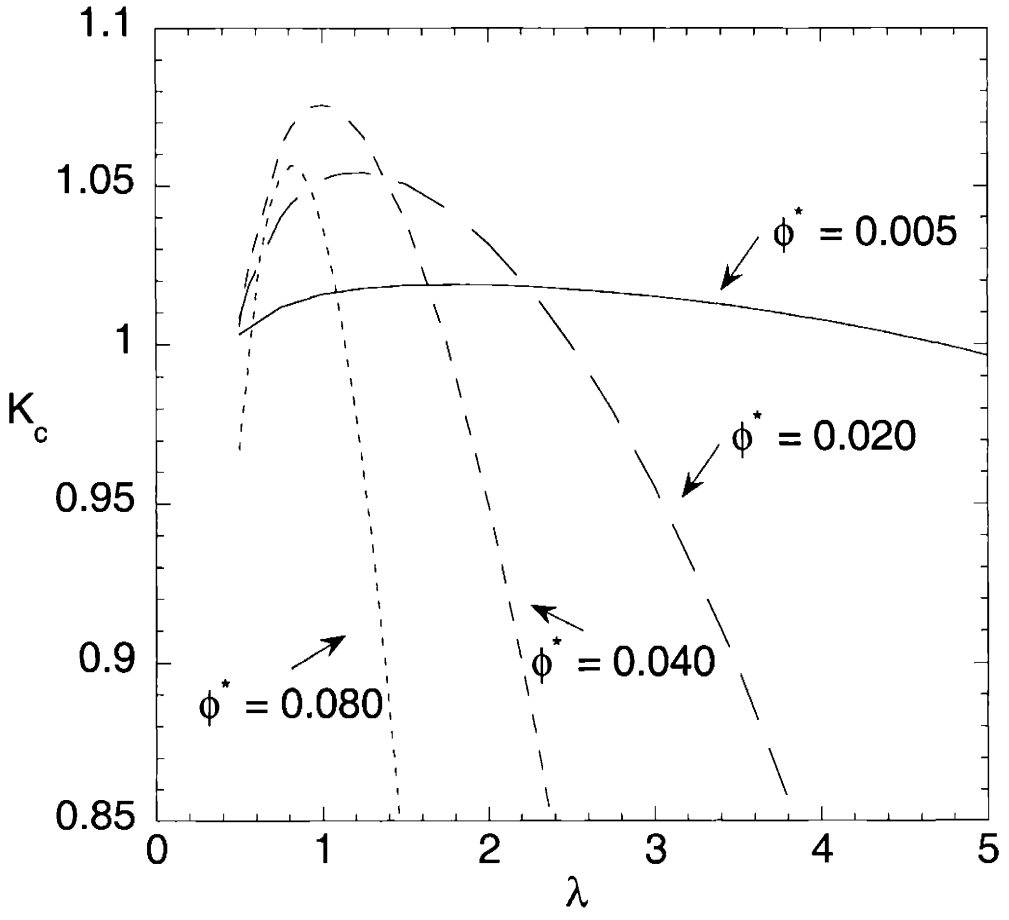

Figure 4.12 Convective hindrance factor (K_c) predictions from Phillips et al. (1990) for a square array of parallel bead-and-string fibers, as a function of the ratio of the solute to fiber radius (λ). Predictions are shown for several different bead-and-string fiber volume fractions (ϕ^*) ranging from 0.005 to 0.080, for a fiber radius of 1.6 nm.

result, predictions for κ will not improve if a fiber radius of 1.6 nm is used, which was recently found by Lazzara and Deen (2004) based on partitioning studies of BSA and Ficoll in agarose gels. The poor κ predictions in agarose gels may be due to heterogeneities in the agarose matrix. Additionally, the effective pore size or fiber spacings of agarose gels measured via nuclear magnetic resonance (Chui et al., 1995) and atomic force microscopy (Pernodet et al., 1997) were shown to have relatively broad distributions that increased in spread as agarose volume fraction decreased.

The indications of fiber spacing heterogeneity in agarose prompted a careful examination of the effects of interfiber spacing heterogeneity on the partitioning and sieving experiments. Assume, for illustrative purposes, that there are two differently sized spaces between fibers through which solute and water can flow. This heterogeneity will cause the apparent K_c to almost always exceed that of a gel with homogeneous interfiber spacings equivalent to either of the two interfiber spacings in the heterogeneous gel. As described in detail below, the measured partition coefficient of a gel with heterogeneous fiber spacings is averaged by fractional area (or volume), while the sieving coefficient at high Pe, which equals ΦK_c, is averaged by fractional volumetric flow. For a given area of gel, flow is always faster in the region with larger interfiber openings. As a result, in a gel with two different sizes of fiber spacings, the fractional area of the region with more closely spaced fibers will exceed its volume flow fraction. For the portion with more distantly spaced fibers, the opposite is true (i.e. the fractional area will always be less than the fractional volume flow). Compared to a homogeneous gel with only close fiber spacings, the heterogeneous gel has a greater value of Φ and ΦK_c. Since the fractional volume flow of the region with fibers spaced farther apart exceeds its fractional area, it has a greater effect on ΦK_c than on Φ, so ΦK_c increases to a greater extent than Φ when heterogeneity is introduced. Therefore, the apparent K_c for the heterogeneous gel is greater than K_c for the homogeneous gel with close fiber spacings. Likewise, the heterogeneous gel has a smaller value of Φ and ΦK_c compared to a homogeneous gel with only wide fiber spacings. Again, the region with the fibers

spaced farther apart has a greater effect on ΦK_c than Φ, so the apparent K_c for the heterogeneous gel will also exceed that for the homogeneous gel with wide fiber spacings.

The hindered convection theory of Phillips et al. (1989; 1990) was investigated to explain the $(\Phi K_c)_s/\Phi$ results since it is the only available theory specifically based on fibrous media. Recall that although this model is based on flow normal to a square array of parallel fibers, it predicted ΦK_c in our gels relatively accurately based on κ. For illustrative purposes, a gel comprised of both a high and a low fiber volume fraction region will be considered, with $r_f = 1.6$ nm in both regions. Since the fibers in both regions have identical r_f and are arranged in square arrays, different fiber volume fractions correspond to different spacing between fibers. The high volume fraction region will have more closely spaced fibers than will the low volume fraction region. In the analysis that follows, parameters based upon the gel region with the more closely spaced fibers (high fiber volume fraction region) and more distantly spaced fibers (low fiber volume fraction region) have the subscript i = 1 and 2, respectively. This exercise is intended to illustrate the effects of interfiber spacing heterogeneity, but the analysis can be extended to account for more than two regions, which probably more closely resembles the actual gels. It is assumed that there is only one macromolecular species involved.

In a gel, the experimentally measured equilibrium partition coefficient (concentration of solute within the gel ($\overline{C}$) based on total gel volume, to that in the bulk solution (C_∞)) for a given macromolecule of radius r_s can be calculated from

$$\Phi = \frac{m}{VC_\infty} \tag{4-25}$$

where m is the total mass of a given macromolecule within a gel of total volume V and thickness L. For the case of two regions i, each with a surface area exposed to flow given as A_i,

$$m = \sum_{i=1}^{2} A_i L \overline{C}_i \tag{4-26}$$

and $$V = \sum_{i=1}^{2} A_i L \tag{4-27}$$

As a result, the average equilibrium partition coefficient, given by Eqs. (4-25) - (4-27), is

$$\Phi = \frac{\sum_{i=1}^{2} A_i \Phi_i}{\sum_{i=1}^{2} A_i} = \sum_{i=1}^{2} \omega_i \Phi_i \tag{4-28}$$

where ω_i is the fraction of gel area (or gel volume) attributed to region i. That is,

$$\omega_i = \frac{A_i}{\sum_{i=1}^{2} A_i} \tag{4-29}$$

Thus, the observable equilibrium partition coefficient of a gel with two regions with different interfiber spacings is an average of the partition coefficients in each of the individual regions weighted by its cross sectional area (or volume).

To determine $(\Phi K_c)_S$, as measured via high Pe sieving experiments in a gel with fiber spacing heterogeneity, recall that the sieving coefficient is given by the concentration of the solute in the filtrate (C_f) divided by that at the upstream surface of the membrane (C_m). C_f can be calculated as the total solute filtered (numerator of Eq. (4-30)) divided by the total volume filtered (denominator of Eq. (4-30)). That is,

$$C_f = \frac{\sum_{i=1}^{2} N_i A_i}{\sum_{i=1}^{2} v_i A_i} \tag{4-30}$$

where v_i is the superficial fluid velocity in region i. At high Pe, the pseudo steady flux evaluated at the upstream membrane surface using external solution concentrations is

$$N_i = \Phi_i K_{ci} v_i C_m \tag{4-31}$$

Substituting Eq. (4-31) into Eq (4-30), noting that v_i is proportional to κ_i for a given ΔP across both regions of the gel, simplifying, and solving for the sieving coefficient gives

$$\Theta = \left(\Phi K_c\right)_S = \frac{\sum_{i=1}^{2} A_i \kappa_i \Phi_i K_{ci}}{\sum_{i=1}^{2} A_i \kappa_i} \tag{4-32}$$

Comparing Eqs. (4-28) and (4-32), it is seen that whereas the equilibrium partition coefficient is averaged by exposed surface area, the convective hindrance is averaged by volume flow. As a result of these inherent differences in averaging, the apparent K_c does not equal K_{c1} or K_{c2}, but almost always exceeds them both, as will be shown later.

To determine the expected magnitude and variation in $(\Phi K_c)_S/\Phi$, the partition and sieving coefficients that would be measured in a heterogeneous gel were compared with those of homogeneous gels that had fiber spacings identical to those in one of the regions of the heterogeneous gel. Based on a volume fraction ϕ_i within region i, values of K_{ci}, κ_i, and Φ_i were calculated via Eqs. (4-9) - (4-10), (4-14), and (4-15), respectively. The average values that would have been observed in partitioning or sieving measurements in the assumed heterogeneous gel were calculated according to Eq. (4-28) and (4-32), respectively, and used to compute $(\Phi K_c)_S/\Phi$. The ratio F_i, defined as

$$F_i \equiv \frac{\left(\Phi K_c\right)_S/\Phi}{K_{ci}} \tag{4-33}$$

will be used in comparing the apparent K_c in the gel with two regions of different fiber spacings to that of the regions themselves.

The magnitude of F_i varies significantly depending on ϕ_i (spacing between fibers), λ, and ω_i, as shown in Figs. 4.13 and 4.14. Figure 4.13 illustrates variations in F_i with ϕ_1/ϕ_2, where ϕ_2 = 0.0077 and $\lambda = 2$. Figure 4.14 shows the variation in F_i with λ, where $\phi_1/\phi_2 = 10$, and ϕ_2 = 0.0046. In each figure, the larger volume fraction region of the gel is indicated by $i = 1$. Results for fractional areas in region 1 of 0.9, 0.5, and 0.1 are shown. As indicated by Fig. 4.13, when ϕ_1/ϕ_2 is close to 1, both regions of the gel have approximately equal interfiber spacing, so as expected, F_i is about 1 for both i. For the three fractional areas shown, F_i steadily increases with ϕ_1/ϕ_2 or λ, with the effects becoming more pronounced as ω_i increases. For the range of volume fractions over which the Phillips' (1989; 1990) model is valid, F_i of around 2 - 2.5 were reached for $\omega_1 = 0.9$ at the maximum ϕ_1/ϕ_2 or λ in Figs. 4.13 and 4.14, respectively. In both comparisons, F_1 is initially less than F_2, but as ϕ_1/ϕ_2 or λ increase, it equals and then surpasses F_2. This trend occurs because in both cases, K_{c2} is always about 1, while K_{c1} initially increases to just above 1 and then decreases below 1.

Based on the analysis of parallel fibers in a square array, values of the apparent K_c within the range of magnitudes shown in Figs. 4.10 and 4.11 for the agarose and agarose-dextran gels are expected. Qualitative trends between the parallel fiber theory predictions and the gel data can also be compared. As shown in Figs. 4.10 and 4.11, for a given gel composition, as r_s increased, $(\Phi K_c)_g/\Phi$ generally increased, except for the largest r_s = 5.9 nm. To compare with the parallel fiber model predictions, an increase in r_s corresponds to larger λ and $(\Phi K_c)_g/\Phi$ (or F_i).

4.4.5 Comparison of Hindered Convection in Synthetic Gels and Isolated GBM

As noted at the outset, the agarose-dextran composite gels were developed as a possible experimental model for glomerular basement membrane (GBM). As reviewed in Deen et al. (2001), measurements using isolated rat GBM have yielded estimates of ΦK_c for Ficolls of

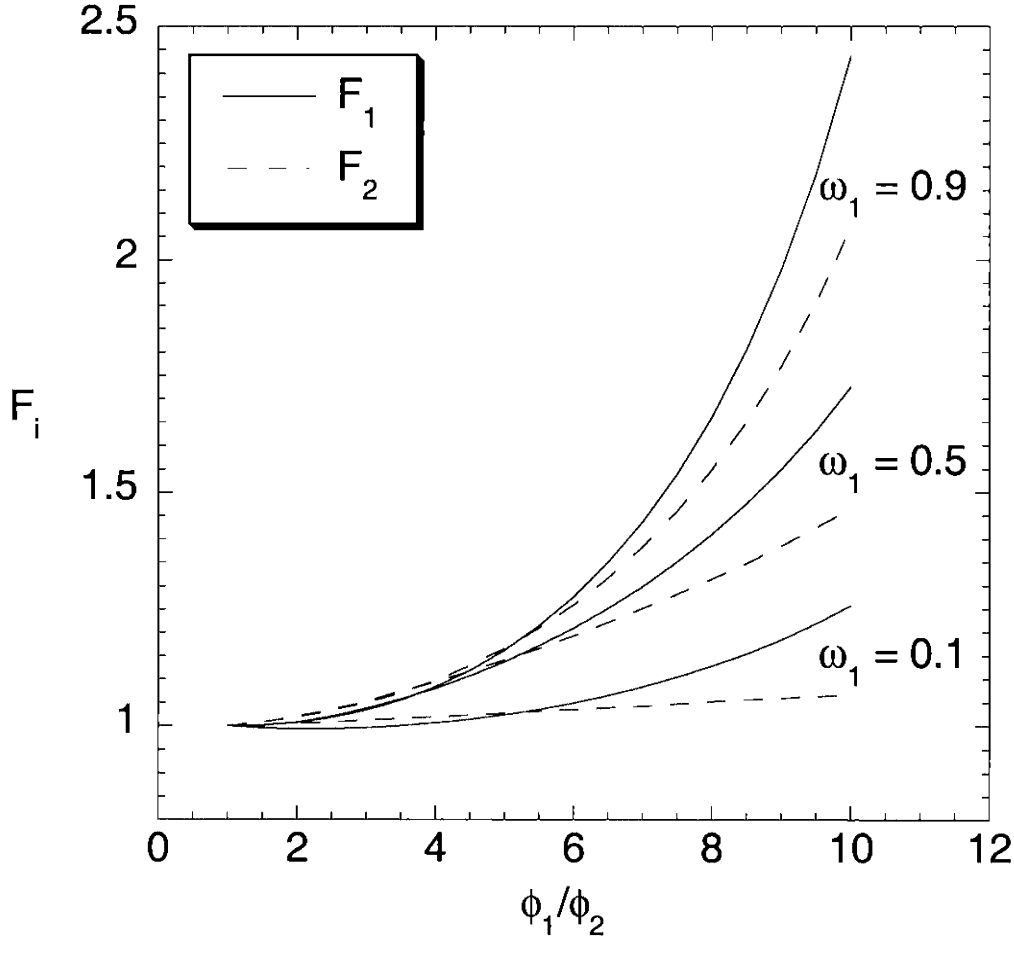

Figure 4.13 Variations in F_i, defined by Eq. (4-33), in a gel with two regions i that have different interfiber spacings, as a function of ϕ_1/ϕ_2. The region with closer fiber spacings is indicated by $i = 1$. Results for fractional areas in region 1 (ω_1) of 0.9, 0.5, and 0.1 are shown for $\phi_2 = 0.0077$ and $\lambda = 2$.

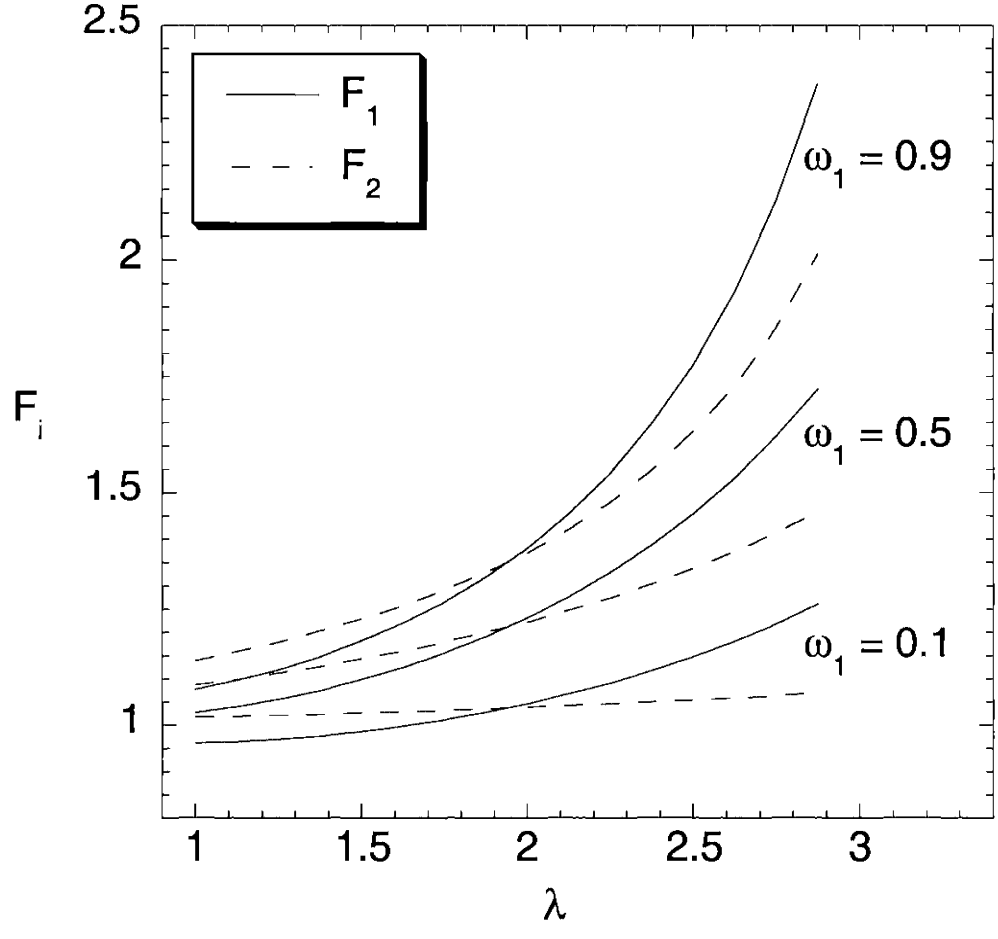

Figure 4.14 Variations in F_i, defined by Eq. (4-33), in a gel with two regions i that have different interfiber spacings, as a function of λ. The region with closer fiber spacings is indicated by $i = 1$. Results for fractional areas in region 1 (ω_1) of 0.9, 0.5, and 0.1 are shown for $\phi_1/\phi_2 = 10$ and $\phi_2 = 0.0046$.

varying size. In choosing a suitable agarose-dextran gel for comparison, we note that a composite with $\phi_a = 0.08$ and $\phi_d = 0.01$ (i.e., 8% agarose with "high" dextran) has a total fiber volume fraction of 9%, similar to the 7-10% solid volume reported for GBM (Robinson and Walton, 1987; Comper et al., 1993). This agarose-dextran composite has been shown in this and a study by White and Deen (2002) to have a Darcy permeability of 1.6-3.0 nm^2 similar to the 1-2 nm^2 typically found for isolated GBM in vitro (Daniels et al., 1992; Edwards et al., 1997b; Bolton et al., 1998). Additionally, diffusional hindrances in this synthetic gel were very consistent with those measured in vitro in isolated GBM, as discussed in section 3.3. Accordingly, it is the one we selected for the comparison in Fig. 4.15, in which values of ΦK_c are shown as a function of the Stokes radius. As may be seen, the values of ΦK_c in the agarose-dextran composite (circles) were qualitatively similar in the decline of ΦK_c with r_s to those of isolated GBM, but they were on average about twice the in vitro value.

The 8% agarose, 1% dextran gel had an average Darcy permeability of 2.9 nm^2, which is slightly higher than those measured in isolated GBM. As indicated in Fig. 4.5, at very small Darcy permeabilities, ΦK_c is very sensitive to changes in κ. Consequently, it is likely that a small addition of dextran would produce even better agreement with the in vitro GBM convective hindrance, while maintaining good diffusive hindrance agreement, since ΦK_d is less sensitive to small changes in κ than is ΦK_c. For a random fiber matrix, there is always the possibility that one pathway will be large enough to accommodate the solute even if it is excluded from all the others, so ΦK_c versus κ probably passes through the origin for moderate r_s. Since the slope of ΦK_c versus κ for small κ is so steep, it can be approximated as a straight line from the data point for the most concentrated gel to the origin. Values of ΦK_c extrapolated to κ = 1.15 nm^2 (Bolton et al., 1998), which was measured in the same isolated GBM used to determine in vitro values of ΦK_c, are also shown in Fig. 4.15. The agreement between ΦK_c extrapolated from the synthetic gel data and that measured in isolated GBM is remarkable. The similarity of these composite gels to ϕ, κ, ΦK_ϕ and ΦK_c of in vitro GBM supports the hypothesis

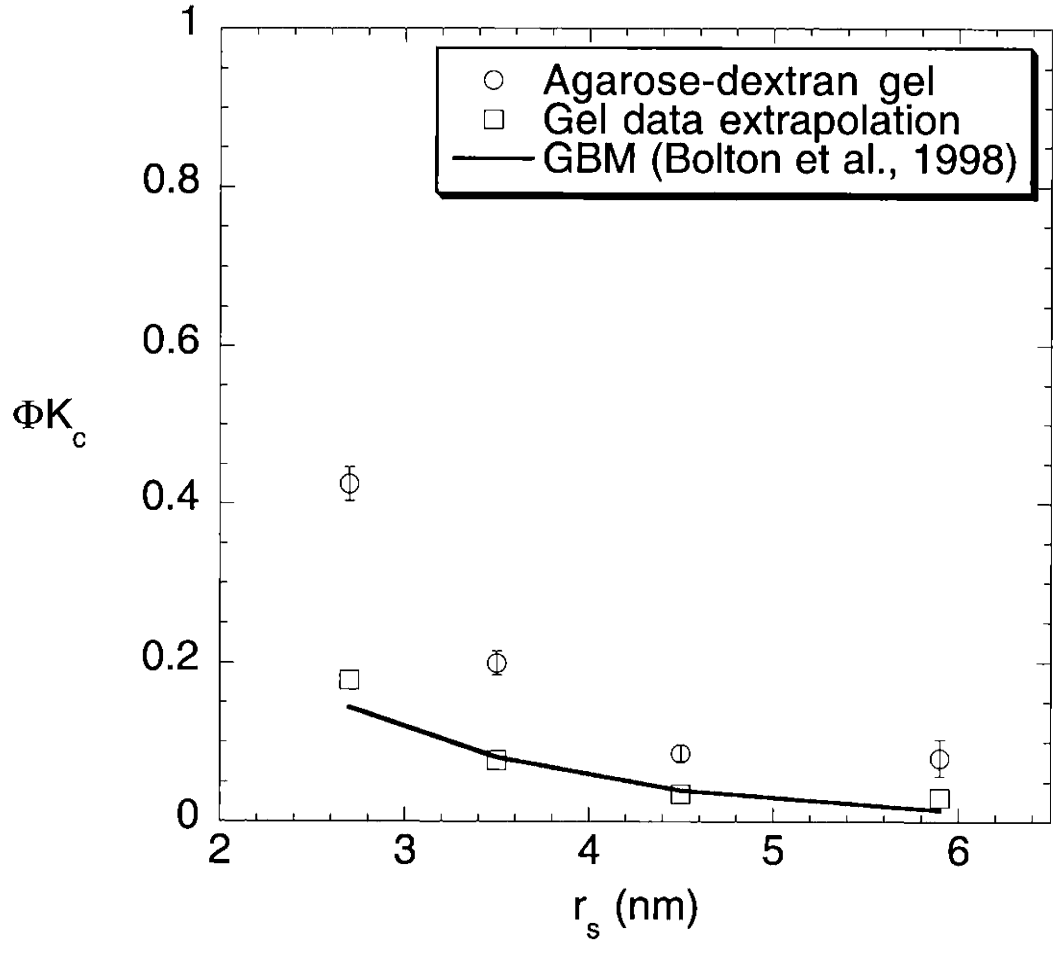

Figure 4.15 Comparison of Ficoll convective hindrances of an agarose-dextran gel (8% agarose with 1% dextran) and isolated rat glomerular basement membrane (GBM). The ordinate is the product of the partition coefficient (Φ) and the ratio of solute velocity in the gel to the superficial fluid velocity (K_c). The GBM results are based on Ficoll sieving across filters prepared from isolated GBM (Bolton et al., 1998). Also shown are ΦK_c extrapolated to the corresponding isolated GBM Darcy permeability, 1.15 nm^2 (Bolton et al., 1998).

that the permeability properties of GBM are determined primarily by its mixture of coarse and fine fibers. That is, its precise chemical composition seems to be secondary.

A Appendix

A.1 Fluorescence Recovery After Photobleaching (FRAP) Extensions

A.1.1 FRAP Users' Manual

The FRAP system described in section 2.2.5 is currently located in Prof. T. Alan Hatton's laboratory, 66-317. Since the system involves a class IIIb laser and is located in the vicinity of class IV lasers, MIT students and affiliates are required to attend laser safety training, administered through the Radiation Protection Office, prior to operating the system. Additionally, laser safety glasses that are appropriate for the wavelength of the laser light must be worn. The following manual instructs the user regarding normal operations of the FRAP system based on current capabilities and setup. An additional manual describing possible configuration changes, troubleshooting, and system maintenance is located with the FRAP system in 66-317.

Safety

1. Wear safety glasses that offer protection in the range of 488 nm (current laser output).
2. Turn on the laser warning lights, using the switch located on the light switch panels near the two entrances to 66-317 (only one needs to be turned on). The "Laser In Use" light and the red spinning light outside the two respective entrances to 66-317 will turn on as a warning to persons entering the room.

Laser Operation

1. Ensure that the laser shutter is closed so that light will not be emitted until needed. The laser shutter, which is manually controlled, is a circular cap covering the front of the laser

where the beam is emitted. When the small hole in the cap and the knob on the shutter are off center from the vertical, the shutter is closed.

2. Check the settings on the laser remote control prior to turning on the laser. In order for the laser to emit light, the "discharge" setting must be "on." For general FRAP operation, it is recommended that the laser be operated in "power" mode, so that the laser emission is maintained at a constant output power. Also set the "display" control to "power" so the number indicated on the remote control display will be the power of the laser emission in mW. The first of the "mode" switches should be in "standby" anytime the laser is not being used for more than about 15 minutes in order to preserve the lifetime of the laser tube. When starting the laser, that switch should be in "standby", so the laser will begin running at the low current threshold. As a result of starting the laser in "standby" mode, the position of the "current" and "power adj." knobs is unimportant at start up.

3. Flip the lever on the breaker box to "on." The breaker box for the FRAP system's power supply is labeled "panel M3 25-27-29, RM 304." Turn the laser power supply switch "on" and turn the key to the right (vertical to horizontal position). The laser and laser power supply fans should turn on and begin to make some noise. Initially, the laser remote control display will indicate ~0 mW (assuming the display is in the "power" setting). After a few minutes, if the laser is in "standby," the display will read a number less than ~10 (As more hours are put on the tube, as the laser drifts out of alignment, or as the internal laser optics get dirty, this number will slowly decrease), which corresponds to the power output at the low current threshold of the laser. Allow the laser to warm up for about 15 minutes.

Sample Loading and Focusing

1. The current sample clamp will easily hold a rectangular microslide capillary tube or a microscope slide. It can be altered to accommodate many different sample cells or setups, if needed. Place the slide in the sample clamp (see Fig. 2.1) and position it

roughly in front of the dichroic mirror. Remember that at the current wavelength setting, 488 nm, the diffusion coefficient of the solute of interest can only be determined if the solute is tagged with a fluorophore that fluoresces when exposed to 488 nm light.

2. Double click on the "Measurement and Automation" icon located on the FRAP system's computer desktop. In the window that opens, double click on "Devices and Interfaces" which is located under "My System" in the "Configuration" box. Double click on "IMAQ PCI-1409 - img0" followed by the "Channel 0: RS-170." In the tool bar at the top of the window that appears, click on "Grab." The video camera should begin to send images to the screen. With some adjustment and focusing, the image shown on the screen should be of your sample. The platform on which the sample clamp is located can be moved up and down by adjusting the levels of the two posts holding the sample stage. The sample can be brought into focus by turning the micrometer on the microtranslation stage upon which the sample platform is attached.

Beam Alignment

1. Ensure that the laser is in "standby" mode, as indicated on the laser remote control, since it is always best to align optics at the lowest power possible for safety. As shown in Fig. 2.1 and detailed in section 2.2.5, the laser is split into two beams, each of which passes through a shutter. Each shutter is controlled by the shutter driver to which it is connected. The driver is connected to the IMAQ A6822 breakout board which connects to the IMAQ PCI-1409 frame grabber board in the computer. At this point, the shutters should both be closed. On the front of the shutter drivers, there is an "on/off" switch and an "N.O./N.C." switch. Make certain that the shutter drivers are both "on" and identify which driver controls which shutter (the attenuated beam shutter driver is generally located directly on top of the bleaching beam shutter driver).
2. Turn the iris (see Fig. 2.1) to its smallest opening so it will be easy to tell if the laser is aligned properly.

3. Turn the shutter on the laser until the small hole and knob are in the vertical position so the laser beam can exit. Use a piece of cardstock to see if the beam passes through the center of the iris (the laser glasses prevent the user from seeing the 488 nm light, so cardstock is useful in tracing the beam). If the beam does not pass through the opening of the iris, either the laser or some of the optics have been moved and the system must be realigned according to Fig. 2.1, so it operates as discussed in section 2.2.5.
4. Assuming the laser beam passes through the iris and contacts the beamsplitter, the attenuated beam shutter should be manually opened by switching from "N.C." to "N.O." on the appropriate shutter driver.
5. Using the knobs on the mirrors in the attenuated beam path, adjust the beam so that it illuminates the sample as uniformly as possible. Switch the laser from "standby" to "run" on the laser remote control. Assuming the laser is in "power" mode with the display also set to "power," this allows the user to turn the "power adj." knob and adjust the laser power (in mW) to the desired level. In order to preserve the laser tube, a power of less than 20 - 35 mW is recommended. (Note that this range is associated with the current needed to obtain a given power. As the laser ages, a higher current will be needed to achieve the same output. As a result, the optimal operation range will decrease as the maximum power the system can produce decreases due to tube aging.) Adjust the power so the sample is relatively bright (in the image on the computer screen), but far from saturated (all white pixels). Notice that there is a filter holder within the attenuated beam path where a neutral density filter can be added to dim the attenuated beam in case it causes the sample to fluoresce too brightly, even at very low power. Alternatively, the concentration of the fluorophore in the sample could be reduced.
6. Once the attenuated beam is aligned and the laser power adjusted to give the desired brightness, manually close the attenuated beam shutter by switching the attenuated beam shutter driver switch from "N.O." to "N.C.". Open the bleaching beam shutter by switching the bleaching beam shutter driver from "N.C." to "N.O.". Remember that this

beam is very concentrated and strong by the time it reaches the sample, so the user may want to switch back into "standby" mode while aligning the bleaching beam. Adjust the bleaching beam, the camera, and/or the dichroic mirror so the beam is centered in the region on which the camera is focused. It may help to open the shutter for a minute, then close it, and make adjustments until the bleached spot is centered in the area of image acquisition (remember, the bleached spot will disappear over time as it "recovers"). When the bleaching beam is centered, close the bleaching beam shutter by switching from "N.O." to "N.C." on the bleaching beam shutter driver.

7. Repeat steps 4 and 5 again to ensure the attenuated beam is still centered and at the appropriate power level, since some of the changes in step 6 might mean that more adjustments are required. Ensure that the laser has been returned to "run" mode.
8. Shift the sample slightly by moving the sample stage along the rail to which it is attached until an area that has not been exposed to the bleaching beam (during alignment) is reached.
9. Once both beams are centered in the region where the camera is acquiring images, ensure that both shutters are closed, but both shutter drivers are still "on."
10. Click on "Grab" again in the window on the computer screen so that the frame grabber will stop acquiring images. Also, minimize the "Measurement and Automation" window.

FRAP Experiment

1. On the desktop of the FRAP system computer, double click on "FRAP program 051904". The front panel of the FRAP program should open.
2. For general FRAP system operation, under "Experiment Options," ensure that "Acquire Images," "Center Laser Before Bleaching," "Bleach a Line," "Bleach a spot," and "Analyze Data" are set to "Yes," "No," "No," "Yes," and "Yes," respectively. Given this configuration, several parameter entries on the front panel may be ignored since they control capabilities of the system that are not used in the standard FRAP system

operation. The motion controller is not used, so ignore the motion controller "Hardware Specifications," "Slot #" and "Axis #," and the entire box of parameters entitled "Motion Control Parameters." In the "Hardware Specifications" box, also ignore the setting for "Camera Channel 2" since only one camera is currently used. In the "Hardware Specifications" box, make sure "Camera Channel 1," "Bleaching Beam Shutter," and "Attenuated Beam Shutter" are set to "0," "External Trigger 0," and "External Trigger 1," respectively. In the "Image Filenames" box, specify the folder in which you would like the image data and the times the images were taken to be stored. By default, the images will be stored in the folder specified under the filename "img(followed by the image number)" and "times(followed by the image number to which it refers)." Under "Image Acquisition and Analysis," "Number of Images" to be taken can be specified (default is 25 images). Also, for each of the 25 (default) images, 5 (default) pictures are taken back to back and averaged together, as indicated by the "Number of Images to Average" setting. The "Time Between Images" can be specified (in ms) by entering the wait time between images in the time array. (The actual time between images will be slightly longer than that specified by the user because actually taking the images requires a small amount of time. The user can specify the wait time after one image acquisition is complete and before the next begins, but that time is not exactly the time between images (see VI descriptions below)). The "Region of Interest" should be set at "0," "0," "720," and "480." The "Number of Spatial Frequencies" has a default of "3." This indicates that the lowest 3 wavenumbers will be used in calculating both the spatial frequency pairs (i.e. wavenumber pairs (0,0), (0,1), (0,2), (1,0), (2,0), (1,1), (1,2), (2,1), and (2,2) will be included in the analysis).

3. Once all the parameters are set properly, run the program by pressing the forward arrow on the Labview toolbar.

4. A window should appear that prompts the user to enter a folder name in which the data from the experiment will be stored. By default, the prompt opens up to the folder specified on the front panel. Enter a folder name and press return.
5. An image of the focused sample is found in the window that appears next. This gives the user one last opportunity to ensure that the sample is centered and the beam intensity is appropriate. Steps 4-9 of "Beam Alignment" may be repeated here, if necessary. When everything is centered, click on the "Camera is Centered on Beam" button at the bottom of the window.
6. A window will appear instructing the user that the experiment is about to begin. Click on "Continue."
7. Under computer control, the attenuated beam shutter will open and a pre-bleach image will be taken. Then, the attenuated beam shutter will close and the bleaching beam shutter will open and bleach the sample for approximately 1 second (default setting in code). The bleaching beam shutter will close. Then, the attenuated beam shutter will open and close every so often, according to the specifications set by the user on the front panel. Each time it opens, an image is taken.
8. When all the images have been acquired, the virtual instrument entitled "Analyze 2D Data5 and Save Images at End" will open automatically. Move the screen around until a set of directions and parameter boxes entitled "x-axis start" and "x-axis end" appears. Follow the instructions on the screen to choose the region of data to analyze.
9. After pressing the "Finished Choosing Analysis Region," move the screen to the right and several images will appear. The image with the white background shows 3D images of the data just acquired at each time step. By placing the cursor over this plot and holding down the left mouse button, the user can change the perspective of the image. The larger rectangular plot below the 3D plot is a 2D plot of a slice through the middle of the image acquisition region for data from select time points. If the screen is moved even farther to the right, a plot of the frequency scaled time verses the negative of the natural logarithm

of the ratio of the Fourier transformed fluorescence intensity is shown. If there is only one fluorescent diffusing species, the slope of this plot gives the diffusivity of the solute. However, even if there is only a single diffusing species, the data should be more closely analyzed to remove the DC component that does not provide any useful information (always indicates an infinite diffusivity), eliminate any frequency pairs that deviate significantly from the others, and truncate the data to ensure that the full profile was included in the analysis region. An explanation of the analysis of the FRAP data in this study is given in section 2.2.6 along with relevant references. The Labview code used to perform the analysis in section 2.2.6 can be found on the FRAP desktop as "FRAP finishing touches FINAL.vi." Additionally, the remaining subsections following this one provide more insight regarding the theory and analysis of FRAP data.

A.1.2 Virtual Instrument Explanations for the FRAP Code

Folder For Future Saved Images.VI

This VI is executed if the "Acquire Images" button is set to "yes." It creates a folder in the default path, "C:\Program Files\National Instruments\FRAP data (K)," to save the sample pre and post bleach images. The user is prompted to enter the name of the folder beginning with Exp. All data for that experiment is automatically stored in the folder named by the user.

Center Laser Before Bleaching 2D.VI

This VI executes if the "Center Laser Before Bleaching" Button is set to "yes." The front panel of this VI contains instructions on how to use it during an experiment. The translation stage must first be initialized if it has just been turned on or if the computer has just been turned on. Once the translation stage is initialized, it does not need to be reinitialized unless the NuDrive or the computer are turned off and then on again. The bleaching beam shutter will open automatically and the user can press the move "forward" and "backward" buttons to move the stage back and forth until the beam is centered on the sample.

The instructions given by the VI are:

1. Enter the increment by which you would like the laser to move, using either the knob or the digital display.

2. Double click on the button indicating the direction you want the laser to move. (If you only single click, the laser will move in the direction indicated by the button you press until you press that button again.) The green light should flash briefly (first click) and then go out (second click).

3. Repeat steps 1 and 2 until the laser is satisfactorily centered on your sample and press the "Laser Centering Finished" button.

After you have finished centering the beam on the sample, the "Preview Camera Alignment" VI executes. The user should move the camera until the beam appears centered in the camera's view. The bleaching beam shutter will then close before the VI completes execution.

Please note that this VI was modified when the system switched from 1D line bleaching to 2D spot bleaching. If this VI were to be reimplemented for 1D line bleaching, a translation should be added in the same case structure as the final shutter close. This will ensure that the stage moves so the beam starts bleaching from one edge and not from the center of the image. If it started in the center, it would bleach unevenly due to the stage startup time

Preview Camera Alignment.VI

This VI executes if the "Bleach a Spot" button is set at "yes" or if the "Center Laser Before Bleaching" button is set to "yes." If the "Center Laser Before Bleaching" button is set to "yes," it will execute after the "Center Laser Before Bleaching" VI and it is just a repeat of the "Preview Camera Alignment" VI contained within the "Center Laser Before Bleaching" VI. This VI simply outputs the images taken by the video camera to the plot on the screen. This

allows the user to adjust the camera position so that the bleached spot will be in the center of the camera's acquisition region. The user can also make sure the bleaching and attenuated beams are centered at this point.

Pre Bleach Image No Filter Wheel

This VI executes if the "Acquire Images" button is set to "yes" and either the "Bleach a Spot" or "Bleach a Line" button is set to "yes." The user is first warned that the image acquisition and bleaching will begin in a certain number of seconds as specified in this VI's code. After the user presses "Continue", that wait time will begin. Following the specified wait time, the attenuated beam shutter will open, an image will be acquired, and the shutter will close again. This VI is named "Pre Bleach Image No Filter Wheel" because a filter wheel used to hold the plano-concave and plano-convex lenses and would switch between the two lenses depending on which type of beam was required. Unfortunately, the filter wheel did not return to precisely the same spot when flipped between the lenses, so this method had to be abandoned.

Open or Close Shutter.VI

This VI creates a TTL signal that operates the shutter via the computer. A BNC connecting cord connects the "pulse O/C" on the back of the shutter driver to one of the trigger BNC ports on the frame grabber breakout board. The "IMAQ generate pulse" VI is used to generate a pulse on the trigger line that will cause the shutter to open if it is closed or visa versa. The default for this VI is a single immediate pulse with a low pulse polarity setting. It is important to use generate pulse again to stop the pulse (the pulse is identified by pulse ID out). Otherwise, it will eventually run out of pulse IDs and the code will stop working.

One Axis, 2-Dir Motion Works.VI

This VI executes when the "Bleach a Line" button is set to "yes." It causes the translation stage to move back and forth a user-specified number of times. Speed and other parameters are also user defined.

Snap 2 Cameras Plus Image Averaging But Save Later.VI

This VI "snaps" a picture of the image. If the user has defined "Camera Channel 1" and "Camera Channel 2" as different numbers corresponding to their locations on the BNC breakout box connected to the frame grabber, this VI will take N back to back images from the camera at channel 1 followed by 1 picture from the camera at channel 2. N is the user defined "Number of Images to be Averaged." Before any images are taken, this VI causes the attenuated beam shutter to open and it closes the shutter after all the images have been acquired. The images are not saved within this VI. The time it takes for the images to be acquired is recorded and the total time divided by two is used as the official image time for the final averaged image.

Picture Sequence Using Wait But Save Later.VI

This VI executes "Snap 2 Cameras Plus Image Averaging But Save Later.vi" in a loop until the user-specified number of pictures has been taken. The user can also specify the time to wait between images on the front panel. The average image time and the wait times are measured and used to calculate the actual time between images. The actual time between images will be slightly longer than that specified by the user because actually taking the images requires a small amount of time. The user can specify the wait time after one image acquisition is complete and before the next begins, but that time is not exactly the time between images.

Time With Wait.VI

This VI calculates the time when the averaged image was taken and saves it in a file called "times" in the folder specified by the user at the beginning of the experiment. The average

image time is the wait time between images plus half the time needed to acquire all the images that end up being averaged together.

Save Average Image Files With 20 Pixel Border.VI

"Save Average Image Files With 20 Pixel Border.vi" saves each image taken by the camera on channel 1. It saves the portion specified by the user in "Analyze 2D data5 and Save Images at End.vi" plus a 20 pixel border (default) in case the user improperly centered the image and needs to re-analyze the images. It does not save any images taken by the camera on channel 2. Originally, the code was developed assuming the attenuated beam would need to monitored and imaged, but this proved to be unnecessary and the code was modified accordingly.

Analyze 2D data5 and Save Images at End.VI

"Analyze 2D data5 and Save Images At End.vi" takes the images and performs 2D spatial Fourier analysis. The diffusion coefficient is determined via images this VI produces along with curve fits etc.

A.1.3 Detailed Derivation of Spatial Fourier Analysis

As discussed in section 2.2.6, spatial Fourier analysis was used to analyze the FRAP images. The following is intended to provide a brief review of the methodology and analysis involved. This method takes advantage of the ease with which the Fourier transformed 2D conservation equation can be solved compared to the 2D conservation equation itself, which is given by

$$\frac{\partial C}{\partial t} = D\left(\frac{\partial^2 C}{\partial x^2} + \frac{\partial^2 C}{\partial y^2}\right) \tag{A-1}$$

where C is the macromolecular concentration, t represents time, D is the macromolecular diffusivity, and x and y are spatial coordinates. The concentration in Fourier form is

$$C(x,y,t) = \sum_{u=-\infty}^{\infty} \sum_{v=-\infty}^{\infty} \tilde{C}(u,v,t) e^{2\pi i u x} e^{2\pi i v y} \tag{A-2}$$

where u and v are spatial frequencies, and $\tilde{C}(u,v,t)$ are Fourier coefficients. Substituting the Fourier representation of the concentration profile into the 2D conservation equation, Eq. (A-1), results in a first order ordinary differential equation, given by

$$\frac{\partial \tilde{C}(u,v,t)}{\partial t} + 4\pi^2(u^2+v^2)D\tilde{C}(u,v,t) = 0 \tag{A-3}$$

The solution to the first order ODE in Eq. (A-3) is given by

$$\tilde{C}(u,v,t) = \tilde{C}(u,v,0) e^{-4\pi^2(u^2+v^2)Dt} \tag{A-4}$$

At every spatial frequency combination of interest, the Fourier coefficients must be calculated at each time step. A diffusivity can be determined from each frequency pair.

Since the image is pixilated rather than continuous, a discrete Fourier transform must be used. The data is collected over a finite region, so the Fourier transform of the image will also be truncated and discrete. The Fourier transform of the image has the same number of discrete frequencies as the image had pixels of data. The frequencies are bound on either end by the Nyquist frequency (f_N), which is

$$f_N = \frac{1}{2\Delta} \tag{A-5}$$

where Δ is the distance between pixels. All allowed frequencies are multiples of the Nyquist frequency, as indicated below. These spatial frequencies, which have the inverse units of the spatial coordinate, are given by

$$u = \frac{\tilde{u}}{N\Delta}, \quad \tilde{u} = -\frac{N}{2}, \ldots, \frac{N}{2} \tag{A-6}$$

$$v = \frac{\tilde{v}}{N\Delta}, \quad \tilde{v} = -\frac{N}{2}, \ldots, \frac{N}{2} \tag{A-7}$$

where $\tilde{u}$ and $\tilde{v}$ are wavenumbers and N is the number of pixels in the sample.

The 2D discrete Fourier transform is calculated by first taking the 1D discrete Fourier transform of each row of data. After transposing the array of pixilated data, another 1D transform is performed on each row (former columns). The 2D transform is completed by transposing the rows and columns a second time. Fourier coefficients for the lowest frequency pairs have the largest values, decay at the slowest rate, and are least influenced by noise. However, the DC component was not used in the analysis since it tended to indicate infinite diffusivity.

Light scattering media such as agarose distort the fluorescence emission profile, which makes many FRAP theories inapplicable to thick or light scattering media. A major advantage of spatial Fourier analysis is its success in predicting diffusivities even in these challenging media (Berk et al., 1993). Notice that the expressions developed above require the Fourier coefficients for the concentration profile, but the camera records the fluorescence intensity profile. The image recorded by the camera is a convolution of the true concentration profile and the point spread function (PSF). The PSF accounts for any aberrations or distortions caused by the microscope lenses, optics, and light absorption or scattering by the sample. The Fourier transform of the PSF is the optical transfer function (OTF). The OTF relates the Fourier transformed concentration to the Fourier transformed image intensity profile. That is,

$$\tilde{I}(u,v,t) = \tilde{C}(u,v,t)\mathrm{OTF}(u,v) \tag{A-8}$$

Generally, the OTF is very difficult to determine accurately and very cumbersome to work with. Luckily, the OTF cancels out of the equation when examining ratios of Fourier transformed intensities and concentrations, so it never needs to be determined. That is,

$$\frac{\tilde{I}(u,v,t)}{\tilde{I}(u,v,0)} = \frac{\tilde{C}(u,v,t)}{\tilde{C}(u,v,0)} \tag{A-9}$$

Additionally, the true concentration profile, which is distorted by thick or light scattering media, does not need to be determined. The decay of the ratio of Fourier transformed image fluorescence intensities is all that is needed to determine the diffusion coefficient, according to

$$\frac{\tilde{I}(u,v,t)}{\tilde{I}(u,v,0)} = e^{-4\pi^2(u^2+v^2)Dt} \tag{A-10}$$

The diffusion coefficient is the slope of a plot of the ratio of the Fourier transformed fluorescence intensities versus frequency scaled time. However, Eq. (A-10) is only strictly applicable to a system containing a single mobile diffusing species.

A.1.4 Application of Spatial Fourier Analysis to Mixtures and Immobile Species

Spatial Fourier analysis can easily be extended to mixtures with more than one diffusing species as immobile components. The concentration profile of a mixture of fluorescent species, $C_{total}(x,y,t)$, at time, t, can be determined by summing the concentration profiles of each species, i, weighted by its fractional contribution, x_i, to the total fluorescence of the mixture. The Fourier

transforms of the fluorescent concentration profiles are similarly additive for a two component mixture, as given by

$$\tilde{C}_{total}(u,v,t) = x_1 \tilde{C}_1(u,v,t) + x_2 \tilde{C}_2(u,v,t) \tag{A-11}$$

where the spatial frequencies are indicated by u and v. Fourier transformed concentration profiles for each individual species are characterized by an exponential decay. That is,

$$\tilde{C}_i(u,v,t) = \tilde{C}_i(u,v,0)e^{-4\pi^2 D_i(u^2+v^2)t} \tag{A-12}$$

Therefore, it is not surprising that when Eq. (A-11) and (A-12) are combined, the diffusion of two components results in biexponential decay. That is,

$$\begin{aligned}\tilde{C}_{total}(u,v,t) = x_1 \tilde{C}_{total}(u,v,0)e^{-4\pi^2 D_1(u^2+v^2)t} \\ + x_2 \tilde{C}_{total}(u,v,0)e^{-4\pi^2 D_2(u^2+v^2)t}\end{aligned} \tag{A-13}$$

As in single species spatial Fourier analysis, the ratio of Fourier transformed intensities equals the corresponding ratio of Fourier transformed concentrations. This is particularly useful since fluorescence intensity is the quantity actually measured by experiment. The equality is

$$\frac{\tilde{I}_{total}(u,v,t)}{\tilde{I}_{total}(u,v,0)} = \frac{\tilde{C}_{total}(u,v,t)}{\tilde{C}_{total}(u,v,0)} \tag{A-14}$$

Dividing Eq. (A-13) by $\tilde{C}_{total}(u,v,0)$ and applying the equality from Eq. (A-14),

$$\frac{\tilde{I}_{total}(u,v,t)}{\tilde{I}_{total}(u,v,0)} = \frac{x_1\tilde{C}_1(u,v,0)}{x_1\tilde{C}_1(u,v,0)+x_2\tilde{C}_2(u,v,0)} e^{-4\pi^2 D_1(u^2+v^2)t} + \frac{x_2\tilde{C}_2(u,v,0)}{x_1\tilde{C}_1(u,v,0)+x_2\tilde{C}_2(u,v,0)} e^{-4\pi^2 D_2(u^2+v^2)t} \tag{A-15}$$

Assuming that the time between bleaching and capturing the first picture is small, the fluorescence concentration profiles of all species should be nearly identical at time $t = 0$. That is,

$$\tilde{C}_1(u,v,0) \approx \tilde{C}_2(u,v,0) \approx \tilde{C}(u,v,0) \tag{A-16}$$

Hence, Eq. (A-15) can be greatly simplified to

$$\frac{\tilde{I}_{total}(u,v,t)}{\tilde{I}_{total}(u,v,0)} = x_1 e^{-4\pi^2 D_1(u^2+v^2)t} + x_2 e^{-4\pi^2 D_2(u^2+v^2)t} \tag{A-17}$$

Obviously, when one species is present in excess of the other, $x_2 << x_1$, then Eq. (A-17) simplifies to the usual single species result. However, Eq. (A-17) can also be simplified at long times when one species diffuses much faster than the other, $D_2 >> D_1$, to give

$$\frac{\tilde{I}_{total}(u,v,t)}{\tilde{I}_{total}(u,v,0)} = x_1 e^{-4\pi^2 D_1(u^2+v^2)t} \tag{A-18}$$

Rearranging Eq. (A-18) to the linear form $y = mx + b$ and replacing 1 with $x_1 + x_2$,

$$-\ln\left[\frac{\tilde{I}_{total}(u,v,t)}{\tilde{I}_{total}(u,v,0)}\right] = \left(4\pi^2(u^2+v^2)t\right)D_1 + \ln\left(1+\frac{x_2}{x_1}\right) \tag{A-19}$$

If x_2/x_1 is very small, then Eq. (A-19) simplifies to

$$-\ln\left[\frac{\tilde{I}_{total}(u,v,t)}{\tilde{I}_{total}(u,v,0)}\right]=\left(4\pi^2(u^2+v^2)t\right)D_1+\frac{x_2}{x_1} \tag{A-20}$$

For a mixture of two species in which one species diffuses much faster than the other, the diffusivity of the slower species can be easily determined at long times using spatial Fourier analysis. Physically, "long times" correspond to complete recovery of the fast component within the detection limits of the system. After the fast species has recovered, the data will only be influenced by the recovery of the slower species. Therefore a plot of the negative of the natural logarithm of the intensity ratio at time t to that at time 0 versus frequency scaled time is a straight line with a slope equal to the more slowly diffusing species. The y-intercept is approximately equal to the ratio of the fraction of the fluorescence attributable to the fast species to that of the slow component.

If two species diffuse at similar rates so that both contribute to the recovery over the entire time scale of the experiment, then the recovery will be biexponential as indicated by Eq. (A-17). Another simplification of Eq. (A-17) occurs when one species diffuses so slowly that it can be considered immobile, or $D_2 = 0$. In this case, spatial Fourier analysis indicates a different relationship than when one species is simply much slower than the other. The result is

$$\frac{\tilde{I}_{total}(u,v,t)}{\tilde{I}_{total}(u,v,0)}=x_1e^{-4\pi^2D_1(u^2+v^2)t}+x_2 \tag{A-21}$$

Equation (A-21) can be rearranged to the linear format used to determine the diffusivity, which is given by

$$-\ln\left[\frac{\tilde{I}_{total}(u,v,t)}{\tilde{I}_{total}(u,v,0)}-x_2\right]=\left(4\pi^2(u^2+v^2)t\right)D_1+\ln\left(1+\frac{x_2}{x_1}\right) \tag{A-22}$$

If the immobile fraction x_2 is small, then Eq. (A-22) can be simplified to

$$-\ln\left[\frac{\tilde{I}_{total}(u,v,t)}{\tilde{I}_{total}(u,v,0)}-x_2\right]=\left(4\pi^2(u^2+v^2)t\right)D_1+\frac{x_2}{x_1} \tag{A-23}$$

The y-intercept in Eqs. (A-20) and (A-23) can be eliminated by plotting $-\ln\left[\frac{\tilde{I}_{total}(u,v,t)}{\tilde{I}_{total}(u,v,0)}\cdot\frac{1}{1-x_2}\right]$ or $-\ln\left[\left(\frac{\tilde{I}_{total}(u,v,t)}{\tilde{I}_{total}(u,v,0)}-x_2\right)\cdot\frac{1}{1-x_2}\right]$ respectively versus frequency scaled time. The slope of such plots is D_1. This type of analysis could easily be extended to include more than two diffusing species, although the ability to fit the data accurately will depend on their relative magnitudes, as discussed above.

A.2 Diffusivities of Macromolecules in Dextran Solutions

The diffusivities of fluoresceinated proteins and Ficoll were measured in dextran solutions of varying concentrations using fluorescence recovery after photobleaching (FRAP). The proteins were ovalbumin and bovine serum album (BSA) and the Ficolls had weight-average molecular weights (M_W) of 21, 61, and 105 kDa. These macromolecules were purchased from the same suppliers, underwent the same preparation, and were characterized by the same properties as those detailed in section 2.2.4. Therefore, the properties of the five test macromolecules can be found in Table 2.1. A measured amount of 500 kDa dextran (Sigma, St.

Louis, MO) was dissolved in a 0.1 M KCl, 0.01 M sodium phosphate buffer at pH 7.0 to make solutions with dextran concentrations of 3.3, 12.0, 33.0, and 41.0 mg/mL.

Half of the volume of each dextran solution was subjected to electron beam irradiation while the other half was left untreated. A small amount of each fluoresceinated macromolecule was added to a fresh sample of the treated and untreated solutions, with the concentration of fluoresceinated solute in the sample less than 1 mg/mL. The samples were mixed and drawn into microcapillary tubes (Vitro Dynamics, Rockaway, NJ) using a syringe connected to the capillary microslide via tubing. To prevent evaporation, each end of the capillary tube was sealed with Hematoseal (Fisher Scientific, Pittsburgh, PA).

The macromolecular diffusion coefficients were measured at three different locations in each of the irradiated and unirradiated dextran solution samples using image-based FRAP (Tsay and Jacobson, 1991; Berk et al., 1993). Details of the FRAP system, operating conditions, and data analysis are given in sections 2.2.5 and 2.2.6. The diffusion coefficients were computed from the FRAP data using spatial Fourier analysis of the digitized images. The dextran solutions were mixed directly with the fluoresceinated macromolecules, rather than via equilibration which was necessary for the gel samples discussed in chapter 2. As a result, for all the macromolecules except BSA, the FRAP data was fit accurately based on a single diffusing species since the contaminants quantified in Table 2.1 had a negligible influence on the fit. The BSA diffusivity (D_∞) was calculated using the contaminant fractions obtained from size-exclusion chromatography (Table 2.1). So that the diffusivity of the predominant component (protein monomer) would be the only fitted parameter, D_∞ of the dimer was estimated from its chromatographic radius. The D_∞ of free fluorescein was assumed to equal that measured for DTAF (Table 2.1).

The relative diffusivities of the proteins and Ficolls in the four different treated and untreated dextran solutions are given in Table A.1. Relative diffusivities in the unirradiated and irradiated dextran solutions are plotted as a function of dextran concentration in Figs. A.1 and A.2, respectively. The relative diffusivity is the diffusivity in the gel (D) divided by that in free

Table A.1 Relative Diffusivities (D/D_∞) of Proteins and Ficolls in Irradiated and Unirradiated Dextran Solutions. Relative diffusivities are given as the mean ± the standard error as detailed in the text. Unless otherwise noted 4 samples were analyzed.

Dextran Concentration (mg/mL)	Ovalbumin D/D_∞	BSA D/D_∞	21 kDa Ficoll D/D_∞	61 kDa Ficoll D/D_∞	105 kDa Ficoll D/D_∞
3.3	0.94 ± 0.00*	0.98 ± 0.01*	0.91 ± 0.01	0.93 ± 0.01	0.91 ± 0.01
12.0	0.83 ± 0.01*	0.78 ± 0.01*	0.78 ± 0.01	0.77 ± 0.00	0.75 ± 0.00
33.0	0.60 ± 0.00*	0.52 ± 0.00*	0.60 ± 0.00	0.51 ± 0.00	0.48 ± 0.00
41.0	0.54 ± 0.00*	0.43 ± 0.01*	0.55 ± 0.01*	0.47 ± 0.01*	0.42 ± 0.00*
3.3 (irradiated)	0.97 ± 0.00	0.99 ± 0.01	0.97 ± 0.01	0.95 ± 0.01	0.97 ± 0.00**
12.0 (irradiated)	0.87 ± 0.01	0.87 ± 0.01	0.90 ± 0.01	0.92 ± 0.01	0.84 ± 0.05
33.0 (irradiated)	0.68 ± 0.01	0.58 ± 0.01	0.69 ± 0.00	0.67 ± 0.01	0.63 ± 0.00
41.0 (irradiated)	0.60 ± 0.01	0.52 ± 0.02	0.64 ± 0.00	0.58 ± 0.00	0.55 ± 0.00

*Two samples were measured.

**Three samples were measured.

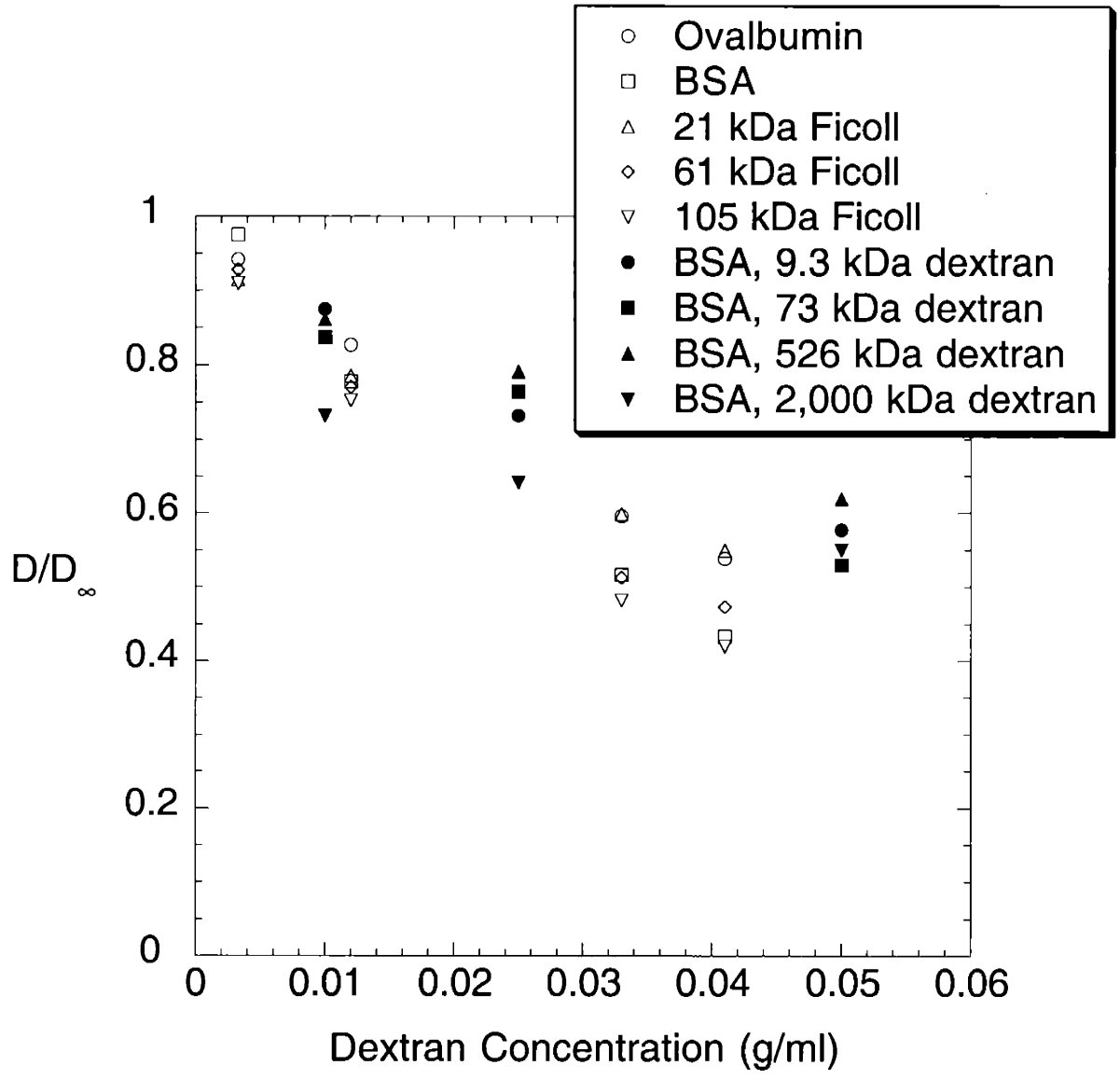

Figure A.1 Diffusivities in unirradiated dextran solutions (D) relative to those in free solution (D_∞). Results from the current study (open symbols) are compared with those of Kosar and Phillips (1995) (filled symbols). In the current study, 500 kDa dextran was used in all cases. The relative diffusivities shown are the mean of 2-4 samples. The standard errors were left off because they were so small (Table A.1) that they complicated the plot without adding any additional information.

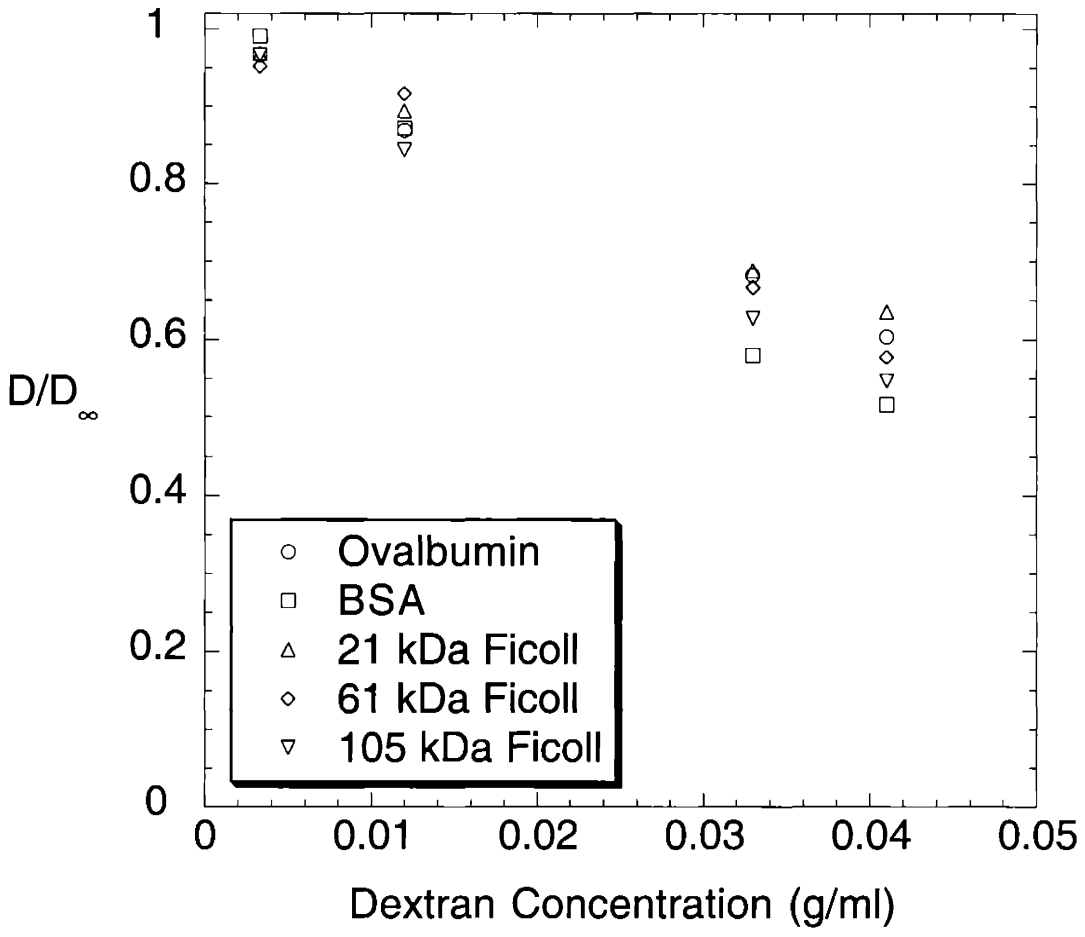

Figure A.2 Diffusivities in irradiated dextran solutions (D) relative to those in free solution (D_∞). The relative diffusivities shown are the mean of 3-4 samples. The standard errors were left off because they were so small (Table A.1) that they complicated the plot without adding any additional information.

solution (D_∞). They are given as the mean ± the standard error when 3-4 measurements were taken. When only 2 samples were examined, the error measure used was one-half of the difference between the two samples, plus the average standard error of the replicates. As expected, as the concentration of dextran increased, the relative diffusivity of a given macromolecule generally decreased. The decrease in relative diffusivity as the size of the macromolecule increased was relatively small. In general, for a given solute and dextran concentration, the relative diffusivity was higher in the irradiated dextran than in the untreated dextran.

In Fig. A.1, the relative diffusivities given in Table A.1 are also compared with the results of Kosar and Phillips (1995). Kosar and Phillips (1995) used holographic interferometry to measure the diffusion of BSA in unirradiated 9.3, 73, 526, and 2,000 kDa dextran solutions. They found that for a given dextran concentration, the diffusivities for the different molecular weights of dextran were not significantly different from each other. The results of Kosar and Phillips (1995) tended to be slightly higher than those in the current study.

A.3 Theoretical Predictions of Water Permeability in Agarose-Dextran Gels

The agarose-dextran composite gels, described in sections 2.2.1 - 2.2.2 and elsewhere, are comprised of a rigid agarose backbone with a small amount of flexible dextran incorporated into the gel. The detailed structure of these gels was probed by White and Deen (2002) who compared the predictions of several different Darcy permeability (κ) models to their data. As detailed in section 2.2.2, a more reliable technique was used to determine ϕ_d than that used by White and Deen (2002), which necessitates that the structure of the agarose-dextran gels be re-examined. In review, possible structures included a random fiber matrix composed of agarose

and dextran fibrils with water filled interstices, a homogeneous dextran gel with agarose fiber barriers, and a homogeneous agarose gel with spherical dextran coils as barriers.

Theories based on a homogeneous dextran gel containing regularly or randomly oriented agarose barriers provided by far the best prediction of κ in this study. Ethier (1991) used Brinkman's equation to describe flow through the homogeneous gel containing a cubic lattice of large rods, such as coarse agarose fibrils. Since theoretical predictions of the Darcy permeability of agarose are unreliable, experimental values were used and incorporated into Ethier's model by White and Deen (2002). The resulting expression, which is rather complex, is of the form

$$\kappa = \frac{f(\phi_a, \kappa_d / r_a^2)}{f(\phi_a, \infty)} \kappa_a \tag{A-24}$$

where κ_i is the Darcy permeability of a medium containing only component i with volume fraction ϕ_i, and fiber radius r_i. An alternate theory explored by White and Deen (2002) utilizes the analogy between Darcy flow and steady heat conduction in a composite medium (Deen, 1998). It is based on flow through randomly oriented coarse fibers within a homogeneous gel. For impermeable cylinders, the expression is

$$\frac{\kappa}{\kappa_d} = 1 - \frac{5}{3}\phi_a + O(\phi_a^2) \tag{A-25}$$

White and Deen (2002) suggested that the Darcy permeability of pure dextran can be estimated using the fit to numerical lattice-Boltzmann simulations from Clague et al. (2000), which is given by

$$\frac{\kappa_d}{r_d^2} = \left[\frac{1}{2}\left(\frac{\pi}{\phi_d} \right)^{\frac{1}{2}} - 1 \right]^2 \left[0.71407 \exp(-0.51854\phi_d) \right] \tag{A-26}$$

Their simulations describe Stokes flow through randomly oriented arrays of uniform radius cylinders.

The Darcy permeability of 4% and 8% agarose gels with three different levels are dextran are shown in Figs. A.3 - A.4, respectively. For the 4% agarose gels, Deen's (1998) model slightly underestimates κ, while Ethier's (1991) overestimates κ. In the 8% agarose gels, Eq. (A-25) does a better job of predicting the composite gel Darcy permeabilities than Eq. (A-24). Aside from being unbounded at zero ϕ_d, Eq. (A-25) may be more appropriate since, as mentioned by Johnson, E. M. et al. (1996), the agarose gels under investigation must have some degree of irregularity because they exhibit a nonzero D/D_∞ past the critical volume fraction when all the fibers in a cubic array would touch.

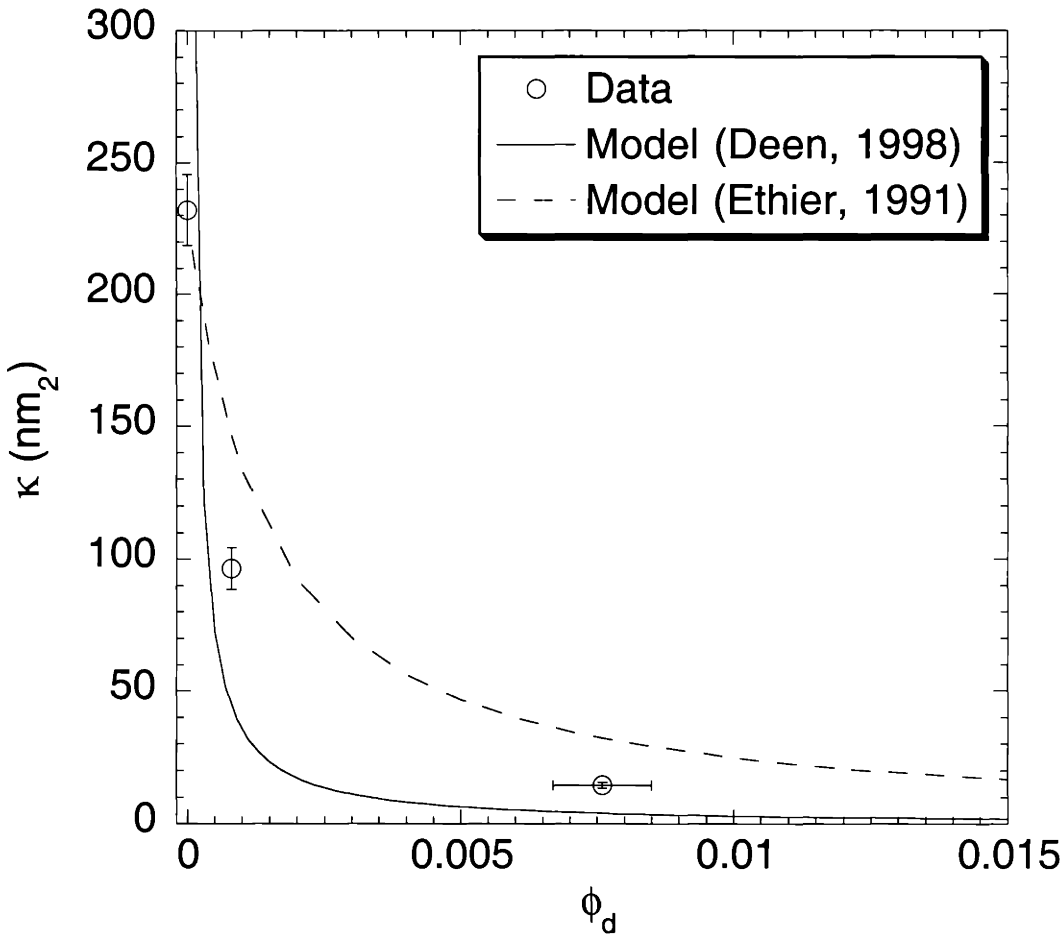

Figure A.3 Measured and predicted Darcy permeabilities (κ) of 4% agarose gels with zero, low, and high dextran levels. The predicted curves are given by Eq. (A-25) (solid curve) and Eq. (A-24) (dashed curve). Both models assume a homogeneous dextran gel containing agarose fiber barriers.

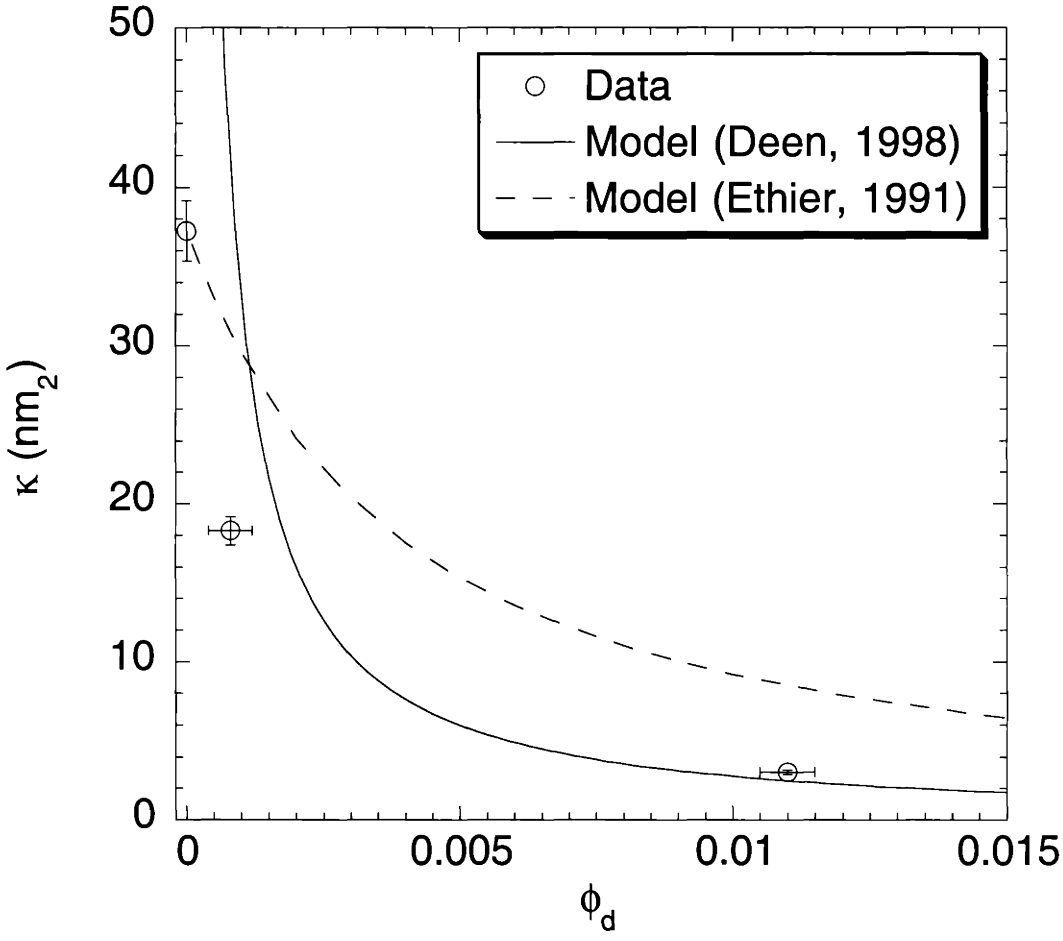

Figure A.4 Measured and predicted Darcy permeabilities (κ) of 8% agarose gels with zero, low, and high dextran levels. The predicted curves are given by Eq. (A-25) (solid curve) and Eq. (A-24) (dashed curve). Both models assume a homogeneous dextran gel containing agarose fiber barriers.

Bibliography

Amsden, B., "Solute Diffusion within Hydrogels. Mechanisms and Models," *Macromolecules*, **31**, 8382 (1998).

Anderson, J. L., "Configurational Effect on the Reflection Coefficient for Rigid Solutes in Capillary Pores," *J. Theor. Biol.*, **90**, 405 (1981).

Anderson, J. L. and D. M. Malone, "Mechanism of Osmotic Flow in Porous Membranes," *Biophys. J.*, **14**, 957 (1974).

Anderson, J. L. and J. A. Quinn, "Restricted Transport in Small Pores. A Model for Steric Exclusion and Hindered Particle Motion," *Biophys. J.*, **14**, 130 (1974).

Arnott, S., A. Fulmer, W. E. Scott, I. C. M. Dea, R. Moorhouse, and D. A. Rees, "The Agarose Double Helix and Its Function in Agarose Gel Structure," *J. Mol. Biol.*, **90**, 269 (1974).

Arnott, S. and W. E. Scott, "Accurate x-ray Diffraction Analysis of Fibrous Polysaccharides containing Pyranose Rings. I. The Linked-Atom Approach." *J. Chem. Soc., Perkin Trans.*, **2**, 324 (1972).

Belton, P. S., B. P. Hills, and E. R. Raimbaud, 'The Effects of Morphology and Exchange on Proton NMR Relaxation in Agarose Gels," *Molecular Physics*, **63**, 825 (1988).

Berk, D. A., F. Yuan, M. Leunig, and R. K. Jain, "Fluorescence Photobleaching with Spatial Fourier Analysis: Measurement of Diffusion in Light-Scattering Media," *Biophys. J.*, **65**, 2428 (1993).

Bohrer, M. P., G. D. Patterson, and P. J. Carroll, "Hindered Diffusion of Dextran and Ficoll in Microporous Membranes," *Macromolecules,* **17**, 1170 (1984).

Bohrer, M. P., W. M. Deen, C. R. Robertson, J. L. Troy, and B. M. Brenner, "Influence of Molecular Configuration on the Passage of Macromolecules Across the Glomerular Capillary Wall," *J. Gen. Physiol.*, **74**, 583 (1979).

Bolton, G. R., W. M. Deen, and B. S. Daniels, "Assessment of the Charge-selectivity of Glomerular Basement Membrane Using Ficoll sulfate," *Am. J. Physiol. Renal Physiol.*, **274**, F998 (1998).

Bolton, G. R. and W. M. Deen, "Limitations in the Application of Fiber-Matrix Models to Glomerular Basement Membrane," In: *Membrane Transport and Renal Physiology*, edited by Layton, H. E. and A. M. Weinstein. New York: Springer-Verlag, (IMA Volumes in Mathematics and its Applications Ser.) (2001).

Bosma, J. C. and J. A. Wesselingh, "Partitioning and Diffusion of Large Molecules in Fibrous Structures," *J. Chromat. B.*, **743**, 169 (2000).

Brady, J., "Hindered Diffusion," *In* Extended Abstracts, AIChE Annual Meeting, San Francisco, CA, 320 (1994).

Brinkman, H. C, "A Calculation of the Viscous Force Exerted by a Flowing Fluid in a Dense Swarm of Particles," *Appl. Sci. Res. A*, **1**, 27 (1947).

Buck, K. K. S., N. I. Gerhardt, S. R. Dungan, and R. J. Phillips, "The Effect of Solute Concentration on Equilibrium Partitioning in Polymeric Gels," *J. Colloid Interface Sci.*, **234**, 400 (2001).

Bungay, P. M. and H. Brenner, "The Motion of a Closely Fitting Sphere in a Fluid-Filled Tube," *Int. J. Multiphase Flow*, **1**, 25 (1973).

Burczak, K., T. Fujisato, M. Hatada, and Y. Ikada, "Protein Permeation through Poly(Vinyl Alcohol) Hydrogel Membranes," *Biomaterials*, **15**, 231 (1994).

Chui, M. M., R. J. Phillips, and M. J. McCarthy, "Measurement of the Porous Microstructure of Hydrogels by Nuclear Magnetic Resonance," *J. Colloid Interface Sci.*, **174**, 336 (1995).

Clague, D. S., B. D. Kandhai, R. Zhang, and P. M. A. Sloot, "Hydraulic Permeability of (Un)Bounded Fibrous Media Using the Lattice Boltzmann Method," *Phys. Rev. E.*, **61**, 616 (2000).

Clague, D. S. and R. J. Phillips, "Hindered Diffusion of Spherical Macromolecules through Dilute Fibrous Media," *Phys. Fluid*, **8**, 1721 (1996).

Clague, D. S. and R. J. Phillips, "A Numerical Calculation of the Hydraulic Permeability of Three-Dimensional Disordered Fibrous Media," *Phys. Fluids.*, **9**, 1562 (1997).

Comper, W. D., A. S. N. Lee, M. Tay, and Y. Adal, "Anionic Charge Concentration of Rat Kidney Glomeruli and Glomerular Basement Membrane," *Biochem J.*, **289**, 647 (1993).

Curry, F. E. and C. C. Michel, "A Fiber Matrix Model of Capillary Permeability," *Microvasc. Res.*, **20**, 96 (1980).

Daniels, B. S., E. B. Hauser, W. M. Deen, and T. H. Hostetter, "Glomerular Basement Membrane: In Vitro Studies of Water and Protein Permeability," *Am. J. Physiol.*, **262**, F919 (1992).

Daniels, B. S., W. M. Deen, G. Mayer, T. Meyer, and T. H. Hostetter, "Glomerular Permeability Barrier in the Rat: Functional Assessment by In Vitro Methods," *J. Clin. Invest.*, **92**, 929 (1993).

Davidson, M. G. and W. M. Deen, "Hydrodynamic Theory for the Hindered Transport of Flexible Macromolecules in Porous Membranes," *J. Membr. Sci.*, **35**, 167 (1988).

Dea, I. C. M., R. Moorhouse, D. A. Rees, S. Arnott, J. M. Guss, and E. A. Balazs, "Hyaluronic Acid: A Novel, Double Helical Molecule," *Science*, **179**, 560 (1973).

De Belder, A. N. and K. Granath, "Preparation and Properties of Fluorescein-Labeled Dextrans," *Carbohydr. Res.*, **30**, 375 (1973).

Deen, W. M., "Heteroporous Model of Glomerular Size Selectivity: Application to Normal and Nephrotic Humans," *Am. J. Pysiol.*, **249**, F374 (1985).

Deen, W. M, "Hindered Transport of Large Molecules in Liquid-Filled Pores," *AIChE J.*, **33**, 1409 (1987).

Deen, W. M., M. J. Lazzara, and B. D. Myers, "Structural Determinants of Glomerular Permeability," *Am. J. Renal Physiol.*, **281**, F579 (2001).

Djabourov, M., A. H. Clark, D. W. Rowland, and S. B. Ross-Murphy, "Small-Angle X-ray-Scattering Characterization of Agarose Sols and Gels," *Macromolecules*, **22**, 180 (1989).

Dormay, Y. and S. Candau, "Transient Electric Birefrigence Study of Highly Dilute Agarose

Solutions," *Biopolymers*, **31**, 109 (1991).

Drummond, J. E. and M. I. Tahir, "Laminar Viscous Flow Through Regular Arrays of Parallel Solid Cylinders," *Int. J. Multiphase Flow*, **10**, 515 (1984).

Drumond, M. C. and W. M. Deen, "Structural Determinants of Glomerular Hydraulic Permeability," *Am. J. Physiol.*, **266**, F1 (1994).

Dubois, M., K. A. Gilles, J. K. Hamilton, P. A. Rebers, and F. Smith, "Colorimetric Method for Determination of Sugars and Related Substances," *Anal. Chem.*, **28**, 350 (1956).

Edwards, A., W. M. Deen, and B. S. Daniels, "Hindered Transport of Macromolecules in Isolated Glomeruli. I. Diffusion Across Intact and Cell-Free Capillaries," *Biophys. J.*, **72**, 204 (1997a).

Edwards, A., B. S. Daniels, and W. M. Deen, "Hindered Transport of Macromolecules in Isolated Glomeruli. II. Convection and Pressure Effects in Basement Membrane," *Biophys. J.*, **72**, 214 (1997b).

Edwards, A., B. S. Daniels, and W. M. Deen, "Ultrastructural Model for Size Selectivity in Glomerular Filtration," *Am J. Physiol.*, **276**, F892 (1999).

Edwards, D. A., M. Shapiro, P. Bar-Yoseph, and M. Shapira, "The Influence of Reynolds Number Upon the Apparent Permeability of Spatially Periodic Arrays of Cylinders," *Phys. Fluids A*, **2**, 45 (1990).

Ethier, C. R., "Flow Through Mixed Fibrous Porous Materials," *AIChE J.*, **37**, 1227, (1991).

Huang, Y. Q., D. Rumschitzki, S. Chien, and S. Weinbaum, "A Fiber Matrix Model for the Filtration through Fenestral Pores in a Compressible Arterial Intima," *Am. J. Physiol.*, **41**, H2023 (1997).

Fanti, L. A. and E. D. Glandt, "Partitioning of Sperical Particles Into Fibrous Matrices. 1. Density-Functional Theory," *J. Colloid Int. Sci.*, **135**, 385 (1990a).

Fanti, L. A. and E. D. Glandt, "Partitioning of Sperical Particles Into Fibrous Matrices. 2. Monte Carlo Simulation," *J. Colloid Int. Sci.*, **135**, 396 (1990b).

Farquar, M.G., "The Glomerular Basement Membrane: A Selective Macromolecular Filter," In *Cell Biology of the Extracellular Matrix*, S. D. Hay (ed.), Plenum Press, New York (1981).

Happel, J., "Viscous Flow Relative to Arrays of Cylinders," *AIChE J.*, **5** (2), 174 (1959).

Hasimoto, H., "On the Periodic Fundamental Solutions of the Stokes Equations and their Application to Viscous Flow Past a Cubic Array of Spheres," *J. Fluid Mech.*, **5**, 317 (1959).

Gibbs, S. J., E. N. Lightfoot, and T. W. Root, "Protein Diffusion in Porous Gel Filtration Chromatography Media Studied by Pulsed Field Gradient NMR Spectroscopy." *J. Phys. Chem.*, **96**, 7458 (1992).

Gong, J. P., N. Hirota, A. Kakugo, T. Narita, and Y. Osada, "Effect of Aspect Ratio on Protein Diffusion in Hydrogels," *J. Phys. Chem. B.*, **104**, 9904 (2000).

Hou, L., F. Lanni, and K. Luby-Phelps, "Tracer Diffusion in F-actin and Ficoll Mixtures: Toward a Model for Cytoplasm," *Biophys. J.*, **58**, 31 (1990).

Jackson, G. W. and D. F. James, "The Permeability of Fibrous Porous Media," *Can. J. Chem. Eng.*, **64**, 364 (1986).

Jain, R. K., R. J. Stock, S. R. Chary, and M. Rueter, "Convection and Diffusion Measurements Using Fluorescence Recovery after Photobleaching and Video Image Analysis: In Vitro Calibration and Assessment," *Microvasc. Res.*, **39**, 77 (1990).

Johansson, L. and J. E. Lofroth, "Diffusion and Interaction in Gels and Solutions. 4. Hard Sphere Brownian Dynamics Simulations," *J. Chem. Phys.*, **98**, 7471 (1993).

Johnson, E. M., D. A. Berk, R. K. Jain, and W. M. Deen, "Diffusion and Partitioning of Proteins in Charged Agarose Gels," *Biophys. J.*, **68**, 1561 (1995).

Johnson, E. M., D. A. Berk, R. K. Jain, and W. M. Deen, "Hindered Diffusion in Agarose Gels: Test of the Effective Medium Model," *Biophys. J.*, **70**, 1017 (1996).

Johnson, E. M. and W. M. Deen, "Electrostatic Effects on the Equilibrium Partitioning of Spherical Colloids in Random Fibrous Media," *J. Colloid Int. Sci.*, **178**, 749 (1996a).

Johnson, E. M. and W. M. Deen, "Hydraulic Permeability of Agarose Gels," *AIChE J.*, **42**,1220 (1996b).

Johnson, M. E., D. A. Berk, D. Blankschtein, D. E. Golan, R. K. Jain, and R. S. Langer, "Lateral Diffusion of Small Compound in Human Stratum Corneum and Model Lipid Bilayer Systems," *Biophys. J.*, **71**, 2656 (1996).

Johnston, S. T., K. A. Smith, and W. M. Deen, "Concentration Polarization in Stirred Ultrafiltration Cells," *AIChE J.*, **47**, 1115 (2001).

Johnston, S. T. and W. M. Deen, "Hindered Convection of Proteins in Agarose Gels," *J. Membr. Sci.*, **153**, 271 (1999).

Johnston, S. T. and W. M. Deen, "Hindered Convection of Ficoll and Proteins in Agarose Gels," *Ind. Eng. Chem. Res.*, **41**, 340 (2002).

Kapur, V., J. C. Charkoudian, S. B. Kessler, and J. L. Anderson, "Hydrodynamic Permeability of Hydrogels Stabalized within Porous Membranes," *Ind. Eng. Chem. Res.*, **35**, 3179 (1996).

Kapur, V., J. Charkoudian, and J. L. Anderson, "Transport of Proteins through Gel-Filled Porous Membranes," *J. Mem. Sci.*, **131**, 143 (1997).

Key, P. Y. and D. B. Sellen, "A Laser Light-Scattering Study of the Structure of Agarose Gels," *J. Polym. Sci. Poly. Phys. Ed.*, **20**, 659 (1982).

Kosar, T. F. and R. J. Phillips, "Measurement of Protein Diffusion in Dextran Solutions by Holographic Interferometery," *AIChE J.*, **41**, 701 (1995).

Kuwabara, S., "The Forces Experienced by Randomly Distributed Parallel Circular Cylinders or Spheres in a Viscous Flow at Small Reynolds Numbers," *J. Phys. Soc. of Japan*, **14**, 527 (1959).

Langmuir, I., "Report of Smokes and Filters," Part IV of a report for the Office of Scientific Research and Development, OSRD No. 865, Ser. No. 353, "Filtration of Aerosols and the Develpment of Filter Materials," by Rodebush, W. H. et al., September 4, 1942.

Larson, R. J. and M. L. Marx, "An Introduction to Mathematical Statistics and its Applications," 2nd ed. Pentice-Hall, Englewood Cliffs, NJ (1986).

Laurent, T. C., "The Interaction Between Polysaccharides and Other Macromolecules. V. The Solubility of Proteins in the Presence of Dextran," *Biochem. J.*, **89**, 253 (1963a).

Laurent, T. C., "The Interaction Between Polysaccharides and Other Macromolecules. VI. Further Studies on the Solubility of Proteins in Dextran Solutions," *Acta Chem. Scand.*, **17**, 2664 (1963b).

Laurent, T. C., "Determination of the Structure of Agarose Gels by Gel Chromatography," *Biochim. Biophys. Acta*, **136**, 199 (1967).

Laurent, T. C. and J. Killander, "A Theory of Gel Filtration and its Experimental Verification," *J. Chromat.*, **14**, 317 (1964).

Laurie, G. W., C. P. Leblond, S. Inoue, G. R. Martin, and A. Chung, "Fine Structure of the Glomerular Basement Membrane and Immunolocalization of Five Basement Membrane Components to the Lamina Densa (Basal Lamina) and its Extensions in Both Glomeruli and Tubules of the Rat Kidney," *Am. J. Anat.*, **169**, 463 (1984).

Lazzara, M. J., D. Blankschtein, and W. M. Deen, "Effects of Multisolute Steric Interactions on Membrane Partition Coefficients," *J. Colloid Interface Sci.*, **226**, 112 (2000).

Lazzara, M. J. and W. M. Deen, "Effects of Plasma Proteins on Sieving of Tracer Macromolecules in Glomerular Basement Membrane," *Am. J. Physiol.*, **281**, F860 (2001).

Lazzara, M. J. and W. M. Deen, "Effects of Concentration on the Partitioning of Macromolecule Mixtures in Agarose Gels," *J. Colloid Interface Sci.*, **272**, 288 (2004).

Leung, B. K. O. and G. B. Robinson, "Ultrafiltration Properties of Hydrogel Analogues of Basement Membrane: A Comparison of the Pore Theory and Fiber Matrix Hypothesis," *J. Membrane Sci.*, **51**, 141, (1990a).

Leung, B. K. O. and G. B. Robinson, "Ultrafiltration through Hydrogels: Effects of Hydration and Crosslinking," *J. Membrane Sci.* **52**, 1, (1990b).

Ligler, F.S. and G.B. Robinson, "A New Method for the Isolation of Renal Basement Membranes," *Biochim. Biophys. Acta*, **468**, 327 (1977).

Mackie, W., D. B. Sellen, and J. Sutcliffe, "Spectral Broadening of Light Scattered from Polysaccharide Gels," *Polymer*, **19**, 9 (1978).

Moussaoui, M., M. Benlyas, and P. Wahl, "Diffusion of Proteins in Sepharose Cl-B Gels," *J. Chromatogr.*, **591**, 115 (1992).

Nordmeier, E. "Static and Dynamic Light-Scattering Solution Behavior of Pullulan and Dextran in Comparison," *J. Phys. Chem.*, **97**, 5770 (1993).

Ogston, A. G., "The Spaces in a Uniform Random Suspension of Fibers," *Trans. Faraday Soc.*, **54**, 1754 (1958).

Ogston, A. G., B. N. Preston, and J. D. Wells, "On the Transport of Compact Particles Through Solutions of Chain Polymers," *Proc. R. Soc. Lond. A.*, **333**, 297 (1973).

Oliver, J. D., S. Anderson, J. L. Troy, B. M. Brenner, and W. M. Deen, "Determination of Glomerular Size-Selectivity in the Normal Rat with Ficoll," *J. Am. Soc. Nephrol.*, **3**, 214 (1992).

Pallmann, H. and H. Deval, "Über die Wasserdurchlässigkeit von Hydrogelen," *Experientia.*, **1**, 325 (1945).

Pernodet, M., M. Maaloum, and B. Tinland, "Pore Size of Agarose Gels by Atomic Force Microscopy," *Electorphoresis*, **18**, 55 (1997).

Phillips, R. J., "A Hydrodynamic Model for Hindered Diffusion of Proteins and Micelles in Hydrogels," *Biophys. J.*, **79**, 2250 (2000).

Phillips, R. J., W. M. Deen, and J. F. Brady, "Hindered Transport of Spherical Macromolecules in Fibrous Membranes and Gels," *AIChE J.*, **35**, 1761 (1989).

Phillips, R. J., W. M. Deen, and J. F. Brady, "Hindered Transport in Fibrous Membranes and Gels: Effect of Solute Size and Fiber Configuration," *J. Colloid Interface Sci.*, **139**, 363 (1990).

Pluen, A., P. A. Netti, R. K. Jain, and D. A. Berk, "Diffusion of Macromolecules in Agarose Gels: Comparison of Linear and Globular Configurations," *Biophys. J.*, **77**, 542 (1999).

Putnam, F. W., ed., "The Plasma Proteins: Structure, Function, and Genetic Control," 2nd ed. Academic Press, New York, **1**, 62 (1975).

Raj, T. and W. H. Flygare, "Diffusion Studies of Bovine Serum Albumin by Quasielectric Light Scattering," *Biochemistry*, **13**, 3336 (1974).

Robinson, G. B. and H. A. Walton, "Ultrafiltration Through Basement Membrane," In *Renal Basement Membranes in Health and Disease*, R.G. Price and B.G. Hudson (eds.), Academic Press, London, 147-161 (1987).

Robinson, G. B., and H. A. Walton, "Glomerular Basement Membrane as a Compressible Ultrafilter," *Microvasc. Res.*, **38**, 36 (1989).

Saltzman, W. M., M. L. Radomsky, K. J. Whaley, and R. A. Cone, "Antibody Diffusion in Human Cervical Mucus," *Biophys. J.*, **66**, 508 (1994).

Sangani, A. S. and A. Acrivos, "Slow Flow Past Periodic Arrays of Cylinders with Application to Heat Transfer," *Int. J. Multiphase Flow*, **8**, 193 (1982).

Signer, R. and H. Egli, "Sedimentation von Makromolekülen und Durchströmung von Gelen," *Rec. Trav. Chim.*, **69**, 45 (1950).

Solomentsev, Y. E. and J. L. Anderson, "Rotation of a Sphere in Brinkman Fluids," *Phys. Fluids*, **8**, 1119 (1996).

Sparrow, E. M. and A. L. Loeffler Jr., "Longitudinal Laminar Flow Between Cylinders Arranged in Regular Arrays," *AIChE J.*, **5**, 325 (1959).

Tokita, M. and T. Tanaka, "Friction Coefficient of Polymer Networks of Gels," *J. Chem Phys.*, **95**, 4613 (1991).

Tsay, T. T. and K. A. Jacobson, "Spatial Fourier Analysis of Video Photobleaching Measurements: Principles and Optimization," *Biophys. J.*, **60**, 360 (1991).

Walton, H. A., J. Byrne, and G. B. Robinson, "Studies of the Permeation of Glomerular Basement Membrane: Cross-Linking Renders Glomerular Basement Membrane Permeable to Protein," *Biochim. Biophys. Acta*, **1138**, 173 (1992).

Wattenbarger, M. R., V. A. Bloomfield, Z. Bu, and P. S. Russo, "Tracer Diffusion of Proteins in DNA Solutions." *Macromolecules*, **25**, 5263 (1992).

Weiss, N. and A. Silberberg, "Inhomogeneity of Polyacrylamide Gel Structure from Permeability and Viscoelasticity," *Brit. Poly. J.*, **9**, 144 (1977).

White, J. A. and W. M. Deen, "Equilibrium Partitioning of Flexible Macromolecules in Fibrous Membranes and Gels," *Macromolecules*, **33**, 8504 (2000).

White, J. A. and W. M. Deen, "Effects of Solute Concentration on Equilibrium Partitioning of Flexible Macromolecules in Fibrous Membranes and Gels," *Macromolecules*, **34**, 8278 (2001).

White, J. A. and W. M. Deen, "Agarose-Dextran Gels as Synthetic Analogs of Glomerular Basement Membrane: Water Permeability." *Biophys. J.*, **82**, 2081 (2002).

White, M. L., "The Permeability of An Acrylamide Polymer Gel," *J. Phys. Chem.*, **64**, 1563 (1960).

Yurchenco, P. D., and J. C. Schittny, "Molecular Architecture of Basement Membranes," *FASEB J.*, **4**, 1577 (1990).

Yurchenco, P. D. and J. O'Rear, "Supramolecular Organization of Basement Membranes," *In Molecular and Cellular Aspects of Basement Membranes*, D. Rohrbach and R. Timpl. (eds.), Academic Press, New York, 19-47 (1993).

Zhang, X. M., N. Hirota, T. Narita, J. P. Gong, Y. Osada, K. S. Chen, "Invesigation of Molecular Diffusion in Hydrogel by Electronic Speckle Pattern Interferometery," *J. Phys. Chem. B.*, **103**, 6060 (1999).